MRI ASSESSMENT OF BRAIN VASCULAR REACTIVITY TO PHYSIOLOGICAL CHALLENGES

by

BINU PANJIKATTIL THOMAS

Presented to the Faculty of the Graduate School of

The University of Texas at Arlington in Partial Fulfillment

of the Requirements

for the Degree of

DOCTOR OF PHILOSOPHY

THE UNIVERSITY OF TEXAS AT ARLINGTON

August 2014

Acknowlegments

I would like to thank my mentor Dr. Hanzhang Lu for allowing me to be a part of his laboratory. I greatly appreciate him for his guidance and support through my research during the past four years. I am thankful for his confidence in my talents and his capabilities to hone it further under his training.

I would also like to thank Dr. Hao Huang, Dr. George Alexandrakis, Dr. Roderick McColl and Dr. Kevin King for taking time out of their busy schedules to serve on my thesis committee. The inputs extended from all my committee members have been very helpful in improvising my research. I would also like to thank Dr. Hanli Liu for being on my proposal committee and advising me through graduate school. I would like to thank my lab members: Sina Aslan, Feng Xu, Peiying Liu, Uma Yezhuvath, Harshan Ravi, Lisa Crystal Krishnamurthy, Shin-Lei Peng, Deng Mao, Min Sheng, Yang Li, Yamei Cheng and Pan Su and my friends Sandeep Ganji, Virendra Mishra for sharing with me their expertise and providing help whenever needed and making my experience in graduate school an easy and enriching one. I would also like to thank all volunteers who participated in my studies, without which this research would not be possible.

I would like to thank my parents P.T. Thomas and Valsa Thomas, my wife Divya, and my daughter Anaaya for extending their love, blessings, support and encouragement without which I would not be able to embark on and complete my work.

July 21, 2014

Abstract

MRI ASSESSMENT OF BRAIN VASCULAR REACTIVITY

TO PHYSIOLOGICAL CHALLENGES

Binu Panjikattil Thomas, Ph.D.

The University of Texas at Arlington, 2014

Supervising Professor: Hanzhang Lu

With a growing need for specific biomarkers in vascular diseases, the past decade has seen a surging interest in mapping brain vascular reactivity. There is great potential that this CVR mapping can be added to standard clinical MRI protocol, but before this is achieved, we need to better understand the mechanism of BOLD signal change to physiological challenges. A signal increase in the BOLD image is usually seen to CO_2 inhalation, but there are reports of negative CVR as well, i.e. decrease in BOLD signal during inhalation of CO_2 gas. Negative CVR is usually seen in patients with vascular occlusions, which is interpreted as vascular steal i.e. blood being stolen by vascular dilation in the normal regions of the brain. Negative CVR was also reported in normal healthy volunteers, which was also interpreted as vascular steal. To understand the physiologic underpinnings of negative CVR, we performed an Inversion Recovery MRI experiment which showed that negative CVR was because of a volume effect in which blood vessel dilation in the ventricle space displaced the bright CSF which reduced the BOLD signal intensity in the ventricle during CO_2 inhalation. This research from Chapter 2 will impact future interpretations of negative CVR, and also guide intervention studies in patients.

CVR in gray matter has been well characterized and understood, but little is known about CVR in WM. Research performed in Chapter 3 helps better understand and characterize WM CVR in terms of its magnitude and temporal characteristics. CVR in the WM was 0.03±0.002 %/mmHg, but was significantly lower than that in the GM: 0.22±0.01 %/mmHg. More strikingly, the WM response showed a temporal delay of 19±3 seconds compared to the GM, which was attributed to the longer time it takes for extravascular CO_2 to change. With age, WM CVR response was found to become greater and faster, which is opposite to the changes seen in the GM. These data suggest that characteristics of WM CVR are different from that of GM and caution should be used when interpreting pathological WM CVR results.

Vascular response to inhalation of both O_2 and CO_2 were studied further in WM in Chapter 4. WM was classified into major fiber tracts, cerebral lobes and layers of increasing depth from the cortical surface and vascular response was measured from these regions. One of the most striking findings was that vascular response to O_2 was also considerably delayed in most regions examined, but it was still faster than the CVR to CO_2 inhalation. This difference in delay was attributed to the difference in the mechanism of action of the each gas on brain vasculature. It was also found that as the depth of WM from the cortical surface increases, the magnitude of response to O_2 and CO_2 gas decreases, while delay in vascular response increases. We also report an index of measurement reproducibility between scans for the vascular response in WM to O_2 and CO_2.

Research on the application of CVR mapping was performed in Chapter 5 to understand the effect of life-long aerobic exercise on brain vascular health. It was found that exercise preserved blood supply in the brain's default-mode-network against age-related deterioration. On the other hand, its impact on the cerebral vascular system

seems to be characterized by a dampening of CO_2 reactivity, possibly because of desensitization effects due to a higher lifetime exposure to CO_2.

Table of Contents

List of Illustrations

List of Tables

Chapter 1

Introduction

Cerebrovascular reactivity (CVR) refers to the ability of brain vasculature to dilate in response to a vaso-dilative agent. It is an important marker of vascular elasticity; specifically, it is a direct measure of vascular endothelium and smooth muscle function [1, 2]. Measurement of CVR provides information about the dynamic properties of vasculature, such as those measured while the brain is subjected to a challenge. During a challenge, smooth muscle cells on the arterial vessel walls expand and cause increase in blood flow. This increase in blood flow causes an increase in oxygenated blood in venous vasculature, which is then detected by MRI due to the differences in magnetic properties of oxygenated and deoxygenated blood. Information about the vaso-dilative ability of blood vessels is very important; it provides insight into the cerebrovascular reserve capacity or the potential of the vasculature to increase blood flow from baseline, if the brain were to undergo a challenge or stimulation. Information about the dynamic properties of vasculature are far more important than that provided by baseline measurements such as baseline cerebral blood flow (CBF) or cerebral blood volume (CBV), as it can predict impending risk to the vasculature. CVR measurement finds applications in many brain disorders and conditions such as small vessel diseases [3], arterial stenosis [4], arteriovenous malformation [5], Moyamoya disease [6, 7], drug addictive conditions [8], and normal aging [9]. CVR measurement can also be used to normalize fMRI signal and to evaluate brain metabolism.

CVR can be probed by performing vaso-dilative challenges such as inhalation of CO2, breath hold, or injection of acetazolamide. CO2 inhalation is the most commonly used procedure to induce vaso-dilation because it provides the ability to modulate vaso-dilation capacity within a short period of time and obtain multiple measures. The breath

hold technique requires subject cooperation and is not favored especially in impaired patients [10]. Injection of acetazolamide is also less favored because it takes longer time for acetazolamide to penetrate blood-brain barrier and cause vaso-dilation [11], which prevents the researcher from making multiple measurements. All CVR measurements performed as part of this thesis use the CO_2 inhalation technique to induce vaso-dilation. CVR was assessed using MRI. Although MRI techniques to measure CBF and CBV changes have been used [12-16], the Blood-Oxygenation-Level-Dependent (BOLD) MRI sequence is most widely utilized due to its superior sensitivity to detect changes in oxygenation, similar to its widespread use in fMRI. All studies performed in this dissertation work utilized the BOLD MRI acquisition technique to measure the vascular response in brain to physiologic challenges. During a CO_2 inhalation experiment, CO_2 travels via the lungs to the brain and then causes vaso-dilation in the brain. It takes around 15 seconds [17-19]for the response to be detected in the brain after a change in End-tidal (Et) CO_2 was measured in the lungs. In the brain, the vaso-dilation response is detected as an increase in the MRI signal intensity.

With this introduction on CVR, the reader is guided into research described in this dissertation. Four research projects were performed and the importance and purpose of each project is provided in the section below. Each sub-heading introduces a single research project.

1.1 Significance and Objectives of Research

1.1.1 Negative Cerebrovascular Reactivity to CO_2 in Brain

With a growing interest for more specific biomarkers of small vessel diseases [3] and the increasing availability of breathing challenge apparatus, over the past few years the field has seen a surging interest to mapping cerebrovascular reactivity by combining BOLD MRI and hypercapnia. It is conceivable that, in the near future, CVR mapping may

become a new addition to the standard clinical MRI protocol in patients implicated with vascular-related diseases. However, before this promise can be fully exercised, mechanism of BOLD changes during CO_2 challenge need to be better understood. Although majority of the literature on CVR focuses on positive CVR or increase of MRI signal with CO_2 inhalation, negative CVR or a decrease in MRI signal intensity in the brain have also been reported. Negative CVR was reported in Moyamoya disease [6, 7] and other types of steno-occlusive diseases [4]. These results were interpreted as "vascular steal" or blood being stolen by the unaffected hemisphere or region as suggested by earlier studies that made measurements of CBF. The steal phenomenon was hypothesized to be present in the healthy brain, causing a negative CVR in the white matter when adjacent blood vessels in the gray matter dilate in response to CO_2 [20]. The exact mechanism for the negative CVR is still unclear. Chapter 2 focuses on performing a series of systematic studies to understand the physiological mechanism of negative CVR. This research will impact future interpretations of negative CVR findings. BOLD scan with CO_2 inhalation was recommended to guide intervention studies on the use of hypercapnia and hypocapnia to improve outcome of cerebral ischemia patients. For example if negative CVR is seen in an ischemic region in a BOLD scan with hypecapnia (increased level of CO_2) inhalation, the recommended intervention is hypocapnia or hyperventilation with the understanding that hypocapnia will prevent blood from being stolen by the unaffected hemisphere and bring blood to the ischemic regions. This intervention may be guided by the wrong interpretation of negative CVR results. We hypothesize that blood volume increase in CSF rich regions is the cause of negative CVR, with the blood volume increase usually caused by vaso-dilation. This indicates that the vasculature in the regions that show negative CVR are capable of dilating, but it is incorrectly interpreted as vascular steal from the contralateral hemisphere. If our

hypothesis is correct, then this research will change the planning of intervention studies to improve patient outcome.

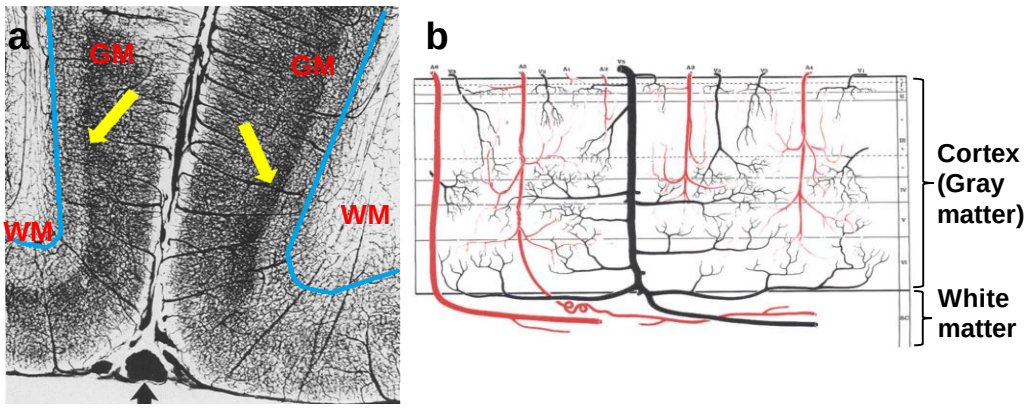

Figure 1-1: (From Duvernoy et al. 1981); Arteries and veins of the GM and WM. (a) Ink labeled vascular network in human striate cortex illustrating reduced vasculature from GM to WM. Layer IV of GM has highest vascular density (yellow arrows). GM and WM boundary is indicated in blue lines. (b) Illustration of arteries (red color) and veins (black) traversing the brain GM and WM tissue space. The arteries originate from the cortical surface. Some arteries penetrate GM, but exclusively supply blood to WM, others perfuse both GM and WM. Veins drain blood from both GM and WM.

1.1.2 Vascular Reactivity in the Brain White Matter

Structural studies using T_2-w, DTI, and magnetization transfer imaging have revealed a wealth of information about the brain's white matter (WM) and its alteration due to aging and diseases. However, physiological properties of WM are still poorly understood, primarily because WM contains 70-75% less vasculature compared to GM [21], as shown in Figure 1-1a, resulting in a considerably lower signal to noise ratio (SNR). Recent technical advances in several methodologies have provided the potential to examine vascular physiology in the WM; specifically baseline CBF in WM can now be reliably estimated [22]. The goal of Chapter 3 is to examine cerebrovascular reactivity in WM microvasculature, which indicates its ability to dilate. CVR is well understood in the GM, but little is known about its characteristics in the WM. Note that vascular deficits in

the WM may be responsible for many abnormalities observed on structural MRI (e.g. WM hyper-intensity, FA decrease) [20], and often precede these structural changes. Characterization of WM CVR will provide new insights into the mechanisms of ischemic and inflammatory responses in the WM, particularly in diseases such as multiple sclerosis [23] and stroke [4]. The knowledge of WM CVR may also improve our understanding of auto-regulatory capacity of vasculature in WM. In Chapter 3, we will use CO_2 inhalation along with BOLD acquisition to determine CVR in the WM and compare it to that in GM. WM CVR response will be examined in the context of both magnitude and temporal characteristics. Effect of aging on these parameters will also be examined by including a group of older and younger participants.

1.1.3 Vascular Response in WM Fiber Tracts, Lobes and Layers to O_2 and CO_2

Neuroanatomical studies have shown that WM contains ordered vascular networks that originate from the cortical surface, penetrate the cortical GM ribbon to reach WM [24] (Figure 1-1). Yet there is a lot more to be learnt regarding WM vasculature, specifically the mechanism of vascular reactivity to CO_2 in WM and its response to O_2 gas. Lately, baseline cerebral blood flow to major fiber tracts in WM was measured, and CBF in these tracts was also found to correlate negatively with fractional anisotropy (structural marker) [25]. This study suggests that individual fiber tracts may have their own blood supply. Chapter 4 will also shed light on WM vascular physiology, but in this research we are interested in studying the vascular response in WM to inhalation of both O_2 and CO_2 gas. Inhalation of O_2 is known to cause minimal vaso-dilation [26, 27]; the O_2 gas acts as a contrast agent and thus may reflect the blood volume. Thus studying the response of vasculature to O_2 gas will provide details about the blood supply to the regions investigated. For a detailed explanation of the volume effect of O2, the reader can refer to section 4.1. A thorough examination of the WM was

performed in Chapter 4; WM was classified into: major fiber tracts, cerebral lobes and multiple layers with increasing depth from the cortical surface. Chapter 4 to our knowledge is the first to measure vascular response on a tract by tract basis and to perform a thorough investigation in the WM. Knowledge of tract specific vascular response in healthy brain may be used as a marker for integrity of vascular function in fiber tracts and may predict impending structural abnormalities. Aside from improving our understanding of the dynamic properties of WM vascular physiology, this work can provide information about the distribution of vasculature in the WM, by examining the O_2 response. This research also has potential clinical relevance. As mentioned earlier, there are very few studies on WM physiology. Most clinical applications rely on anatomic or structural imaging techniques to provide insights on WM physiology. By demonstrating that vascular response of individual fiber tracts can be reliably measured, this study may find application in traumatic brain injury and pathological conditions like stroke, multiple sclerosis, Alzheimer's disease (AD) and mild cognitive impairment. A recent review article mentions that neurovascular dysfunction is the primary cause of cognitive decline and neurodegeneration in AD; neurovascular dysfunction is caused by atherosclerotic plaque buildup inside the lumen, thinning of smooth muscle layer, degeneration of endothelium and thickening of the basement membrane [28]. All these changes can lead to reduced CVR in vasculature. If these changes diminish the CVR of the fiber tracts in WM, then CVR measurement may help predict impending communication problems between brain regions connected by those tracts. Multiple sclerosis is a disease of the autoimmune system, which is characterized by degeneration of the myelin sheath that insulates the fiber tracts [29]; reduced CVR in WM fiber tracts may be an early predictor for WM lesions. Thus this technique of measuring CVR in WM tracts may be applicable in the study of these diseases.

1.1.4 Benefits of Life-Long Aerobic Exercise on Cerebrovascular Function

Benefits of physical exercise on cardiovascular fitness and cognitive functions are increasingly recognized by researchers and public [30-33]. Previous research has demonstrated parenchyma changes in the brain including preserved brain mass, structural integrity, and enhanced neural activity during task performance [34-36]. Efforts are now being directed toward understanding the mechanisms of such beneficial effects. Much of this alteration is thought to be caused by improvement in cerebrovascular function. However, the effect of physical exercise on vascular health in the brain has not been well characterized in humans and is the topic of this investigation. Benefits of short term (< 1 year) aerobic exercise on cerebrovascular health were reported, primarily in animals [37-39]. Chronic exercise in dogs was shown to increase endothelium derived relaxing factor (EDRF) and nitric oxide induced artery dilation [40], which may indicate improved vascular function. We are interested in studying the upper limit of benefits from exercise on cerebral vascular function in humans. We will compare a group of elderly Masters Athletes (MA) to a group of sedentary elders (SE). MA are individuals who represent a unique group of sample on the highest end of the fitness level spectrum. They participate in competitive sports at a very high level even at an age that exceeds the typical peak age for the event. Life-long exercise in MA may improve their vascular dilation capability when compared to SE. In Chapter 5 we will measure CVR to CO_2 inhalation and baseline cerebral blood flow in both MA and SE. To examine the effect of age on vascular function, a group of sedentary young controls (YC) will also be studied. Research has shown that as we age, baseline CBF decreases and so does cerebrovascular reactivity to CO_2; reduction in CVR is more prominent compared to the reduction in CBF [9]. This study will be of importance in aging research to evaluate if exercise can reverse some of the age related changes on cerebral vascular function. This

study may also aid future research on Alzherimer's disease, for example to examine if the diagnosis of AD can be reversed by prescribing aerobic exercise early on during the onset of the disease.

Chapter 2

Physiologic Underpinnings of Negative BOLD Cerebrovascular Reactivity in Brain Ventricles

2.1 Introduction

Cerebrovascular reactivity (CVR) refers to the ability of blood vessels to dilate such as in reaction to vasoactive agents. It is an important marker for vascular function, in particular the integrity of endothelium and smooth muscle in the vessel wall [1, 41]. The measurement of this physiologic parameter may therefore provide insights on brain vasculature beyond those from baseline cerebral blood flow (CBF) or cerebral blood volume (CBV), and may find applications in many brain disorders such as small vessel diseases [3], arteriovenous malformation [5], Moyamoya disease [6, 42], arterial stenosis [4], drug-addictive conditions [8], and normal aging [9]. It has also been shown that CVR can be used for normalization of fMRI signal [43-47] and evaluation of brain metabolism [12, 13].

CVR can be assessed by increasing the blood concentration of CO_2, a potent vasodilator, while monitoring vascular responses using MRI. While MRI techniques to measure CBF and CBV changes have been utilized [4, 12-16], the BOLD sequence is by far the most widely utilized acquisition technique due to its superior sensitivity (similar to the situation in the fMRI field). In the past few years, owing to the increasing availability of breathing challenge apparatus [17, 48, 49], the field has seen a surging interest in quantitative mapping of CVR [42, 50-53]. It is conceivable that in the near future, CVR mapping may become a new addition to the standard clinical MRI protocol. However, before this promise can be fulfilled, mechanism of BOLD changes during CO_2 inhalation challenge needs to be better understood.

Although the majority of CVR literature has focused on BOLD signal increases with CO_2, observations of negative CVR have also been noted. For example, negative CVR has been reported in Moyamoya Disease and other types of steno-occlusive diseases [4, 6, 7]. These findings were interpreted as a result of “vascular steal” by the unaffected hemisphere or regions, as suggested by earlier studies using direct CBF measurements (but see Brian 1998 for a review of alternative findings) [54]. The steal phenomenon was also hypothesized to be present in the healthy brain, causing a negative CVR in the white matter when adjacent blood vessels in the gray matter dilate in response to CO_2 [20]. On the other hand, Blockley et al. noted that the negative CVR was primarily observed in CSF-rich regions in the healthy brain [19]. At present, the exact mechanism of the apparently negative CVR remains unclear.

The goal of this study is to systematically address these questions in a series of three studies. In the first study, we demonstrated the presence of statistically significant clusters that showed apparently negative CVR during CO_2 inhalation and estimated their spatial distributions. In the second study, we used MR signal modeling and numerical simulations to qualitatively explain the observed signal in terms of a CBV increase that is accompanied by a CSF volume reduction during hypercapnia. Also included in the second study was a set of experiments using an inversion recovery (IR) EPI sequence, which allowed us to further test our hypothesis that these findings are attributed to a CBV effect rather than an oxygenation effect. We also studied BOLD responses to hyperoxia challenge to examine whether any negative clusters are present during O_2 inhalation. In a third study, we used Arterial-Spin-Labeling (ASL) MRI to quantitatively evaluate whether CBF increases or decreases in the ventricles.

2.2 Methods

2.2.1 General

Experiments were performed on a 3 Tesla MRI scanner using a 32-channel receive-only head coil (Philips Medical Systems, Best, The Netherlands). The body coil was used for RF transmission. The protocol was approved by the University of Texas Southwestern Medical Center's Institutional Review Board. Foam padding was placed around the head to minimize motion.

2.2.2 Study 1: Location of the Apparently Negative CVR in the Brain

Fourteen healthy volunteers (age 26±4 years, 9 males, 5 females) were scanned. CVR was measured with hypercapnia, in which participants inhaled 5% CO_2 gas, while BOLD MR images were simultaneously acquired. The details of the CVR measurement were described previously [17]. Briefly, during the CVR scan, subjects were fitted with a nose clip, and breathed room air and the prepared gas in an interleaved fashion (50 sec CO_2, 70 sec room air, repeated four times) through a mouthpiece. The prepared gas was a mixture of 5% CO_2, 74% N_2 and 21% O_2 contained within a Douglas bag. The gas was delivered to the subject through a two-way non-rebreathing valve and mouthpiece combination (Hans Rudolph, 2600 series, Shawnee, KS). A research assistant was inside the magnet room throughout the experiment to switch the valve and monitor the subject. BOLD MR images were acquired continuously during the entire experimental period. The end-tidal CO_2 (Et CO_2), the CO_2 concentration in the lung which approximates that in the arterial blood, was also recorded throughout the breathing task using a capnograph device (Capnogard, Model 1265, Novametrix Medical Systems, CT). The total duration for the CVR scan was 9 minutes. The BOLD sequence used following imaging parameters: TR = 1500ms, flip angle (FA) = 60°, field-of-view (FOV) = 220x220 mm^2, matrix = 64x64, 29 slices, thickness = 5mm, no gap between slices, 360 volumes. The

TE was chosen to be 30ms, which provides a balance between BOLD sensitivity and the number of slices acquired [55]. In addition, a T_1-weighted high-resolution image was acquired using the Magnetization-Prepared-Rapid-Acquisition-of-Gradient-Echo (MPRAGE) sequence (voxel size = 1x1x1mm^3, scan duration = 4 min).

Data analysis was conducted using the software Statistical Parametric Mapping (SPM), (University College London, UK) and in-house MATLAB (MathWorks, Natick, MA) scripts. Pre-processing of the BOLD images included motion correction, registration with T_1-weighted anatomic images, and normalization to Montreal-Neurological-Institute (MNI) template space, with a resolution of 2x2x2 mm^3.

The Et CO_2 time course, which is the input function to the vasculature, was shifted by a delay so that it is synchronized to the BOLD time course in terms of timing [17, 19]. This delay time was computed on a subject-by-subject basis using procedures reported previously [17] and it represents the time it takes for the blood to travel from the lung to the heart then to the brain.

For each subject, voxel-by-voxel analysis of General Linear Model (GLM) was performed in which the Et CO_2 time course was the independent variable and the BOLD time course was the dependent variable. This analysis provides a map of CVR in units of % per mmHg CO_2. Group-level one sample t test was then conducted to identify voxels with significantly negative CVR using a false-discovery-rate (FDR) corrected $p<0.05$. Averaged BOLD time course in these voxels was also obtained for each subject.

2.2.3 Study 2: Examination of the Mechanism of the Apparently Negative CVR

2.2.3.1 Modeling and Numerical Simulations

Having established the presence of a negative BOLD signal, next we sought to understand its underlying mechanism. We performed theoretical investigations by modeling of the BOLD signal. Numerical simulations were also conducted to provide an

estimation of the general characteristics of the signals. However, fitting of the experimental data to the model was not performed due to the limited number of experimental measures.

The theoretical investigations focused on the voxels showing negative CVR in Study 1, in this case the brain ventricles. For a typical voxel in the ventricle, we can model it using a two-compartment model consisting of CSF and blood, the BOLD signal of which can be written as:

$$S = f_{CSF} \cdot C_{CSF} \cdot M_{CSF,BOLD} \cdot e^{-TE/T_{2,CSF}^{*}} + (1 - f_{CSF}) \cdot C_{blood} \cdot M_{blood,BOLD} \cdot e^{-TE/T_{2,blood}^{*}} \quad (1)$$

where f_{CSF} and $1 - f_{CSF}$ are the volume fractions of CSF and blood in the voxel, respectively. Note that it is assumed that MR signal in a ventricular voxel contains minimal contributions from parenchyma tissue (gray or white matter). C_{CSF} and C_{blood} are water density of CSF and blood. $M_{CSF,BOLD}$ and $M_{blood,BOLD}$ are terms related to T_1 relaxation, and in a BOLD sequence are given by:

$$M_{i,BOLD} = \frac{1 - e^{-TR/T_{1,i}}}{1 - \cos(FA) \cdot e^{-TR/T_{1,i}}} \cdot \sin(FA) \quad (2)$$

in which i denotes either CSF or blood. A hypercapnia-induced signal decrease could be attributed to a reduction in the T_2^{*} terms in Equation (1). Alternatively, it could be attributed to a decrease in f_{CSF} as a consequence of possible dilation of blood vessels inside the ventricle. The latter mechanism becomes clear when we replace symbols in Equations (1) and (2) with realistic values. Based on the assumed parameter values in Table 2-1, Equation (1) under a BOLD EPI sequence can be written as:

$$S = f_{CSF} \cdot 0.39 + (1 - f_{CSF}) \cdot 0.29 \quad (3)$$

Table 2-1: Parameters used in the numerical simulations.

T_1 (ms)		T_2 (ms)		T_2^* (ms)		C (ml/ml)		TR (ms)		TE (ms)		TI (ms)	FA (°)	
CSF	Blood	CSF	Blood	CSF	Blood	CSF	Blood	BOLD	IR	BOLD	IR	IR	BOLD	IR
4163[a]	1624[d]	2000[b]	73.8[e]	1082.5[c]	44.2[e]	1[b]	0.87[b]	1500	7000	30	25	2500	60	90

[a][56]

[b][57]

[c][58]

[d][59]

[e][60]

In effect, Equation (3) states that unit-volume CSF signal is greater than unit-volume blood signal, which can be also appreciated by the bright ventricular signal in the BOLD image itself (Figure 2-1c). Thus, a reduction in CSF partial volume (replaced by blood volume) can result in an overall signal reduction in the voxel. Numerical simulations were performed using Equation (3) for a range of f_{CSF} values under normcapnic and hypercapnic states.

To specifically test the f_{CSF} mechanisms, we further model the MR signal under a different pulse sequence, an inversion recovery (IR) EPI sequence. In the IR sequence, the signal in the ventricle (consisting of CSF and blood compartments) can be written as:

$$S = f_{CSF} \cdot C_{CSF} \cdot M_{CSF,IR} \cdot e^{-TE/T_{2,CSF}} + (1 - f_{CSF}) \cdot C_{blood} \cdot M_{blood,IR} \cdot e^{-TE/T_{2,blood}} \quad (4)$$

where the M terms in Equation (4) is given by:

$$M_{i,IR} = \frac{1-2e^{-TI/T_{1,i}}+e^{-TR/T_{1,i}}}{1+e^{-TR/T_{1,i}}\cdot\cos(FA)\cdot}\cdot\sin(FA) \quad (5)$$

Using assumed parameters listed in Table 2-1, the signal equation becomes:

$$S = f_{CSF}\cdot 0.09 + (1-f_{CSF})\cdot 0.36 \quad (6)$$

which indicates that unit-volume CSF signal is lower than unit-volume blood signal. Therefore, if f_{CSF} reduction is the primary mechanism, a signal increase should now be observed.

2.2.3.2 Experiments to Test the Theoretical Predictions

Ten healthy volunteers (age = 27±5 years, 5 males, 5 females) were scanned in Study 2. The IR sequence used TR/TI = 7000/2500ms, FA = 90°, FOV = 220x220 mm^2, matrix = 64x64, 20 slices, thickness = 5mm. To facilitate the detection of the volume effect (which is our hypothesized mechanism), a spin-echo (SE) EPI was used so that the oxygenation effect is reduced, compared to gradient-echo EPI [61]. We used an empirical TR/TI combination such that CSF was not completely nulled, but instead was suppressed to about 9% of equilibrium. This was to ensure that SNR in the ventricle was still sufficiently high. The hypercapnia paradigm was similar to that of Study 1 (50 sec CO_2 interleaved with 70 sec room air), except that five cycles were used and the total duration was 11 min. This longer duration can increase the sensitivity of the data, partly offsetting the SNR penalty as a result of long TR (7000ms) used. Note that, even with the longer duration, the total number of volumes acquired in the IR-EPI scan was only 95.

In addition to the IR-EPI scan, a BOLD EPI scan was also performed to delineate the negative CVR voxels in this new cohort and to reproduce the results found in Study 1. The hypercapnia timing and imaging parameters of the BOLD EPI were identical to those

used in Study 1, except that the number of slices was 20 to match that of IR-EPI and TR was 1 sec (minimum time to acquire 20 slices).

To further confirm that the apparently negative CVR observed during CO_2 inhalation was attributed to vasodilation, we also performed the BOLD sequence under another physiologic challenge, inhalation of 98% O_2 (supplemented by 2% CO_2 to maintain a constant Et CO_2 level in the presence of slight hyperventilation by the subject). Hyperoxia was previously shown by some studies [26, 27] to cause minimal vasodilation (but see [62] for alternative findings). We hypothesized that negative BOLD-CVR should not be seen with the O_2 challenge. The imaging parameters for the O_2 challenge were the same as those used for the hypercapnia BOLD-EPI in Study 2. End-tidal O_2 (Et O_2) was measured using an O_2 sensor (Analox Sensor Technology, North Yorkshire) in addition to the physiologic parameters monitored during the CO_2 challenge.

Data analysis for the BOLD hypercapnia data was identical to that of Study 1 and a CVR map was generated. Similarly, an IR-CVR map was calculated by a GLM analysis between the Et-CO_2 time course and the IR-EPI time course. A one-sample t test was performed on the group-level CVR map to identify any clusters with apparently negative CVR and this analysis was carried out for BOLD-CVR and IR-CVR maps separately. If a negative cluster is detected on the group level analysis in one map (e.g. BOLD-CVR map), it is saved as a mask and applied to the other map (e.g. IR-CVR map) to examine how these voxels behaved when using a different pulse sequence.

For the hyperoxia BOLD data, a GLM analysis was performed between the Et-O_2 time course and the BOLD time course, resulting in a map of O_2 response in units of % per mmHg O_2. One sample t test was performed to detect any negative clusters on a group level.

2.2.4 Study 3: Assessment of Blood Flow Changes in the Ventricle

Experiments in Study 2 investigated whether f_{CSF} reduction is an important cause of the apparently negative CVR in the BOLD hypercapnia data. However, possible changes in oxygenation (therefore T_2^*) were not investigated. Assuming that blood oxygenation and flow are coupled in the ventricles, we examined CBF in the brain ventricles during room air and during CO_2 inhalation.

The data for this study were collected as part of a previous report [63]. However, the analysis of CBF in the ventricle is new and was not performed in the previous report. Eight young healthy normal volunteers (age 29±7 years, 6 males, 2 females) were scanned. CBF was measured twice in the same scan session, first when the subject was breathing room air and then during CO_2 breathing. Each CBF measurement lasted for approximately 5 minutes and included a Pseudo-continuous Arterial-Spin-Labeling (PCASL) MRI (4.5 min) and a phase-contrast MRI (0.5 min). The purpose of the phase-contrast MRI, which provides a global but quantitative evaluation of CBF, is to account for potential variations in the labeling efficiency of PCASL across physiologic states and across subjects [63]. Imaging parameters for the PCASL sequence were: single-shot gradient-echo EPI, TR/TE = 4020/14ms, FOV = 240x240 mm^2, matrix = 80x80, voxel size = 3x3 mm^2, 27 slices acquired in ascending order, slice thickness = 5mm, no gap between slices, labeling duration = 1650ms, post labeling delay = 1525ms, interval between consecutive slice acquisitions = 35.5 ms, number of control/label scans = 30 pairs, scan duration 4.5 minutes. The phase-contrast scan was performed at the level of 3^{rd} cervical spine, placed perpendicular to the internal carotid and vertebral arteries. Other imaging parameters were: TR/TE = 20/7ms, FA=15°, thickness = 5 mm, maximum arterial blood velocity encoding = 80cm/sec, and scan duration = 30 sec.

Voxel-by-voxel maps of CBF were obtained using procedures described previously [63]. One sample t test was performed to detect any clusters with a negative CBF change due to hypercapnia. Furthermore, the masks of negative BOLD-CVR voxels delineated in Study 1 and 2 were applied to the CBF data to estimate CBF values during normocapnia and hypercapnia in these regions.

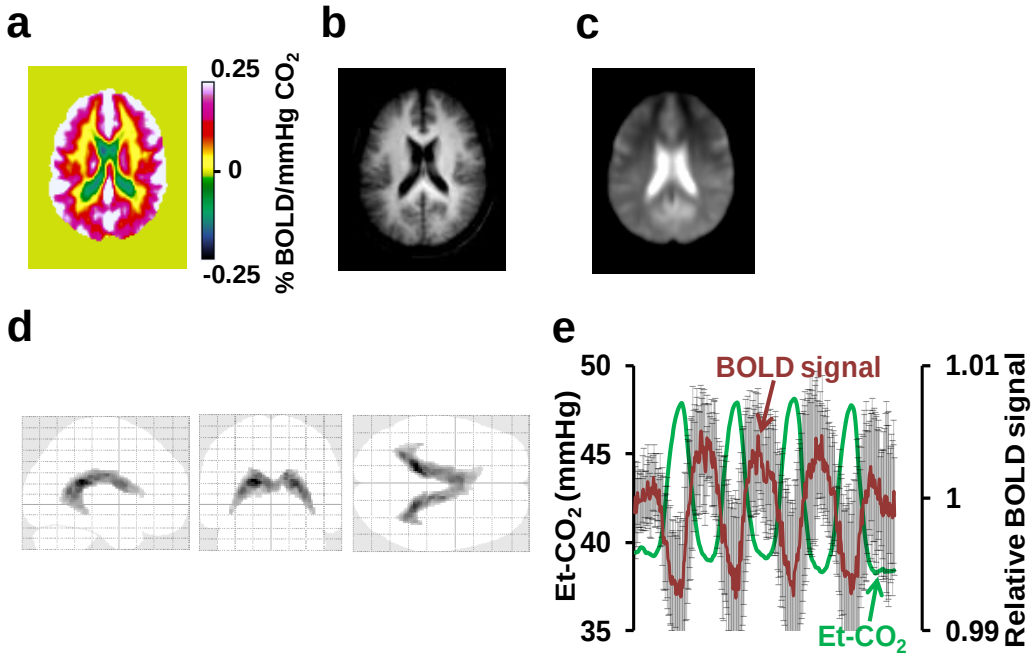

Figure 2-1: Summary of BOLD-CVR results from Study 1. (a) Group-averaged CVR map (N=14) in a representative slice (z=47 in MNI template) illustrating regions with apparently negative CVR values (cold color). The unit of BOLD-CVR is percent BOLD signal change per mmHg change in Et-CO_2. (b) and (c) show corresponding T_1-weighted and BOLD EPI images, respectively, to provide anatomic references. The image in (c) also demonstrates the intense signals in the ventricular regions, compared to brain parenchyma. (d) Voxels with significantly negative CVR (FDR corrected $p<0.05$) using group-level one-sample Student's t tests. (e) Averaged BOLD time course (red) from the voxels in (d) and the corresponding Et-CO_2 (green). Error bars indicate standard deviations of the BOLD signal across subjects.

2.3 Results

2.3.1 Study 1

Table 2-2 shows Et CO_2 values during normocapnia and hypercapnia. Group-averaged CVR map from the CO_2 BOLD experiment is shown in Figure 2-1a. The color scale is such that positive CVR is shown in warm color whereas negative CVR, if present, is shown in cold color. As expected, brain parenchyma mostly manifests positive CVR. However, a region that shows negative CVR can be clearly seen. Figure 2-1b and Figure 2-1c show the averaged MPRAGE and BOLD EPI images, respectively, to provide an anatomic reference. It is apparent that the negative CVR voxels are mainly located in the ventricle regions. Figure 2-1d shows the results of one sample t test of the CVR maps, confirming the presence of statistically negative clusters (total volume 20.4 cm^3). Applying CSF probability map obtained from segmentation of the MPRAGE image, we found that the voxels identified in Figure 2-1d had a CSF probability of 0.77±0.10 (mean±SD). Average BOLD time course of these voxels averaged over all subjects and the corresponding Et CO_2 time course are plotted in Figure 2-1e. The BOLD signal change was -0.51±0.44% in these voxels.

Table 2-2: Summary of end-tidal (Et) CO2 and O2 parameters during the physiologic maneuvers. All values are written in units of mmHg.

Study 1		Study 2						Study 3	
BOLD Hypercapnia		BOLD Hypercapnia		IR Hypercapnia		BOLD Hyperoxia		PCASL Hypercapnia	
Room air Et-CO_2	5% CO_2 Et-CO_2	Room air Et-CO_2	5% CO_2 Et-CO_2	Room air Et-CO_2	5% CO_2 Et-CO_2	Room air Et-O_2	98% O_2 Et-O_2	Room air Et-CO_2	5% CO_2 Et-CO_2
40±4	49±3	41±2	49±2	40±2	49±2	121±4	664±21	40±4	49±2

$p<0.001$ for all comparisons between the room air and the CO_2/O_2 gas mixture.

2.3.2 Study 2

Group-averaged CVR map from the CO_2 BOLD experiment is shown in Figure 2-2a. Again, positive CVR is displayed in warm color and negative CVR is shown in cold color. These results reproduced findings in Study 1. That is, while the majority of voxels showed a positive CVR to CO_2 inhalation, an area in the ventricles showed a statistically significant negative response (Figure 2-2b). Due to a smaller sample size used (N=10), the volume of the clusters (6.9 cm^3) was smaller than that of Study 1, but the location is again primarily in the ventricles (CSF probability = 0.76±0.08).

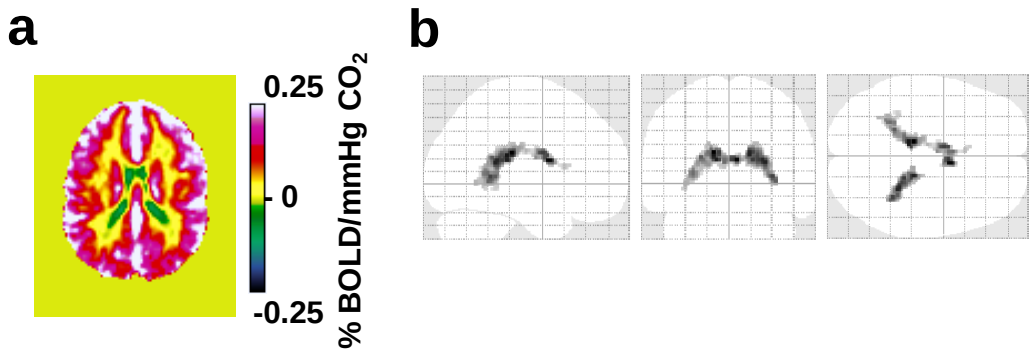

Figure 2-2: BOLD-CVR response to hypercapnia from data in Study 2. (a) Group-averaged CVR map (N=10) in a representative slice (z=47 in MNI template) illustrating regions with apparently negative CVR values (cold color). (b) Voxels with significantly negative CVR (FDR corrected p<0.05) as detected from the BOLD hypercapnia data in Study 2.

The image from the IR-EPI experiment (Figure 2-3a) shows that the CSF signal is effectively suppressed (ventricles appear dark compared to surrounding tissue). CSF signal was not completely nulled, but maintained at about 9% of the equilibrium signal to assure sufficient SNR within the ventricle. Figure 2-3b shows the averaged IR-CVR map (N=10), which reveals positive CVR in the ventricles. When examining the IR-EPI time course (red curve, Figure 2-3c) in voxels that manifested a negative signal change in the

BOLD hypercapnia experiment (i.e. voxels in Figure 2-2b), a positive correlation (cc = 0.60±0.12, p<0.001, N = 10) with the Et CO_2 time course (green curve, Figure 2-3c) is now observed. The IR-EPI signal change was 0.66±0.25% in these voxels. We were not able to identify any clusters with negative signal change when the IR-EPI sequence was used. These data suggest that CSF volume reduction as a consequence of blood volume increase is a major physiological response in brain ventricles during hypercapnia challenge, and appears to be responsible for the observation of the apparently negative CVR when using the BOLD sequence.

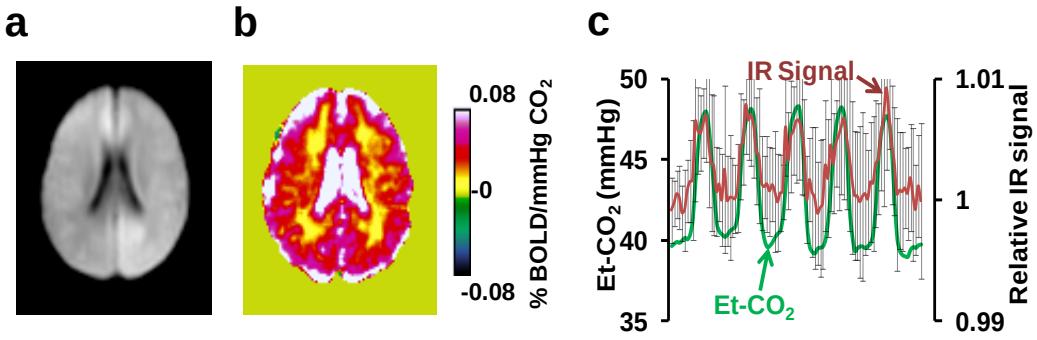

Figure 2-3: Results of IR EPI experiment in Study 2. (a) Representative image using the IR EPI sequence, illustrating the suppressed CSF signal. (b) Group-averaged IR-CVR map (N=10). Shown here is the same slice as in Figure 2-1 (i.e. z=47 in MNI template). No regions manifested a negative response. (c) Averaged IR signal time course from the voxels depicted in Figure 2-2b and the corresponding Et-CO_2. Error bars indicate standard deviations of the IR signal across subjects.

Et O_2 values during hyperoxia are listed in Table 2-2. Figure 2-4 shows the results of the hyperoxia experiment, which is known to alter oxygenation (like the CO_2 challenge) but thought to not cause vasodilatation (different from the CO_2 challenge). No voxels showed a negative signal change in the response map (Figure 2-4b). Even in the voxels manifesting a negative BOLD response to CO_2 inhalation (voxels in Figure 2-2b), the time course now shows a positive change with the O_2 challenge (Figure 2-4c). These

data suggest that vasodilatation is necessary in order to observe a negative BOLD response, again supporting the volume change as a mechanism for the apparently negative CVR in the CO_2 experiment. In the hyperoxia experiment, Et CO_2 showed a negligible difference between normoxia (38±2 mmHg, mean±SD) and hyperoxia (38±2 mmHg) periods.

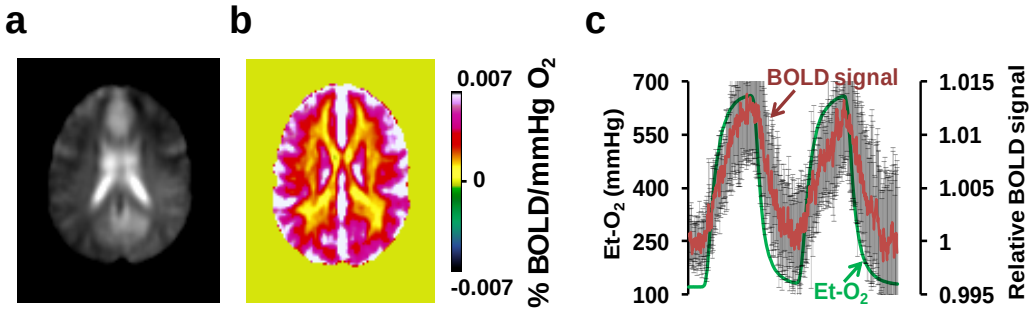

Figure 2-4: Results of BOLD responses to hyperoxia. (a) Representative BOLD image acquired during the hyperoxia scan for anatomical reference. (b) Group-averaged (N=10) map of BOLD responses to inhalation of 98% O_2. The unit of the map is percent BOLD signal change per mmHg change in Et-O_2. (c) Averaged BOLD time course from the voxels depicted in Figure 2-2b and the corresponding Et-O_2. Error bars indicate standard deviations of the BOLD signal across subjects.

2.3.3 Study 3

Whole-brain CBF changed from 45±9ml/100g/min during normoxia to 70±14ml/100g/min during hypercapnia, an increase of 58±24%. When applying the mask of negative-CVR voxels delineated in Study 1 (Figure 2-1d) to these CBF data, average CBF showed a significant (paired t test, p = 0.025, N = 8) change from a normocapnic value of 15±8ml/100g/min to a hypercapnia value of 22±7ml/100g/min, an increase by 49%. For the negative-CVR voxels delineated in Study 2 (Figure 2-2b), a similar finding was observed, with a normocapnic CBF of 16±9ml/100g/min and a hypercapnic value of 24±10ml/100g/min (paired t test, p = 0.021). Therefore, it appears that CBF in the ventricular regions increased during hypercapnia. Assuming a coupled relationship

between blood flow and oxygenation [64], it is most plausible that blood oxygenation also increases, unless oxygen metabolic rate would increase more than that of CBF in the ventricles, which has not been reported in the literature.

2.3.4 Simulation

By simulating the MR signal under normocapnic and hypercapnic states using Equation (3), one can calculate the BOLD response, $(S_{hypercapnia} - S_{normocapnia}) / S_{normocapnia}$, as a function of $f_{CSF,normocapnia}$ and Δf_{CSF} ($= f_{CSF,hypercapnia} - f_{CSF,normocapnia}$), which is shown in Figure 2-5a. It is apparent that a small f_{CSF} change of 0.01-0.02 (absolute value) is sufficient to cause the observed negative BOLD response in the ventricle during hypercapnia. Similar simulation was performed for the IR-EPI sequence using Equation (6), and the results are shown in Figure 2-5b. As expected, a f_{CSF} decrease results in a signal increase using this pulse sequence.

We point out that the purpose of the simulation is to demonstrate a qualitative correspondence between the theoretical expectations and the experimental findings. An exact matching of the response amplitudes or fitting of the data to the model was not possible, due to the limited number of experimental measures and the large number of unknowns (i.e. $f_{CSF,normocapnia}$ and Δf_{CSF}, but also T_1 and T_2 values of the various spin compartments). Also note that possible T_2 or T_2^* changes in the ventricular space during hypercapnia were not accounted for in the simulations.

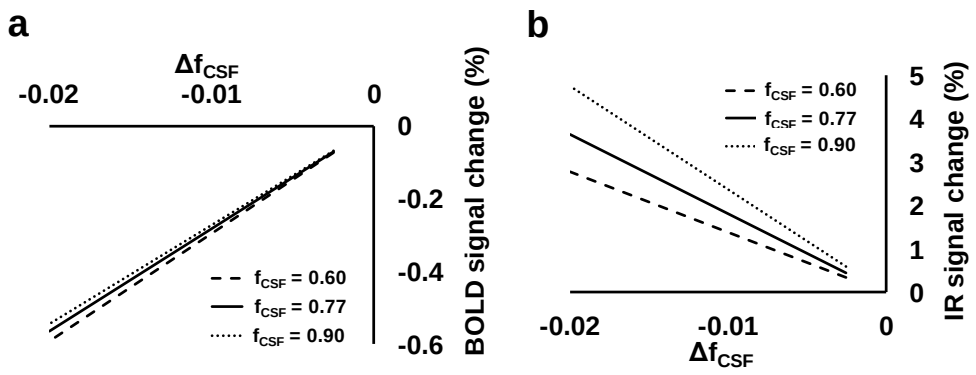

Figure 2-5: Results from numerical simulations using Equations [3] and [6]. (a) BOLD signal change as a function of baseline CSF fraction, $f_{CSF,normocapnia}$, and hypercapnia-induced reduction in CSF fraction, Δf_{CSF} ($= f_{CSF,hypercapnia} - f_{CSF,normocapnia}$). The results are shown in a series of 2D profiles at $f_{CSF,normocapnia}$ of 0.60, 0.77, and 0.90. Note that 0.77 is the CSF probability of the significantly negative voxels according to our experimental data. (b) IR signal change as a function of $f_{CSF,normocapnia}$ and Δf_{CSF}.

2.4 Discussion

In the present work, we report an intriguing but robust observation of apparently negative CVR in response to CO_2 inhalation, which is primarily located in brain ventricles. This finding appears to be associated with CSF volume reduction as a consequence of blood volume increase. CSF has a hyperintensive signal in BOLD image due to greater water density and longer T_2^*. Thus, a reduction in CSF volume would result in an apparent decrease in BOLD signal. When the CSF signal was made dark with an IR EPI sequence, the opposite signal change was observed. The volume-origin of the observation was further verified by the absence of the negative response when using an O_2 challenge, which has a similar effect to CO_2 in terms of blood oxygenation but is thought to have no vasodilatory effect. Absolute measurement of blood oxygenation in

the ventricular vessels is technologically difficult at present, but CBF assessment suggested that their oxygenation levels should increase rather than decrease.

Cerebrovascular reactivity to CO_2 reflects the ability of the brain vasculature to dynamically regulate blood supply and is a more direct measure of vascular endothelium and smooth muscle function, compared to baseline CBF. The majority of BOLD-CVR literature has focused on the positive BOLD response upon hypercapnia, as should be expected from the vasodilatory effects of CO_2 in healthy brain. Earlier work of Blockley et al. suggested an apparently negative CVR when using the BOLD sequence [19]. However, the small sample size used did not allow a statistical evaluation of the location and extent of the negative voxels. In the present work, we conducted a systematic study to establish the presence and potential physiological mechanism of this effect. Another study by Mandell et al. suggested that white matter regions that tend to have hyperintensities later in life (e.g. periventricular white matter) showed some negative CVR at young age [20]. However, since these authors specifically masked out the ventricles and only examined brain parenchyma, it is not possible to assess whether these negative CVR values could be attributed to a "spillover" of the ventricle voxels. Note that, in the present study, all voxels in the brain were examined for negative responses.

Our results show that negative CVR is to be expected in brain ventricles when the BOLD sequence is used for image acquisition. The negative response, however, should not be interpreted as a sign of blood oxygenation decrease or vasoconstriction, but rather reflects a dilation of the ventricular vessels decreasing the relative proportion of CSF per unit volume. Thus, this observation is a CBV effect, in some sense similar to the VASO effect [65]. In the brain parenchyma, CBV increase in the voxel is largely accommodated by a volume reduction in tissue. In the ventricle, on the other hand, it seems that CBV increase is achieved at the expense of CSF volume, as there is no brain

tissue surrounding the vessels in the ventricles. We note that several previous studies have suggested a possible CSF volume reduction even in the brain parenchyma, when the blood vessels dilate due to neural activation [66] or hypercapnia challenge [67]. Some investigators estimated that this effect is sizable while others reported that it is relatively small [68]. In the present work, the negative BOLD CVR clusters were found exclusively in the ventricular regions in both Study 1 and Study 2, suggesting that parenchymal CSF volume did not decrease significantly in healthy brain. Similarly, in the IR CO_2 data, we did not observe any negative clusters in the cortex, indicating that parenchymal CSF volume did not increase significantly either. Thus it is most plausible that, during hypercapnia, CSF in the ventricle was partially displaced to the spinal space [69].

The findings from the present study have several implications for clinical applications of the CO_2 modulation techniques. Both hypercapnia and hypocapnia have been proposed as an intervention to improve the outcomes of cerebral ischemia (see [54] for a review). The researchers proposing hypercapnia reason that inhalation of CO_2 would increase the blood supply to the ischemia regions, thus would benefit the ischemic regions [70]. However, other researchers argue that vessels in ischemic regions cannot be further dilated by hypercapnia and, when the surrounding normal vessels dilate in response to CO_2, the blood flow to the ischemic brain may actually decrease, often referred to as a vascular steal phenomenon [54]. Under these situations, a hypocapnic intervention is actually proposed. Therefore, the management of individual patient may be dependent on whether a vascular steal is identified in the ischemic regions. Due to the advantages of BOLD CVR mapping techniques mentioned earlier, a few investigators have proposed and demonstrated the possibility of using negative BOLD CVR to identify vascular steal in Moyamoya and other steno-occlusive diseases [4, 6, 7]. The results from the present study suggest that negative CVR could also be due to CBV increase in

CSF-rich regions. This possible interpretation should be considered for regions with prior infarct or edema, which usually contain a large amount of fluid.

The results from the present study also have implications for vascular physiology in brain ventricle. As can be seen in Figure 2-1d, the voxels with apparently negative CVR are located in the lateral ventricles. However, they do not cover all divisions of the lateral ventricles. Specifically, a careful review by an experienced neuroradiologist (K.K.) suggested that the frontal horns of the lateral ventricle contain no voxels with apparently negative CVR. This is consistent with the well-documented observations that the frontal horns do not have choroid plexus, the primary form of blood vessels in the ventricle [71]. Another important finding is that the choroid plexus does indeed undergo vasodilation. The choroid plexus themselves do not contain smooth muscles [72] and it was unknown whether they are capable of dilating. This has important clinical and physiological implications since hypocapnia is used clinically to acutely reduce intracranial pressure [73, 74].

The anti-correlation between ventricular and parenchymal BOLD responses during hypercapnia may also have important implications in resting-state fMRI (rs-fMRI) analysis strategies. It has been suggested that certain fluctuations in rs-fMRI data are attributed to respiratory variations with time and that the regression of these physiological fluctuations from the rs-fMRI data is useful in removing this nuisance effect [75-77]. Recent investigations reported interesting observations that such fluctuations in visual cortex and ventricles are opposite in phase [78]. The findings from the present study support the notion that the effect of P_aCO_2 fluctuation in the cortex is dominated by oxygenation effect whereas in the ventricle the effect is mainly driven by blood/CSF volume changes, which results in a signal change opposite in sign. Bright et al. also

reported that, during hypocapnia, cortical and ventricular BOLD time courses are anti-correlated [79].

To reduce the volume effect so that BOLD-CVR can be predominantly sensitive to oxygenation effect, one needs to minimize the difference between the two numerical values in Equation [3]. Simulation suggested that an increase in the flip angle or a decrease in TR or TE in the BOLD sequence is useful for this purpose. For example, when using TR = 800ms, TE = 23ms, and flip angle of 60°, CSF and blood magnetizations per unit volume are approximately equal, thus a change in f_{CSF} is not expected to show any effect on the BOLD signal. However, such a protocol would reduce the spatial coverage of the scan and the sensitivity to T_2^* effect is also attenuated.

The findings from the present study need to be interpreted in view of a few limitations. First, this study has only examined the cerebrovascular reactivity using fixed CO_2 inhalation, but has not tested other types of vasodilatative challenges such as breath hold [80], injection of acetazolamide [81], prospective end-tidal targeting [49], or dynamic end-tidal forcing [48]. Thus, our results should be interpreted within the scope tested. In particular, the fixed CO_2 inhalation maneuver may have also altered the Et-O_2 level due to hyperventilation, although this effect is expected to be relatively small according to our previous testing (Et O_2 increased from 115mmHg to 137mmHg) [82]. Second, the present study did not directly test the possible contribution of CSF inflow or pulsation to the negative BOLD response. Increased CSF flow rate during hypercapnia could allow more saturated spins to enter the imaging slice, causing a signal decrease [19]. Our IR hypercapnia experiment provided some evidence that this effect is not a major factor as otherwise negative responses should still be observed in the IR data. However, a more direct study to measure CSF flow rate during hypercapnia would be more useful to address this issue. Third, when interpreting the hyperoxia-induced signal increase, we

have used the assumption that hyperoxia influences the BOLD signal only by the oxygenation effect, but did not consider the potential T_1 shortening effect of dissolved oxygen, which could also result in a signal increase. Thus, if this effect is present, the hyperoxia-induced signal change could be due to a combination of three contributions, including oxygenation (T_2^*) effect, partial volume effect, and T_1 effect. However, the characterization of this mechanism is beyond the scope of the present study. Finally, it should be kept in mind that, although hypercapnia is often assumed to be iso-metabolic and represent a purely vascular challenge, there is some evidence in the literature that suggests that brain activity and metabolism may be slightly suppressed during hypercapnia [82, 83]. The effect of reduced oxygen consumption in face of an enhanced blood supply could result in a BOLD response that is greater than the true vascular effect alone. Thus, the value of CVR may be over-estimated when using hypercapnia challenge in general. However, the vascular effect of CO_2 is still expected to be the predominant factor in the measured CVR, considering that each unit (mmHg) of increase in Et CO_2 results in about 6% increase in CBF, but only about 1.5% decrease in metabolic rate [82].

2.5 Conclusions

When using typical BOLD imaging parameters to study MR signal response to hypercapnia challenge, an apparently negative CVR should be expected in brain ventricles. The physiologic underpinning of this observation appears to be a reduction of CSF volume fraction as a consequence of blood vessel dilation, causing bright CSF signal being replaced by less intensive blood signal. As far as the blood oxygenation level of the ventricular vessels is concerned, measurement of CBF suggested that it most likely increased rather than decreased during hypercapnia.

Chapter 3

Cerebrovascular Reactivity in the Brain White Matter: Magnitude, Temporal Characteristics, and Age Effects

3.1 Introduction

White matter (WM) comprises about half of the brain and is composed of bundles of myelinated nerve cell processes that connect various brain regions to each other [84]. WM dysfunction is implicated in a number of neurological diseases such as stroke [85], Alzheimer's Disease [86], multiple sclerosis [87], and traumatic brain injury [88]. At present, imaging studies of WM diseases primarily rely on structural imaging techniques such as T_2-weighted MRI, Diffusion Tensor Imaging (DTI), and Magnetization Transfer (MT) imaging [89, 90]. Unfortunately, relatively little is known about the physiologic underpinnings that led to these alterations. Moreover, by the time structural changes can be detected, irreversible damage often has occurred and treatment options are limited. Physiologic changes usually takes place before structure is altered, thus imaging of physiologic parameters may provide an early marker for disease diagnosis and progression. The present study aims to examine vascular parameters in the brain WM.

Compared to the gray matter (GM), vascular physiology of WM is still poorly understood. This is primarily because WM contains 70-75% less vasculature compared to GM [21], resulting in a considerably lower signal to noise ratio (SNR) [91]. Recent technical advances in imaging methodologies have mitigated some of these challenges and have provided the potential to examine vascular physiology in the WM [22]. For example, it has been suggested that baseline cerebral blood flow (CBF) of WM can be quantitatively assessed with Arterial-Spin-Labeling (ASL) MRI on a region-by-region and tract-by-tract basis and that WM CBF is inversely correlated with diffusion fractional anisotropy [22, 25]. The present study is focused on the examination of another important

property of microvasculature: its ability to dilate upon stimulation. This physiological property, referred to as Cerebrovascular Reactivity (CVR) [17, 92, 93], is a critical function of healthy blood vasculature [92, 93]. In the GM, this index has been measured using breath-hold [94-98], pharmacological challenge with acetazolamide [81], and inhalation of CO_2 [17, 48, 97], and is of great importance in functional MRI and its quantitative interpretation [13, 99-103]. To date, CVR in the WM has not been studied systematically. Characterization of WM CVR may provide new insights into the mechanisms of ischemic and inflammatory responses in the WM, in particular in diseases such as, multiple sclerosis [23] and stroke [4]. The knowledge of CVR may also improve our understanding of autoregulatory capacity of vasculature in the WM.

In the present study, we determined CVR by using CO_2 inhalation as a vaso-dilatory challenge and measured blood-oxygenation-level-dependent (BOLD) signal changes during this physiologic maneuver. WM CVR responses were examined in the context of both magnitude and temporal features. The most striking observation was that WM response to CO_2 inhalation was considerably delayed compared to that in the GM, and this was interpreted as the time it takes for the extravascular CO_2 to build up and reach a new steady state. The effect of age on these parameters was investigated by comparing WM CVR between younger and older participants. For comparison, baseline CBF in WM was also measured with ASL in these participants.

3.2 Methods

3.2.1 Participants

This study was approved by the Institutional Review Board of the University of Texas Southwestern Medical Center and the University of Texas at Dallas. All subjects gave informed written consent before participation. Fifteen younger (age = 27±1.4 years, range = 20-35 years, 5 males and 10 females) and fifteen older (age = 75±2 years, range

= 62-86 years, 8 males and 7 females) subjects were examined. Participants were recruited through flyers and advertisements in the local media. All participants recruited underwent extensive health screening and had no contra-indications to MRI scanning (pacemaker, implanted metallic objects, and claustrophobia) and were generally in good health, with no serious or unstable medical conditions such as neurological disease, brain injury, uncontrollable shaking, past bypass surgery or chemotherapy, or use of medications that affect cognitive function. All participants had a Mini-Mental-State-Exam (MMSE) [104] score of 26 or greater.

3.2.2 Experimental Procedures

Experiments were performed on a 3 Tesla MRI scanner using an 8-channel receive-only head coil (Philips Medical Systems, Best, The Netherlands). The body coil was used for RF transmission. Foam padding was placed around the head to minimize motion during MRI scan acquisition.

CVR was measured with a hypercapnia challenge, in which participants inhaled 5% CO_2 gas while BOLD MR images were simultaneously acquired. The details of the CVR measurement were described previously [17]. Briefly, during the CVR scan, subjects were fitted with a nose clip, and breathed room air and the prepared gas in an interleaved fashion (60 sec CO_2, 60 sec room air, repeated three times) through a mouthpiece. The prepared gas was a mixture of 5% CO_2, 74% N_2 and 21% O_2 contained within a Douglas bag. The gas was delivered to the subject through a two-way non-rebreathing valve and mouthpiece combination (Hans Rudolph, 2600 series, Shawnee, KS). A research assistant was inside the magnet room throughout the experiment to switch the valve and monitor the subject. BOLD MR images were acquired continuously during the entire experimental period. The end-tidal CO_2 (Et CO_2), the CO_2 concentration in the lung which approximates that in the arterial blood, was also recorded throughout

the breathing task using a capnograph device (Capnogard, Model 1265, Novametrix Medical Systems, CT). The total duration for the CVR scan was 7 minutes. The BOLD sequence used the following imaging parameters: single-shot EPI, field-of-view (FOV) = 220×220 mm^2, matrix size = 64×64, 43 axial slices, thickness = 3.5 mm, no gap, TR/TE/flip angle = 2000 ms/25ms/80˚, and 210 volumes.

Baseline CBF was measured using a Pseudo-continuous Arterial-Spin-Labeling (PCASL) sequence, which has been shown to provide an improved sensitivity compared to previous ASL methods [105, 106]. Scan parameters were: pseudo-continuous labeling with a labeling duration of 1.65s, post-label delay = 1.525s, labeling RF duration = 0.5 ms, pause between RF pulses = 0.5 ms, labeling pulse flip angle = 18°, single-shot EPI, FOV = 240×240 mm^2, matrix = 80×80, 27 axial slices, thickness = 5mm, TR/TE = 4020ms/14ms, 30 pairs of label and control images, duration = 4 minutes.

In addition, a T_1-weighted high-resolution image was acquired using the Magnetization-Prepared-Rapid-Acquisition-of-Gradient-Echo (MPRAGE) sequence (voxel size = 1×1×1mm^3, scan duration = 4 minutes).

3.2.3 Data Processing

CVR data were analyzed using the software Statistical Parametric Mapping (SPM), (University College London, UK) and in-house MATLAB (MathWorks, Natick, MA) scripts [17]. Pre-processing of the BOLD images included motion correction and registration with T_1-weighted anatomic images. The data were analyzed in individual space. This is because spatial normalization to standard space usually results in smoothing of the image, which could increase the partial voluming effect of gray matter on white matter regions-of-interest (ROIs).

Quantitative analyses of the data have primarily focused on the ROI results as they are more reliable than voxel-wise results in the WM. The WM ROI was defined using following two steps in order to minimize GM contribution (

Figure 3-1).

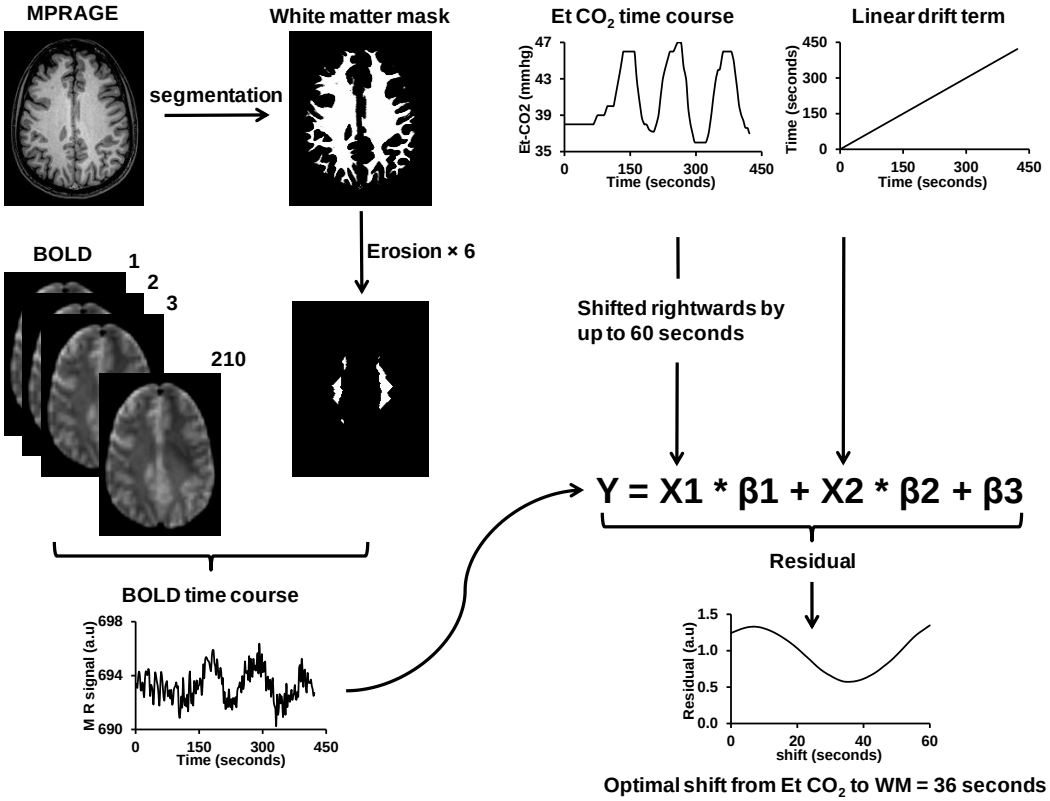

Figure 3-1: Illustration of analysis steps for the quantification of WM CVR and delay time. Upper left: MPRAGE T_1 weighted image is segmented using SPM5 to obtain a mask of white matter (voxels with >90% WM probability). To further reduce the likelihood of GM partial volume, the mask is eroded three-dimensionally by 6 times. Thus the final mask is considerably small, but is expected to contain minimal GM contribution. The final mask is then applied on the BOLD image series to obtain a BOLD time course in the WM, which is used as the dependent variable in the linear regression analysis. Upper right: End-tidal (Et) CO_2 time course and a linear drift term are used as independent variables in the linear regression analysis. To identify the optimal delay time, the Et CO_2 curve is shifted rightwards by 0 to 60 seconds at an interval of the acquisition TR (2.0 seconds). At each shift, the linear regression analysis was performed and a residual error term is calculated. The optimal delay time is then determined based on the shift that yields the least residual error.

In the first step, the T_1-weighted MPRAGE image was segmented (SPM5, University College London, UK) to obtain a WM probability map and only voxels with a WM probability of 90% or greater were included in the preliminary ROI. Second, recognizing that the BOLD resolution (3.4×3.4×3.5 mm^3) is considerably lower than MPRAGE and that there could be slight misregistration between BOLD and MPRAGE, we further eroded the preliminary WM ROI (i.e. peeling off a 1mm layer) three-dimensionally by six times, resulting in a rather small but minimally contaminated WM ROI (see

Figure 3-1 for an example). BOLD time courses of the voxels within the final ROI were subsequently averaged. For comparison, a GM ROI was also delineated by selecting voxels with a GM probability of 90% or greater. These voxels were identified from a single slice immediately above the lateral ventricles, where it contains cortical gray matter only (no deep gray matter) and the coregistration between MPRAGE and BOLD images is highly reliable. GM ROIs from other slices were also investigated, but no dependency of the results on sampling position was found.

From the averaged BOLD time course, two measures were obtained: the delay time and magnitude. Previous studies have established that the trace of end-tidal CO_2 and GM BOLD signal have a time shift of around 15 seconds [17, 19], which is the time it takes for the blood to travel from the lungs to the brain tissue and for the vessels in the tissue to react to the change in CO_2-concentration. This delay time may be different for WM, thus was specifically determined in the present study. The procedure was based on conducting a series of multi-regression analyses with a range of delay times and identifying the delay that corresponds to the best fit. Specifically, in each regression analysis, the BOLD time course was used as the dependent variable, and the time-

shifted end-tidal (ET) CO_2 curve and a linear curve to account for BOLD signal drift were used as the independent variables (

Figure 3-1). The range of Et CO_2 shift tested was from 0 to 60 seconds. A residual error was obtained for each regression analysis. The different regression analyses used an increasing amount of shift in Et CO_2. The shift that yielded the least residual errors was determined to be the optimal delay between Et CO_2 and the BOLD signal. Next, the magnitude of CVR was calculated using the coefficients from linear regression at the optimal delay [17], and is written in %BOLD signal per mmHg. The above analyses were conducted separately for gray and white matter time courses.

Arterial-Spin-Labeling MR images were used to calculate a quantitative CBF map by subtraction of the control and label image sets following procedures established previously [107]. The 30 repeated scans were averaged to improve SNR. The WM and GM ROIs described were applied to the ASL data to obtain baseline CBF values in these regions.

3.2.4 Statistical Analysis

All parametric values are reported in mean ± standard error. Data from younger and older groups were compared with a two-sample Student's t test. GM and WM results were compared with a paired Student's t test. A p value of 0.05 or less is considered significant.

3.2.5 Exploratory Analysis on the Curvature Differences between White Matter and Gray Matter Time Courses

In the regression analysis, the temporal differences in WM and GM time courses have mainly been modeled as simple time shift. Another possibility is that the two signals could have different curvatures. Specifically, the WM time course may have a smoother and broader response compared to the GM due to dispersion of the bolus in WM

vasculature [24]. We therefore tested this possibility by convolving the GM time courses, $Y_{GM}(t)$, with a mono-exponential "dispersion" function, $d(t) = e^{-t/\tau}$, to yield a smoothed version of the GM time course, $\bar{Y}_{GM}(t) = Y_{GM}(t) \otimes d(t)$. Multi-regression analysis was then performed in which $Y_{WM}(t)$ was used as the dependent variable and $\bar{Y}_{GM}(t)$ was the independent variable and a linear term was a covariate, similar to that shown in

Figure 3-1 This regression analysis was performed for a range of τ values (0-60 seconds) in the dispersion function. The optimal value for the time constant τ was determined based on minimal residual errors.

3.3 Results

Volumes of WM ROI were 10.9±1.0 cm^3 (N = 15) and 5.7±1.0 cm^3 (N = 15) in younger and older participants, respectively. Both were sufficiently large for accurate signal estimation, although the younger group had a significantly greater volume ($p<0.001$). The average WM probability of these ROIs was 0.9989±0.0001 and 0.9981±0.0003 for younger and older subjects, respectively, suggesting that GM partial volume was minimal. GM ROI volumes were 5.0±0.1 cm^3 and 3.86±0.08 cm^3 in younger and older subjects, respectively.

Average time courses of Et CO_2, GM and WM BOLD signals in young subjects are shown in Figure 3-2a. The most interesting feature is that there is a clear temporal delay in the WM time course relative to the GM. Table 3-1 summarizes the quantitative results. It can be seen that, in young subjects, GM signal lags behind the Et CO_2 time course by approximately 15 seconds, which is in agreement with previous literature [17, 19]. In the WM, BOLD signal appears to manifest a further and drastic delay of 19 seconds, compared to the GM. The magnitude of WM CVR was 14±1% of that in the GM, significantly different at a $p<0.001$.

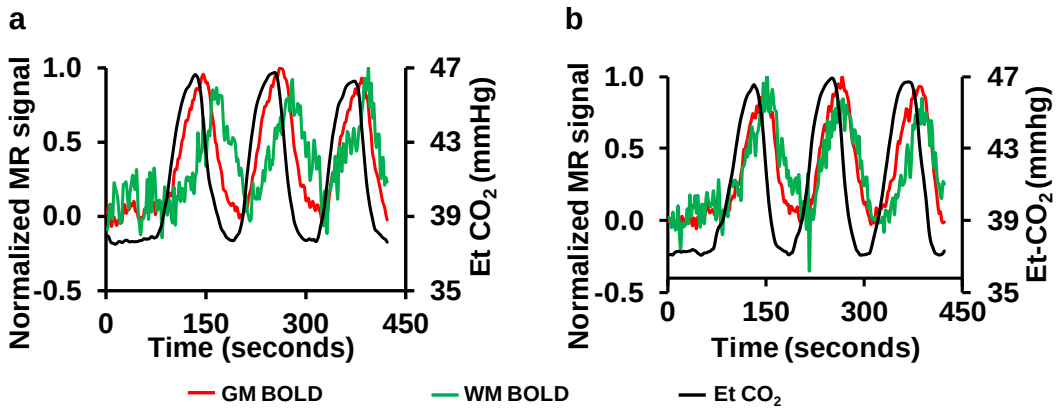

Figure 3-2: Time courses of End-tidal (Et) CO_2, GM BOLD, and WM BOLD signal in (a) younger and (b) older subjects. To highlight the timing differences, the MR signals have been normalized such that normocapnic signal is 0 and hypercapnic signal is 1. The Et CO_2 values are plotted in units of mmHg (right axis). It can be seen that the WM time courses lag behind the GM signal, which in turn lags behind the Et CO_2. The curves were obtained from averaging across all subjects. Error bars are not plotted for clarity.

End-tidal CO_2, GM and WM BOLD signals in older subjects are shown in Figure 3-2b. CVR parameters in older subjects showed several important differences from that in young. First, the lag between Et CO_2 and GM time courses in elderly was significantly greater ($p = 0.003$) than that in young (Table 3-1). Second, the delay between GM and WM BOLD time course is considerably shorter in elderly (from 19 seconds in young to 8 seconds in elderly, $p = 0.002$). Moreover, the magnitude of WM CVR was found to be greater ($p=0.003$) in older than in younger subjects (Table 3-1). As a result, the WM/GM CVR ratio in elderly was 29±2.7%, much greater ($p<0.001$) than that in young (14±1% as described above). Baseline CBF data showed similar trends (Table 3-1) in that the WM/GM CBF ratio in elderly (35±2%) was greater ($p<0.001$) than that in young (23±0.9%). Finally, GM CVR in elderly was significantly lower ($p<0.001$) than that in young, which is relatively well established from previous literature [9, 108].

Table 3-1: Summary of CVR and CBF results in the GM and WM ROIs (N = 15 for younger group; N = 15 for older group). Data are presented in mean ± standard error.

	CVR delay (seconds)			CVR magnitude (% BOLD/mmHg CO_2)		CBF (ml/100g/min)		
Group	Et CO_2 to GM	Et CO_2 to WM	GM to WM	GM	WM	GM	WM	WM/GM ratio
Young (N=15)	15.3±0.6	34.4±2.9	19.1±3.0	0.22±0.01	0.03±0.002	68.2±2.5	15.9±0.8	0.23±0.01
Old (N=15)	18.5±0.8	26.9±1.3	8.4±1.0	0.17±0.01	0.05±0.005	52.9±2.8	18.8±1.8	0.35±0.02
p value	0.003	0.029	0.002	<0.001	0.003	<0.001	0.152	<0.001

Further analysis was performed to test the possibility that the WM time course is best matched by the convolution of the GM time course with an exponential dispersion function, rather than by simply shifting the GM time course. The optimal time constant for the exponential function was found to be 26±5 seconds and 8±2 seconds for younger and older subjects, respectively, with a significant group difference ($p = 0.004$). The convolution analysis yielded slightly lower ($p = 0.038$) residual error (1.4±0.3 in units of MR signal) than the shift analysis (1.7±0.3).

3.4 Discussion

The present study conducted a systematic examination of cerebrovascular reactivity in the WM and its dependence on age. Our data suggested that, in addition to the expected difference in response magnitude, CVR in the WM is different from that in the GM in several important aspects. Furthermore, while the amplitude of reactivity decreases with age in the GM, the opposite pattern is seen in the WM.

One of the main findings of the present study is that CVR response in the WM is considerably slower than that in the GM, consistent with a slower rise time reported by Rostrup et al [93]. Using the shift analysis, we found that the WM response lags behind the GM by 19 seconds in young individuals. Using a different analysis based on

dispersion, it was found that the WM signal is equivalent to the GM signal smoothed by an exponential function with a time constant of 26 seconds. This is surprising considering that the WM ROI is located just a few centimeters deeper than the GM. Of course, it is well known that blood arrives later in the WM than the GM due to the known anatomy of the vasculature [84]. However, evidence from ASL and DSC-MRI literature suggests that this should only be 2-3 seconds at most [109]. Therefore, we hypothesize that this large delay is primarily due to a slow response of the WM compared to the GM. Specifically, we propose that it takes considerable amount of time for the extravascular CO_2 in the WM to build up and reach a new steady state, after the arterial CO_2 content has been altered. Figure 3-3 shows a qualitative illustration of this potential mechanism. The longer buildup time is primarily attributed to a low CBF in the WM, such that the amount of additional CO_2 that is brought to the WM per unit time is relatively small. Given the large fraction of tissue in the WM (98% tissue, 2% blood), it is plausible that it takes tens of seconds for the extravascular CO_2 concentration to change. It should also be noted that hypercapnia-induced vasodilation is primarily mediated by extravascular CO_2 concentration rather than intravascular CO_2. This notion is derived from animal data that selective inhibition of vascular endothelium function does not reduce hypercapnic response whereas inhibition of neuronal nitric oxide synthase does [54].

Another interesting finding of the present study is that WM in the older subjects showed a faster CVR response compared to young, in that the GM-to-WM delay in elderly is not as pronounced as those in young. Following our proposed mechanism described in the previous paragraph, this would mean that extravascular CO_2 concentration in the WM of older individuals increases more rapidly upon a change in arterial CO_2 content. This prediction is consistent with the baseline CBF results that WM

CBF was greater in older than in younger subjects, thus it takes less time for the CO_2 to build up.

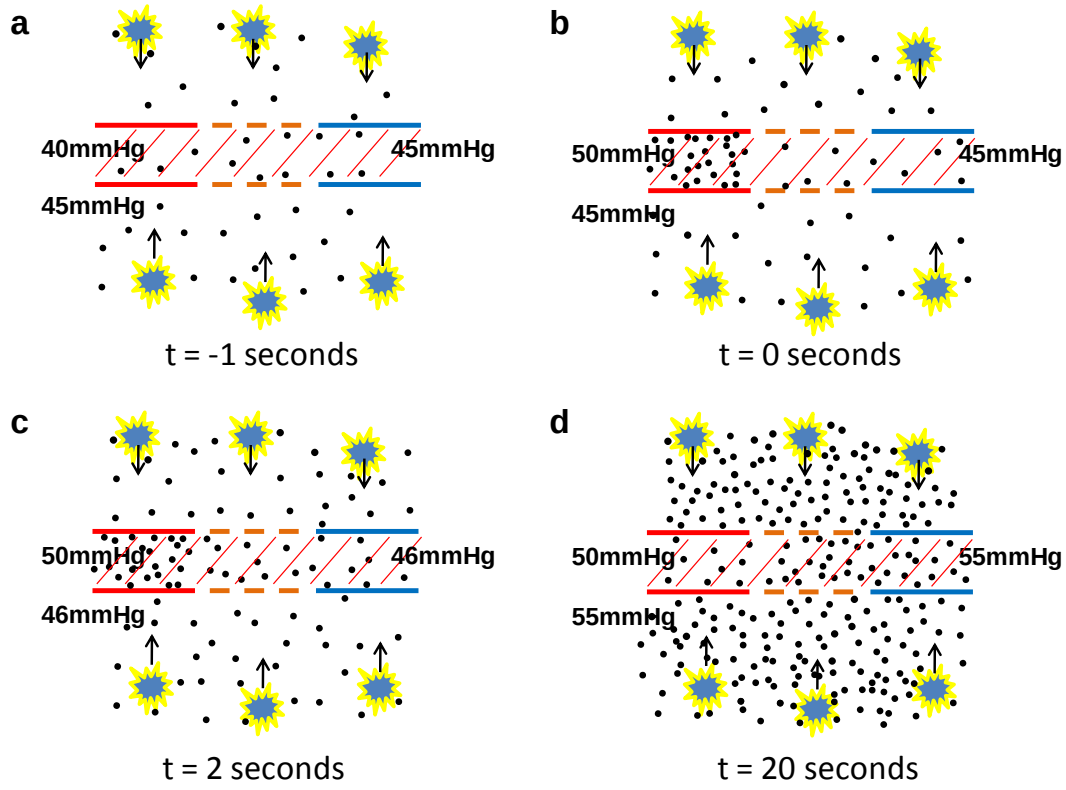

Figure 3-3: A proposed mechanism to explain the delay in CVR response in the WM. (a) Under normocapnic steady state, arterial CO_2 partial pressure is approximately 40 mmHg and tissue CO_2 is about 45 mmHg. Red lines indicate arterial vessel wall. Brown color denotes capillary vessel wall, which is shown in dashed lines to indicate that it is permeable to CO_2 molecules. Blue lines indicates venous vessel wall. It is assumed that tissue and blood CO_2 concentrations have reached equilibrium in capillary, thus venous CO_2 pressure is the same as tissue CO_2. Hatched area indicates intravascular space. Black dots illustrate CO_2 molecules. The yellow symbols indicate tissue cells, which generate CO_2 and the arrows indicate that CO_2 generated by tissue is cleared through blood vessels. (b) When the hypercapnic blood first arrives, arterial CO_2 concentration will increase, delivering extra CO_2 to the tissue. (c) However, tissue and venous CO_2 pressure shows a much slower change than the arterial CO_2, due to the large space of tissue compared to the rate of blood flow. Note that, with a perfusion of 30 ml/100g/min, the amount of blood delivered to the WM per second is only 0.5% of the tissue space. Therefore, during the first few seconds after the arterial CO_2 has changed, extravascular CO_2 may not show a pronounced alteration. (d) With time, extravascular CO_2 concentration increases substantially and a new steady state is reached.

The reason that WM CBF and CVR are greater in elderly than in young may be associated with the mechanical properties of the WM. WM in young subjects is tightly packed with axons and myelin, which makes it difficult for blood to penetrate and for vessels to dilate. This notion is supported by recent findings that, within healthy brain, fiber tracts that have higher fractional anisotropy (i.e. tighter organization with more myelin) tend to have a lower CBF [25]. In older individuals, as age-related demyelination and axon loss takes place, WM becomes less densely packed, thus exhibiting less hindrance for blood to flow through loose WM fibers.

Characteristics of WM CVR have been discussed in two previous studies. Mandell et al. reported that WM CVR could actually be negative (i.e. BOLD signal decreases with CO_2 inhalation), especially in white matter regions adjacent to lateral ventricles [20]. The authors interpreted these findings as a steal phenomenon by the gray matter in response to hypercapnia. Blockley et al. showed in a voxel-by-voxel analysis that WM CVR had a considerable delay, similar to those shown in this study [19]. However, the authors were not able to rule out the possibility of estimation errors and considered these as artifacts due to low SNR in their data [19]. In the present study, we have used several procedures to improve the reliability of our data. First, we have focused our analysis on ROI results, which have greater SNR compared to single-voxel results. Second, to ensure that the voxels included in the ROI are indeed WM voxels and to minimize partial volume of GM, we used tissue segmentation in combination with ROI erosion such that only the core of the white matter region is included in the final ROI. Third, we have used a shift-based analysis, in which the range of shifts tested included both shorter and longer than the expected GM delay. Thus, if noise had caused a difference in GM and WM timing, we should at least observe the WM time course leading the GM in some (e.g. 25%) subjects, which we did not see. Finally, we studied two

separate groups of subjects (younger and older) and both showed a significant GM-vs-WM difference. Thus, the probability of random noise to cause the same false positive observation in two studies is relatively low.

The results in this study have several practical implications for the design and analysis of CVR studies. First, given the considerable differences in delay times between tissue types, frequency-domain data analysis [19] may be a preferred approach over time-domain analysis, as it is less sensitive to the delay in time course. Second, it is desirable to use a breathing paradigm that could generate a BOLD time course of an approximate sinusoidal function, so that the time course would have a prominent frequency peak. To achieve this, one can employ a feedback/feedforward system targeting for a sinusoidal curve [19]. Alternatively, one can use a fixed inspired O_2 method with a short period (e.g. switching gas every minute) [17]. Due to the mixing of gas bolus in the lung and dispersion of blood bolus along its path to the brain, the BOLD time course with this paradigm is also generally similar to a sinusoidal curve. Third, high temporal resolution in data acquisition (e.g. short TR) is desired in order to accurately depict time delays in the signal. Finally, when evaluating WM CVR data under pathological conditions, potential change in both amplitude and temporal features should be considered. Note that, if the delay time is not properly accounted for, the response amplitude may be underestimated leading to mis-interpretation of results.

For the quantification of timing difference between the WM and GM BOLD time courses, we used two analysis methods, one based on shifting the time course and the other based on convolution of the time course with an exponential dispersion function. From our mechanistic model proposed in Figure 3-3, the dispersion and smoothing of the WM response relative to GM seem more plausible. Additionally, the convolution analysis yielded lower residual error compared to the shift analysis, again supporting the

dispersion method. However, given that the WM BOLD time course is generally variable and the residual error is of similar amplitude using the two analyses, the exact determination of the optimal analysis method as well as the physiologic interpretation requires further investigation. A limitation of the present study is that the gender distributions in the younger and older group were not exactly matched. The older group had more male subjects. It is known that females and males could have different blood flow. Therefore, some of the CBF findings (e.g., lower GM CBF in old) could be influenced by this confounding factor.

3.5 Conclusions

White matter CVR in response to hypercapnia is different from that of GM in several important aspects. Aside from the expected reduction in magnitude, WM response was slower than GM by tens of seconds. This could be attributed to the longer time it takes for WM extravascular CO_2 to accumulate and may be related to the lower perfusion in this tissue type. With age, WM CVR becomes greater and faster, which is opposite to the changes seen in the GM.

Chapter 4

Characterization of O_2 and CO_2 Response in the White Matter

4.1 Introduction

Structural imaging techniques such as T_2-weighted MRI, Magnetization Transfer (MT) and Diffusion Tensor Imaging (DTI); and postmortem studies of the brain have revealed a wealth of information regarding the structure of the White Matter (WM).[89, 90, 110, 111] Thus far we have learned that WM is composed of myelinated nerve cell processes that connect different brain regions to each other.[112] We have also learned that WM contains about 70% to 75% less vasculature compared to Gray Matter (GM).[21] This smaller vascular composition in WM results in considerably lower signal to noise ratio (SNR),[91] which is one of the main reasons why WM vascular physiology is still poorly understood compared to vascular physiology in the GM that has been well characterized. It is believed that disruptions in vascular physiology may precede most of the structural abnormalities. To gain insight into the neurological diseases that affect WM such as multiple sclerosis[87], stroke[85], Alzheimer's disease[86] and traumatic brain injury [88], it is very important to understand vascular physiology in the WM.

Recent advances in neuroimaging techniques have mitigated some of the challenges in studying vascular physiology in WM and have helped take the initial steps towards understanding WM vasculature.[22] For example, it has been suggested that baseline Cerebral Blood Flow (CBF) can be mapped in the WM using the Arterial-Spin-Labeling (ASL) MRI technique in a tract-by-tract basis and that WM CBF is inversely correlated with diffusion fractional anisotropy (FA) [25]. Recently, another important property of vasculature in the WM was measured: its ability to dilate upon stimulation, referred to as Cerebrovascular Reactivity (CVR). CVR was measured and characterized in terms of its magnitude and temporal properties in the core of the WM and was

compared to that measured in the GM; and effects of age on the CVR in WM were also reported.[18] Characterization of CVR in WM is important to understand mechanisms of ischemic and inflammatory responses in the WM, which may provide new insights into the patho-physiology of diseases such as multiple sclerosis[23] and stroke[4].

This present study takes a further step into understanding WM vascular physiology; it measures CVR in WM to CO_2 inhalation, and also vascular response in WM to inhalation of oxygen. It is important to measure vascular response to inhalation of O_2, which is an indicator of the passive property of vasculature. The O_2 gas (composed of 98% O_2 and 2% CO_2) is shown by some studies [26, 27] to cause minimal vaso-dilation; the gas itself acts as a contrast agent, i.e. once it enters the venous blood vessels, it can be detected using the Blood-Oxygen-Level-Dependent (BOLD) MRI sequence. The response of vasculature to the O_2 gas is different from its response to the CO_2 gas, i.e. the O_2 gas does not stimulate the smooth muscles on the vascular endothelium, and so, it does not increase CBF, unlike the CO_2 gas which causes an increase in CBF. Thus, vascular response to O_2 inhalation is similar to the measurement of cerebral blood volume (CBV) [21]. In this study, in-depth characterization of vascular response in WM was performed by classifying WM into broad cerebral lobes, 10 major WM fibers and into layers with increasing depth from the cortical GM. One of the most striking findings was that vascular response to O_2 was also considerably delayed in most regions examined, but it was still faster than the CVR to CO_2 inhalation. This difference in delay due to O_2 and CO_2 gas was attributed to the difference in the mechanism of action of the O_2 and the CO_2 gas on brain vasculature. It was also found that as the depth of WM from the cortical surface increases, the magnitude of response to O_2 gas decreases, but for the inner most few millimeters of WM, an increase in the magnitude of response was seen, which may be indicative of the structure of WM microvasculature, i.e. data may indicate

that micro-vessels may penetrate into the WM from both sides (mid-line of the brain as well as the lateral cortical surface of the brain) of each cerebral hemisphere. It was also found that as the depth of WM from cortical GM increases, the CVR to inhalation of CO_2 gas decreases, but the signal plateaus or remains same in the inner most layers of the WM, which may suggest that in the deeper layers of the WM, the micro-vessels may have smaller vaso-dilatory capacity; the effect of smaller vaso-dilatory capacity is balanced out by the increase in micro-vascular concentration as seen from the O_2 data, hence a plateau is seen in the magnitude of the CVR signal in the WM layers located in the core of the WM. Finally, we also report the coefficient of variation between scans for the vascular response in WM to O_2 and CO_2 inhalation, which is an indicator of measurement reproducibility.

4.2 Methods

4.2.1 Participants

This study was approved by the Institutional Review Board of the University of Texas Southwestern Medical Center. All subjects gave informed written consent before participation. Nine young (age = 30±1.4 years, range = 23-33 years, 4 males and 5 females) subjects were examined. Participants were recruited through flyers and advertisements in the local media. All participants recruited had no contra-indications to MRI scanning (pacemaker, implanted metallic objects, and claustrophobia) and were generally in good health, with no serious or unstable medical conditions such as neurological disease, or brain injury.

4.2.2 Experimental Procedures

4.2.2.1 General

Experiments were performed on a 3 Tesla MRI scanner using a 32-channel receive-only head coil (Philips Medical Systems, Best, The Netherlands). The body coil

was used for RF transmission. Foam padding was placed around the head to minimize motion during MRI scan acquisition. Scans were acquired in two separate sessions to maintain participant comfort and to prevent fatigue. In between these two sessions, participants were allowed to come out of the scanner room and relax for 15 minutes. Scan sessions were split based on the type of gas inhaled, i.e. during each session, participants inhaled either the O_2 gas or the CO_2 gas, and during the second scan session, participants inhaled the other gas. For example, if during the first scan session a participant inhaled the CO_2 gas, then during the second scan session, that participant would inhale the O_2 gas. The order in which participants inhaled gas was pseudo-randomized: six participants inhaled O_2 gas during the first session and CO_2 gas during the second session, while three participants inhaled CO_2 gas during the first session and then the O_2 gas. BOLD image acquisitions were performed simultaneously while participants inhaled the gas to measure vascular response to the gas. Each scan session consisted of two BOLD image acquisitions, for measurement of reproducibility of data, and one DTI scan acquisition. The DTI scan acquisition performed during the O_2 scan session consisted of measuring diffusion in 30 directions and was used to trace fiber tracts within the WM; and the DTI scan acquisition performed during the CO_2 scan session consisted of measuring diffusion only in six directions, and was performed to only obtain the B0 image, which was used for image registration between the two scan sessions.

4.2.2.2 Scans Acquired During the O_2 Session

4.2.2.2.1 BOLD Scan with Simultaneous O_2 Inhalation

Vascular response to O_2 was measured by the BOLD MRI sequence while participants inhaled the O_2 gas. The details of the experimental set up and measurement was described previously [17], and are similar to that performed during CVR

measurement with inhalation of the CO_2 gas. Briefly, during the O_2 inhalation scan, subjects were fitted with a nose clip, and breathed room air and the prepared gas in an interleaved fashion (2 min O_2, 2 min room air, repeated three times) through a mouthpiece. The prepared gas was a mixture of 98% O_2 and 2% CO_2 contained within a Douglas bag. 2% CO_2 was supplemented to maintain a constant Et CO_2 level in the presence of slight hyperventilation by the subject. The gas was delivered to the subject through a two-way non-rebreathing valve and mouthpiece combination (Hans Rudolph, 2600 series, Shawnee, KS). A research assistant was inside the magnet room throughout the experiment to switch the valve and monitor the subject. BOLD MR images were acquired continuously during the entire experimental period. The end-tidal O_2 (Et O_2), the O_2 concentration in the lung which approximates that in the arterial blood, was also recorded throughout the breathing task using an O_2 monitoring device (Biopac, Model MP 100, Biopac Systems Inc, CA). The total duration for each vascular response to O_2 scan was 12 minutes. The BOLD sequence used the following imaging parameters: single-shot EPI, field-of-view (FOV) = 200×200 mm^2, matrix size = 80×80, 29 axial slices placed parallel to the AC-PC plane, thickness = 5 mm, no gap, TR/TE/flip angle = 1500 ms/21 ms/88.5°, and 490 volumes. This BOLD scan was acquired twice to assess reproducibility of measurements.

4.2.2.2.2 DTI Scan

To trace major WM fibers in the WM, a DTI scan was performed during the O_2 scan session with following parameters: single-shot EPI, field-of-view (FOV) = 200×200 mm^2, matrix size = 80×80, 58 axial slices, thickness = 2.5 mm, no gap, TR/TE/flip angle = 5000 ms/59 ms/90°; diffusion weighting was encoded along 30 independent orientations and the b value was 1000 seconds per mm^2.

4.2.2.3 Scans Acquired During the CO_2 Session

4.2.2.3.1 BOLD Scan with Simultaneous CO_2 Inhalation

CVR was measured with a hypercapnia challenge, in which participants inhaled 5% CO_2 gas while BOLD MR images were simultaneously acquired. The details of the CVR measurement were described previously [17]. Participant set up in the scanner was similar to that described for the O_2 inhalation scan. Subjects breathed room air and the prepared gas in an interleaved fashion (50 sec CO_2, 70 sec room air, repeated five times) through the mouthpiece. The prepared gas was a mixture of 5% CO_2, 74% N_2 and 21% O_2 contained within a Douglas bag. The end-tidal CO_2 (Et CO_2), the CO_2 concentration in the lung which approximates that in the arterial blood, was also recorded throughout the breathing task using a capnograph device (Capnogard, Model 1265, Novametrix Medical Systems, CT). The total duration for the CVR scan was 11 minutes. The BOLD sequence used the following imaging parameters: single-shot EPI, field-of-view (FOV) = 220×220 mm^2, matrix size = 80×80, 29 axial slices placed parallel to the AC-PC plane, thickness = 5 mm, no gap, TR/TE/flip angle = 1500 ms/21 ms/88.5˚, and 440 volumes. The flip angle and TE used in the scan were optimized to avoid the artifactual negative CVR seen in large fluid filled spaces like the CSF in the brain. This BOLD scan was acquired twice to assess reproducibility of measurements.

4.2.2.3.2 DTI Scan

To co-register images between the O_2 and CO_2 scan sessions, a DTI scan was performed to only obtain the B0 image. Imaging parameters for the DTI scan were same as the parameters used for the DTI scan obtained during the O_2 session, except that diffusion weighting was encoded only along 6 independent orientations instead of the 30 directions encoded in the DTI scan from the O2 session.

4.2.3 Data Processing

BOLD data were processed using Statistical Parametric Mapping (SPM) (University College London, UK), and in-house Matlab (MathWorks, Natick, MA) scripts. Pre-processing of the BOLD images included motion correction and registration with the B0 image (T_2-weighted) obtained from the DTI scan. Briefly, the BOLD image series from each BOLD scan were realigned to the last image, because this was closest to the DTI scan. This was done to obtain good registration between the BOLD and DTI images. The last BOLD image of each BOLD data was then registered to the B0 image from the DTI scan obtained within the same session, and the transformation parameters were applied to all BOLD images. The data were analyzed in individual space. This is because spatial normalization to standard space usually results in smoothing of the image, which could result in increased partial voluming effect of GM on WM regions of interest (ROIs).

Quantitative analyses of the data have primarily focused on the ROI results as they are more reliable than voxel-wise results in the WM. Analysis of WM data was performed by classifying WM into three different types of ROIs: 1. Ten major fiber tracts, 2. Broad lobes in the brain, and 3. WM layers with increasing depth from the cortical surface.

Ten major fiber tracts in the WM were identified from the DTI data acquired during the O_2 session. DTI images were processed in DTI studio (Radiology Department, Johns Hopkins University). Pre-processing of the DTI images included realignment, using a 12-parameter affine registration. The DTI images were then corrected for distortion caused by eddy currents using Automatic Image Registration (AIR) [113]. Six elements of the 3 × 3 diffusion tensor were calculated by least square fitting; the tensor was then diagonalized to obtain the three eigen values (λ_1, λ_2, λ_3) and three eigen vectors (i_1, i_2, i_3).

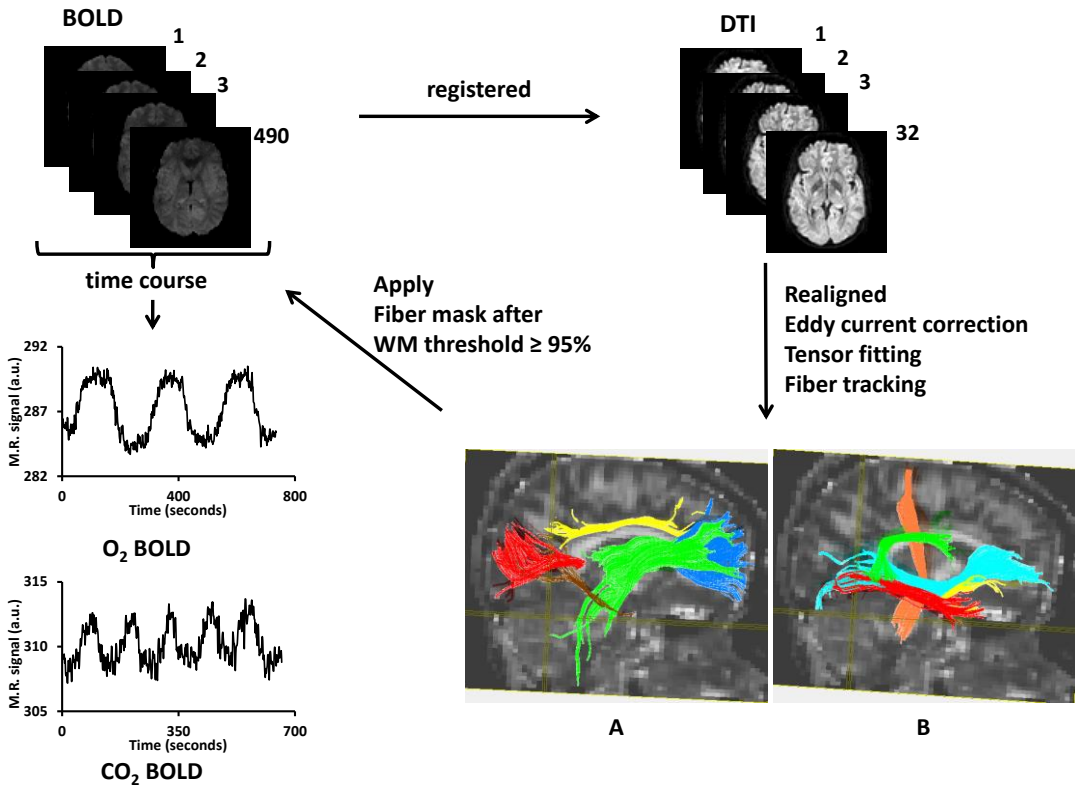

Figure 4-1: Overview of the processing steps used to extract the BOLD time course from the major fiber tracts of the WM. All ten major fiber tracts that were tracked are shown in Figure 4-1 A and B overlaid on the FA map. Shown in Figure 4-1 (A) are forceps major (Fmajor) in red color, cingulum to the hippocampus (CGH) in brown color, anterior thalamic radiation (ATR) in green color, cingulum in the cingulate cortex (CGC) in yellow and forceps minor (Fminor) in blue color, and in Figure 4-1 (B) are inferior longitudinal fasciculus (ILF) in red color, inferior fronto-occipital fasciculus (IFO) in blue, temporal component of the superior longitudinal fasciculus (SLFt) in green, uncinate fasciculus (UNC) in yellow and corticospinal tract (CST) in orange color.

Tensor fitting was performed using DTI studio [114]. Standard whole brain fractional anisotropy (FA) maps were obtained. An overview of the processing steps is shown in Figure 4-1. Fiber tracking was then done in DTI studio. Fiber tracking was only performed on 10 major fiber tracts to avoid potential controversies over validity of smaller fibers. The 10 major fiber tracts are shown in Figure 4-1 A and B. Five fibers are shown in Figure 4-1 A: forceps major (Fmajor) in red color, cingulum to the hippocampus (CGH) in

brown color, anterior thalamic radiation (ATR) in green color, cingulum in the cingulate cortex (CGC) in yellow and forceps minor (Fminor) in blue color and the remaining five fibers are shown in Figure 4-1 B: inferior longitudinal fasciculus (ILF) in red color, inferior fronto-occipital fasciculus (IFO) in blue, arcuate fasciculus, also known as the temporal component of the superior longitudinal fasciculus (SLFt) in green, uncinate fasciculus (UNC) in yellow and corticospinal tract (CST) in orange color. Tracking of these fiber tracts was shown to be very reliable across raters and over different data sets [115]. Fiber tracking protocol specified by Wakana et al. [115] was followed to track these fibers. Fiber tracking for all subjects was performed by a single experienced tracker: VM.

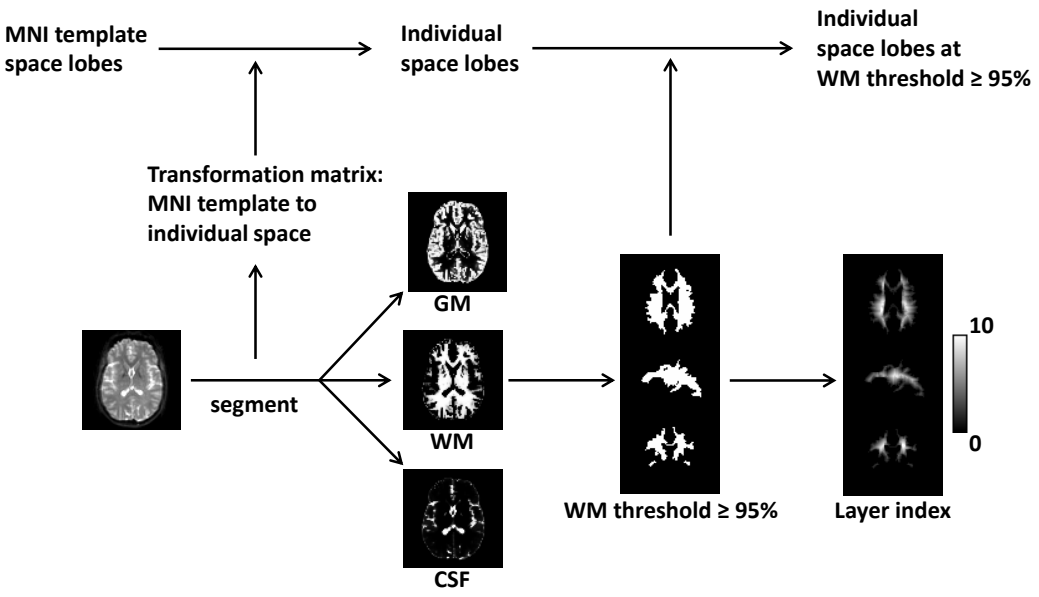

Figure 4-2: Overview of the processing steps to classify WM into broad lobes and into layers. Images are from a representative subject.

To classify each participant's WM into the broad lobes in the brain, the B0 image was first segmented into GM, WM and CSF segments. The inverse transformation matrix obtained from the segmentation step was then applied to the MNI space lobes to

transform the lobes into an individual subject's image space. Data from the five major lobes in the brain: frontal, limbic, parietal, temporal and occipital, were measured. An overview of these steps is shown in

Figure 4-2.

Given that arteries originate on the cortical surface, perfuse GM and then penetrate and perfuse WM. It is possible that CVR in the WM could be dependent on the depth of the WM from the cortical surface, with the understanding that larger arteries on the cortical surface may have higher CVR compared to microvasculature located deeper within the WM (also known as watershed effect). So, we estimated a WM layer index for each voxel within the WM; the layer index would indicate the depth of the voxel from the cortical GM. We used a step-wise erosion process, that involved peeling off a single layer of WM and then assigning all voxels in that layer a layer index. This step was further repeated to peel off multiple layers, resulting in smaller volume of WM with increasing layer index. An example layer index map from a single subject is shown in

Figure 4-2. A region with minimal partial volume effects (PVE) from GM was obtained after peeling off 7 WM layers; this region was called the core of the WM. For comparison with all the WM ROI data, a GM ROI was also identified. All GM slices above the lateral ventricles were included in this GM ROI. Only slices above the ventricles were chosen because registration between BOLD images and the B0 image is more reliable in these regions compared to regions below the ventricles. Brain regions in the lower portion of the brain include the sinuses, which may result in mis-registration because of air pockets that generate poor MRI signal in the BOLD image.

Special care was taken to avoid partial volume effects, so for all ROIs only 95% or higher probability of the particular tissue type was included, avoiding partial volume effects from another tissue. Binary masks of all ROIs were created and applied to the

BOLD image series obtained from the O_2 session, to extract the BOLD time course from each ROI; an example of the time course is shown in Figure 4-1.

From the averaged BOLD time course, two measures were obtained: the delay time and the magnitude of response to the O_2 gas. Previous studies have established that the trace of end-tidal CO_2 and GM BOLD signal have a time shift of ~15 sec [17, 19], which is the time it takes for the blood to travel from the lungs to the brain tissue and for the vessels in the tissue to react to the change in CO_2-concentration. This delay time is different for WM and was previously found to be around 34 sec [18]. We are interested in finding out the delay time during inhalation of the O_2 gas, and comparing it to those found during inhalation of the CO_2 gas. The procedure of obtaining the delay is based on conducting a series of multi-regression analyses with a range of delay times and identifying the delay that corresponds to the best fit, shown in Figure 4-3. Specifically, in each regression analysis, the BOLD time course was used as the dependent variable, and the time-shifted end-tidal (ET) O_2 curve and a linear curve to account for BOLD signal drift were used as the independent variables. A residual error was obtained for each regression analysis. The different regression analyses used an increasing amount of shift in Et O_2. The shift that yielded the least residual errors was determined to be the optimal delay between Et O_2 and the BOLD signal. Next, the magnitude of vascular response was calculated using the coefficients from linear regression at the optimal delay [17], and is written in %BOLD signal per mmHg. The above analyses were conducted separately for each ROI time course.

To obtain the BOLD time course from the CO_2 inhalation session, all ROI masks and the BOLD images from the CO_2 inhalation scan session have to be registered. This was done by registering the B0 image from the O_2 session DTI scan to the B0 image from the CO_2 session DTI scan and applying the parameters to all ROIs.

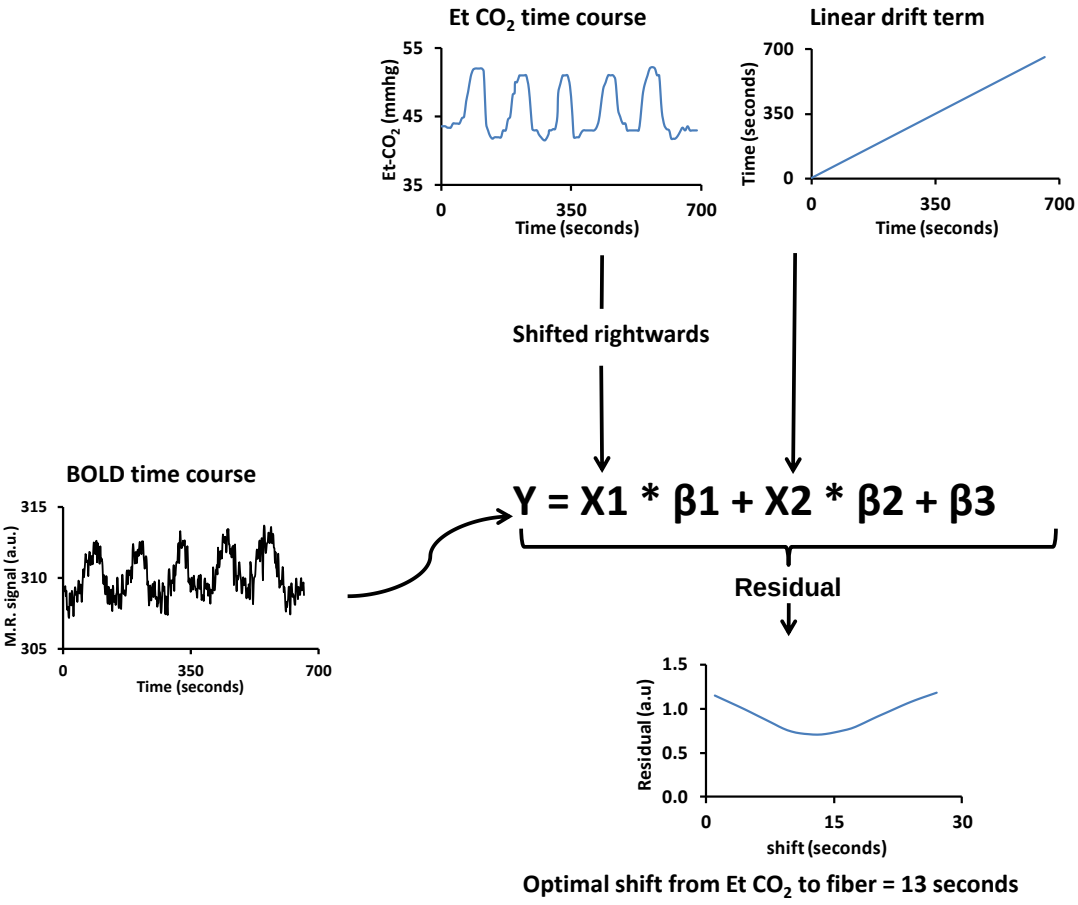

Figure 4-3: Detailed steps in the multi-regression processing to obtain the optimal delay between the end-tidal measurement and the BOLD time course. For illustration purpose, an example Et CO_2 time course and the BOLD time course from a single fiber tract is used. The same procedure can be used with the Et O_2 time course.

This registration procedure will smooth the ROIs. The ROI volume post registration was maintained same as that prior to registration. The average BOLD time courses were then obtained from the CO_2 session data and the same multi-regression analysis that was described for the O_2 session was performed to determine the delay and magnitude of the CVR response to CO_2 inhalation (Figure 4-3). All values reported in this chapter are mean ± standard error.

4.3 Results

4.3.1 Delays

Delay from Et O_2 to the GM ROI was 11.5 ± 0.8 seconds. This delay signifies the time it takes the O_2 gas to travel from the lungs to the brain and to be detected in the brain using the BOLD MR sequence. The delay from the Et CO_2 to the GM ROI was 15.7 ± 0.5 seconds, this delay is similar to that reported previously [18]. The delay to the GM from Et O_2 was significantly different at a Bonferroni corrected $p = 0.002$ compared to the delay to GM from Et CO_2. This data indicates that the vascular response in GM to O_2 gas is significantly faster compared to the CVR in GM to the CO_2 gas. Comparison of delays between GM and the core of WM showed that delays to the GM were significantly shorter compared to the delays to the core of the WM for both the O_2 and the CO_2 gas; significantly different at $p < 0.001$; this is expected given that arteries originate on the cortical surface and then penetrate the WM to perfuse WM.. The delays from the end tidal measurement to the GM, core of the WM and the WM fibers are shown in Figure 4-4 a. The delays measured for all fibers using the O_2 gas were shorter compared to that measured for the CO_2 gas, except for the CST fiber in which the delay measured by the O_2 gas was longer compared to that measured using the CO_2 gas. The comparison of the delays measured to the CGH fiber using the O_2 and the CO_2 gas was significantly different at a $p < 0.05$ (corrected) and the comparison of delays measured to the ATR fiber was significantly different at a $p < 0.05$ (uncorrected).

The delays measured in the WM from the broad lobes is shown in Figure 4-4 b. Delays from frontal occipital and temporal lobes for the CO_2 gas were longer than those measured for the O_2 gas, while delays from the limbic and parietal lobes was shorter for the CO_2 gas compared to that for the O_2 gas. The comparison of the O_2 and CO_2 delays did not show any significant differences in the lobes.

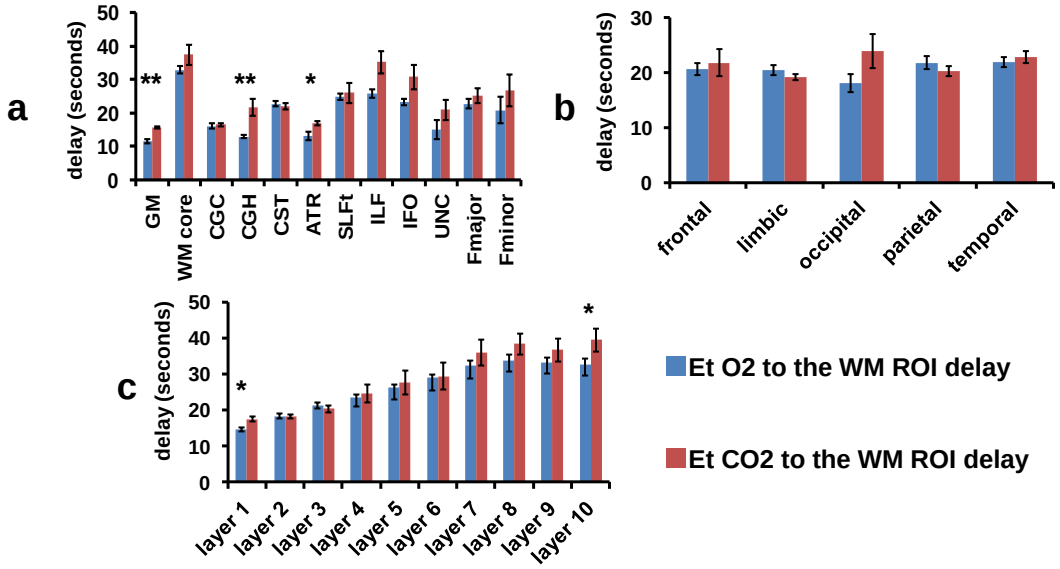

Figure 4-4: Delay from Et O_2 to each ROI and Et CO_2 to each ROI are shown; blue color represents delay from Et O_2 to the ROI and red color represents the delay from Et CO_2 to the ROI. In (a) is shown delays to the GM, the core of WM and the ten major fibers in WM; (b) shows delays to the WM in the broad lobes and (c) shows delays in the individual layers of the WM. **Corrected $p < 0.05$, *Uncorrected $p < 0.05$; Error bar = standard error.

The delays in the layers in WM are shown in Figure 4-4 c. It is evident that as the depth of the WM from the cortical surface increases, i.e. with increase in WM layer index, the delays for both O_2 and CO_2 gas increase. As seem in Figure 4-4 c, all WM layers show longer delays for the CO_2 gas compared to the O_2 gas and delays in layer 1 and layer 10 are significantly different at a $p < 0.05$ (uncorrected).

The delays from Et O_2 to the 10 major fiber tracts in the WM were found to be significantly different between fibers. A difference matrix generated from the p-values of comparisons between fibers is shown in Figure 4-5.

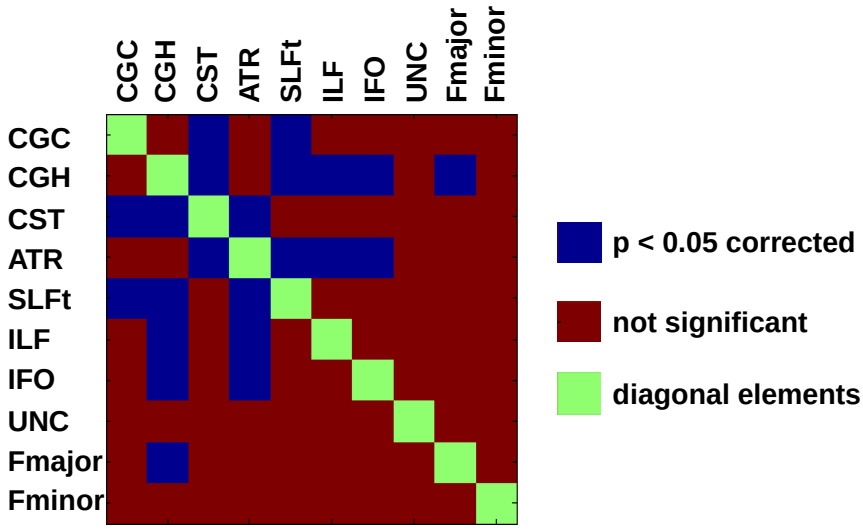

Figure 4-5: Difference matrix of comparison of delays from Et O_2 to WM fibers; green color indicates diagonal elements within the comparison matrix which signifies comparison of the same fiber with itself, blue color indicates differences significant at a Bonferroni corrected $p < 0.05$, and red color indicates differences that are not significant.

We compared the delays from Et CO_2 to individual WM fibers and found that delays between the CGC and CST were significantly different at a Bonferroni corrected $p < 0.05$; delays between all other fibers were not significantly different at the corrected threshold.

We compared the delays from Et O_2 to individual lobes and found that delays between different lobes were not significantly different at a corrected threshold. The delays from Et CO_2 to individual lobes were different between the temporal and limbic lobes and between temporal and parietal lobes at a corrected $p < 0.05$.

We also found that delays from Et O_2 to WM layers were significantly different; shown in Figure 4-6 a, is a difference matrix created from the p-values of comparisons. Colors in Figure 4-6 are similar to the colors used in Figure 4-5; again, blue color indicates differences that were significant at a $p < 0.05$ corrected for multiple

comparisons and red color indicates differences that were not significant after correcting for multiple comparisons. Shown in Figure 4-6 b is the difference matrix of comparison of delays from Et CO_2 to WM layers.

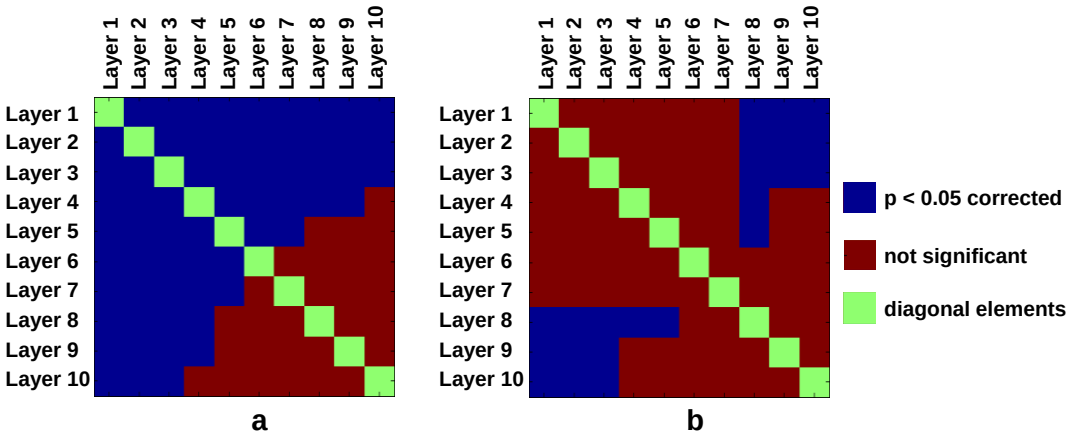

Figure 4-6: Difference matrix of comparison of delays from the end tidal measurement to WM layers; (a) shows the difference matrix for comparison of WM layer delays from Et O_2 and (b) shows the difference matrix for comparison of WM layer delays from Et CO_2. Green color indicates diagonal elements within the comparison matrix which signifies comparison of the same layer with itself; blue color indicates differences significant at a Bonferroni corrected $p < 0.05$ and red color indicates differences that are not significant.

4.3.2 Magnitude of Vascular Response

The magnitude of the vascular response to O_2 in the GM was 0.0052 ± 0.0002 %/mmHg O_2 and in the core of the WM it was 0.0014 ± 0.00005 %/mmHg O_2; significantly different at a $p < 0.001$. These values are shown in Figure 4-7 a. Also shown in Figure 4-7 a, are magnitude of response in all individual fibers in the WM. The average magnitude of response in all the fibers in the WM was 0.0017 ± 0.0001 %/mmHg O_2, which is similar to the value reported in the core of the WM. The magnitude of response to the O_2 gas in the broad lobes of the WM are shown in Figure 4-7 b. Figure 4-7 c shows the magnitude of response in the individual layers in the WM to the O_2 gas. As expected

layer 1 shows the largest magnitude of response to the O_2 gas, this is expected, due to partial volume effects from GM as this layer is closest to the cortical surface. The magnitude of response in the layers of the WM decreases until layer 7 and then it increases in layers 8, 9 and 10; significant difference was seen between layer 8 and layer 9 and between layer 8 and layer 10 at a $p < 0.001$ and $p < 0.05$ respectively.

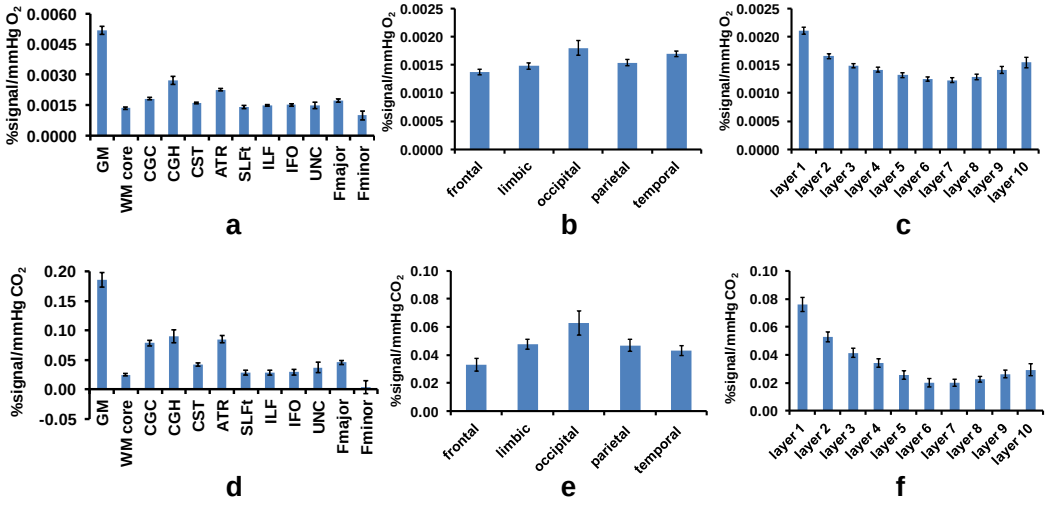

Figure 4-7: BOLD percent signal per mmHg of the gas (%/mmHg) used is shown for each ROI. (a), (b) and (c) show it for the O_2 gas challenge and (d), (e) and (f) show it for the CO_2 gas challenge. (a) and (d) show values for GM, core of the WM and individual fibers in the WM. (b) and (e) show values for the broad lobes in the WM, and (c) and (f) show it for the individual layers in the WM.

The magnitude of the vascular reactivity to CO_2 in the GM was 0.19 ± 0.01 %/mmHg CO_2 and it was 0.02 ± 0.002 %/mmHg CO_2 in the core of the WM; shown in Figure 4-7 d. As expected, the magnitude of response in the core of the WM was significantly smaller than that in the GM at a $p < 0.001$. Also shown in Figure 4-7 d is magnitude of response in the ten major fiber tracts in the WM. The average magnitude of response in all the fibers in the WM was 0.05 ± 0.006 %/mmHg CO_2. The magnitude of response to CO_2 gas in the broad lobes of the WM is shown in Figure 4-7 e. Figure 4-7 f

shows the magnitude of response in the individual layers in the WM to the CO_2 gas. Again, as expected, layer 1 shows the largest magnitude of response to the CO_2 gas. We did not find a significant difference between the response magnitude in layers 8, 9 and 10 in the CO_2 data.

A map of the vascular response to CO_2 and O_2 is shown in Figure 4-8.

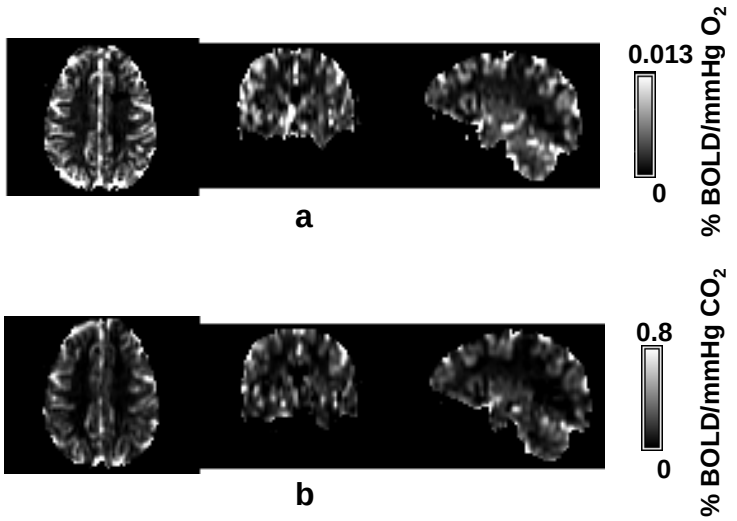

Figure 4-8: Map of the magnitude of vascular response to O_2 and CO_2 in the brain. (a) vascular response to O_2 is reported in the units of % BOLD/mmHg O_2 and (b) shows CVR to CO_2 in the units of % BOLD/mmHg CO_2.

We tested for differences in % signal/mmHg gas between the WM fiber tracts and the result is shown in Figure 4-9. Figure 4-9 a, shows the differences for the O_2 gas and Figure 4-9 c shows it for the CO_2 gas. More fibers are significantly different for delays measured due to the CO_2 gas compared to the number of fibers that show differences in delays measured due to the O_2 gas. Comparison of differences between WM layers for the magnitude of response to O_2 is shown in Figure 4-9 b and the comparison for the magnitude of response to CO_2 is shown in Figure 4-9 d. We also tested differences in % signal/mmHg O_2 between the broad lobes from the WM and

found that only the frontal lobe showed difference from the temporal lobe at $p < 0.05$ Bonferroni corrected. The differences in % signal/mmHg CO_2 between the broad lobes within the WM were different between the frontal and limbic lobes and between frontal and parietal lobe, significant at $p < 0.05$ Bonferroni corrected.

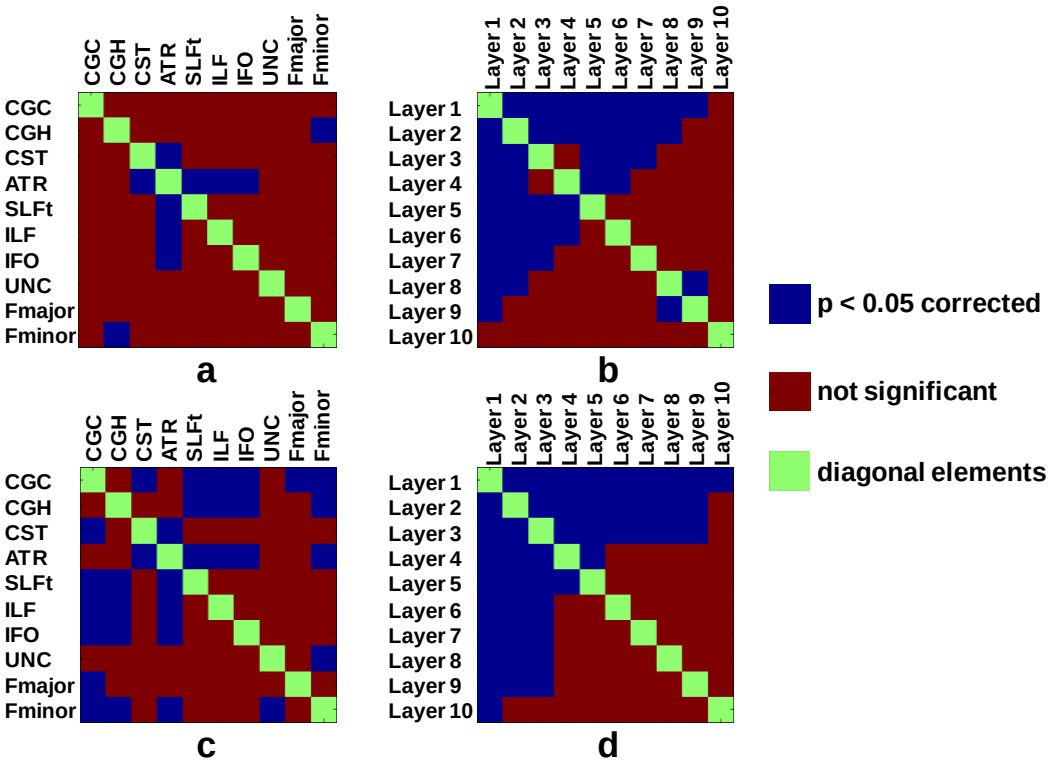

Figure 4-9: Difference matrix of comparison of % signal/mmHg gas between WM fibers and between WM layers; (a) shows the difference matrix for comparison of %signal/mmHg O_2 for WM fibers, (b) shows the difference matrix for comparison of %signal/mmHg O_2 for WM layers. (c) Shows the difference matrix for comparison of %signal/mmHg CO_2 for WM fibers and (d) shows the difference matrix for comparison of %signal/mmHg CO_2 for the WM layers. Green color indicates diagonal elements within the comparison matrix which signifies comparison of the same ROI with itself; blue color indicates differences significant at a Bonferroni corrected $p < 0.05$ and red color indicates differences that are not significant.

4.3.3 Relationship between Delay and Magnitude of Response

Next we wanted to find out if there is a relationship between the measured delay in seconds and the magnitude of response. So, we calculated Pearson's correlation coefficient for delay and the % signal/mmHg. We found a negative correlation between delay and the magnitude of response for O_2 in the WM fibers, significant at $p = 0.03$; shown in Figure 4-10 a. We also found a similar negative correlation when CO_2 gas was inhaled, significant at $p = 0.02$, shown in Figure 4-10 b. This data suggests that if a WM fiber tract shows long delay in vascular response, it will elicit a small signal change magnitude in response to inhalation of either gas: O_2 or CO_2.

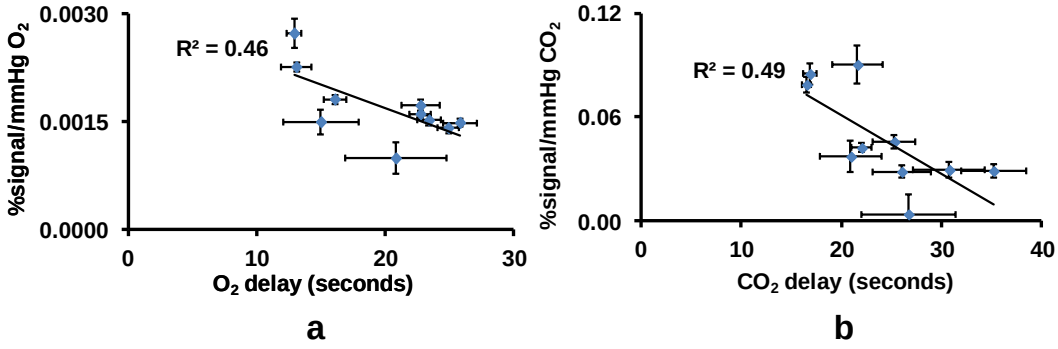

Figure 4-10: Relationship between WM fiber delay and % signal/mmHg gas shows a negative correlation; (a) shows the relationship for the O_2 gas, significant at $p = 0.03$ and (b) shows the relationship for the CO_2 gas, significant at $p = 0.02$. Error bar = standard error.

We also tested this relationship in each fiber across all nine subjects and found that delays were negatively correlated with the %signal/mmHg O_2, but we did not find any significant correlations. We also found a negative correlation between delays and %signal/mmHg CO_2 for each fiber and found significant correlations for the ILF, IFO, UNC and the Fminor fibers, significant at $p < 0.05$, shown in Figure 4-11.

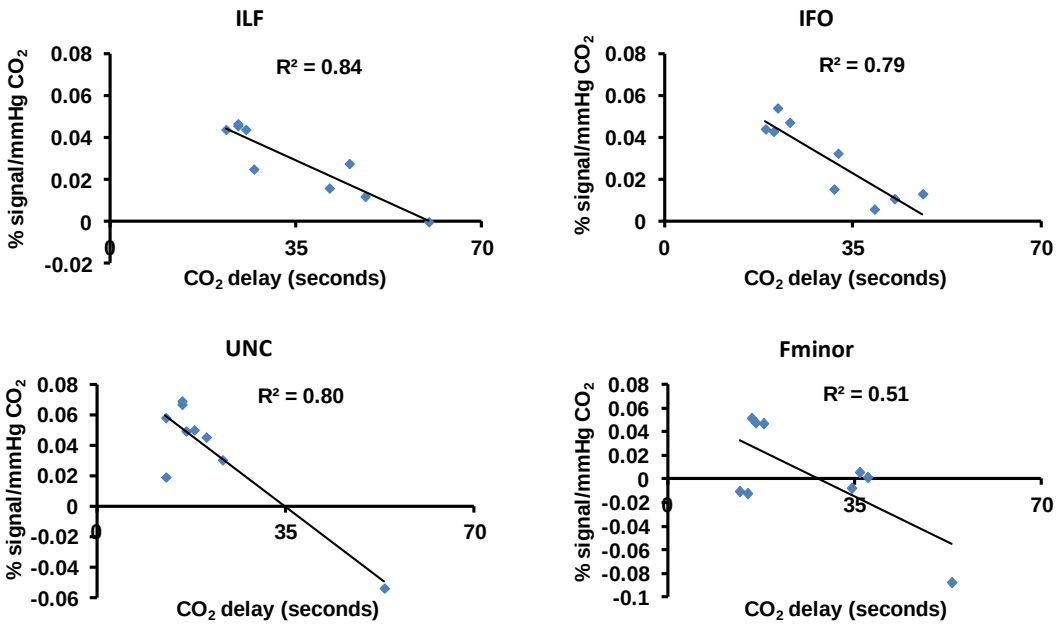

Figure 4-11: Relationship of measured delay in seconds to the % signal/mmHg CO_2 across nine subjects for individual fibers: ILF, IFO, Fminor and UNC, significant at p = 0.0004, p = 0.001, p = 0.03 and p = 0.001 respectively.

We tested for the relationship between the measured delay and the % signal/mmHg in the WM lobes for both O_2 and CO_2 gas, but we did not find any significant correlation. We also tested for this relationship in individual lobes across all nine subjects and found a negative correlation for all lobes except the Frontal lobe for the O_2 data; the correlations were not significant. In the Frontal lobe, we found a small positive correlation, with the slope of the trend line approximately zero; we did not find a significant relationship. We tested for this relationship in the CO_2 data and found a negative correlation between vascular response delay and magnitude of response in all the lobes in WM. We found a significant negative correlation in the frontal lobe, significant at p = 0.02, as shown in Figure 4-12, and in the occipital lobe, we found significance at trend level (p = 0.06).

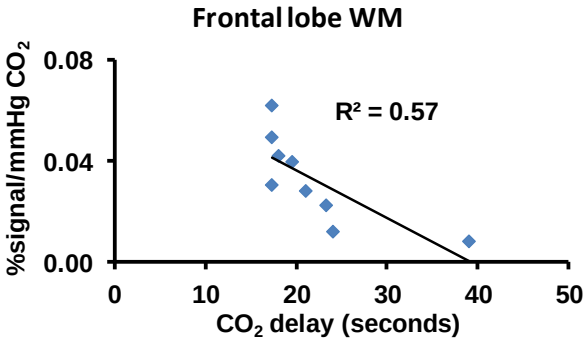

Figure 4-12: Negative correlation between delay in vascular response and magnitude of response to inhalation of CO_2 in the Frontal lobe in WM, significant at p = 0.02.

We also tested for this relationship within the WM layers and found a negative correlation between delays and % signal/mmHg O_2 for the WM layers, significant at p = 0.01, as seen in Figure 4-13 a. We also found a negative correlation between delays and % signal/mmHg CO_2 for the WM layers, significant at p = 0.008, shown in Figure 4-13 b. This data suggests that if a WM layer has a long vascular response delay, then that layer will have a small magnitude of response.

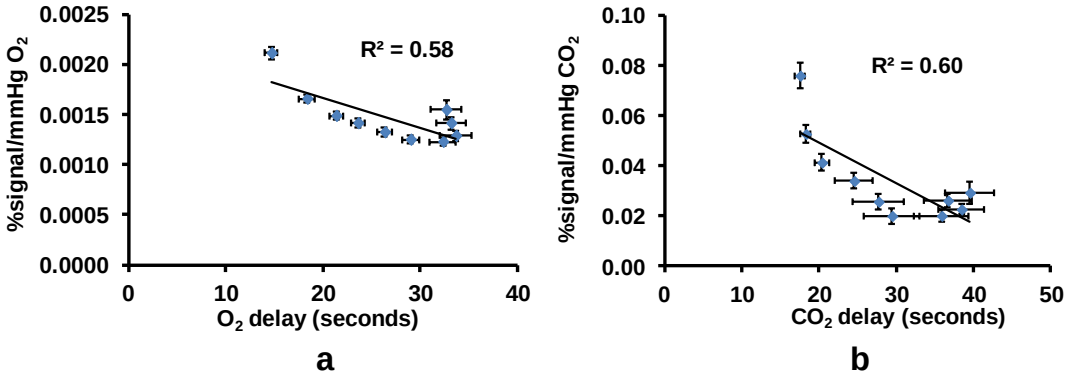

Figure 4-13: Negative correlation between delay in seconds and % signal/mmHg gas in the layers in the WM; (a) shows the relationship for the O_2 gas, significant at p =0.01 and (b) shows the relationship for the CO_2 gas, significant at p =0.008.

For each individual WM layer, across all nine subjects, we checked for the relationship between vascular response delay in a layer and its response magnitude. For the O_2 inhalation data we did not find a significant relationship. For the CO_2 data, we found a negative correlation between the vascular response delay in the layer and its response magnitude in each WM layer except in layer 6 which showed a positive correlation. In WM layers 3, 4 and 9, we found significant correlations as shown in Figure 4-14.

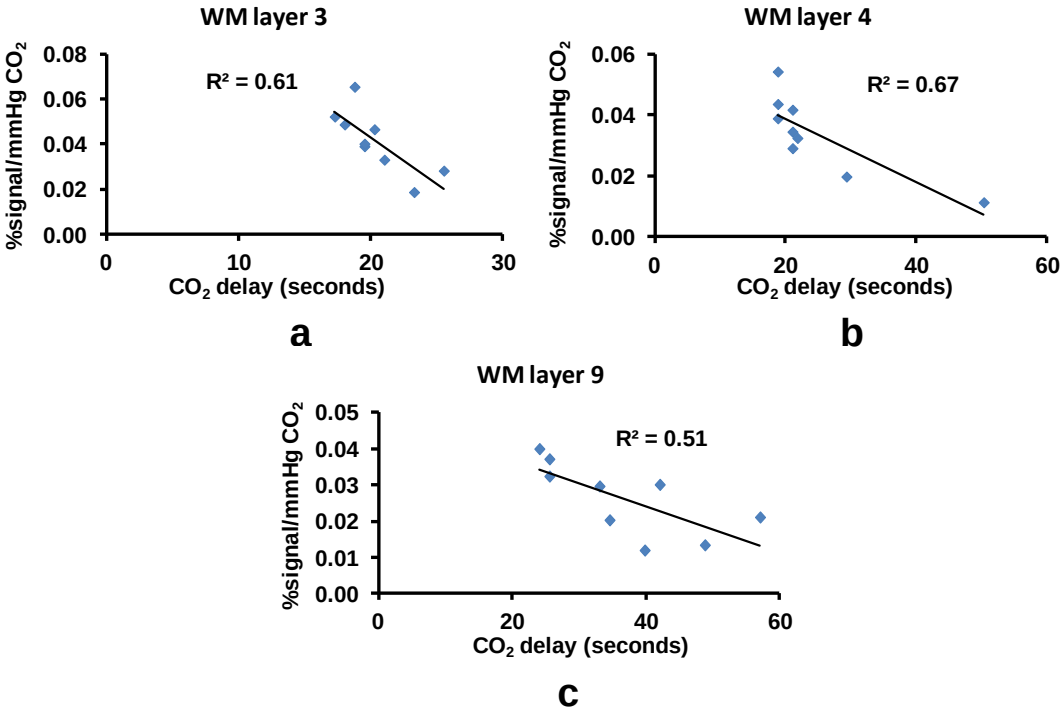

Figure 4-14: Relationship in WM layers across nine subjects between WM layer delay and its response magnitude (%signal/mmHg CO_2) to CO_2 inhalation, which shows a negative correlation; (a) shows this relationship for WM layer 3, significant at p = 0.01 (b) shows this relationship for WM layer 4, significant at p = 0.007 and (c) shows this relationship for WM layer 9, significant at p = 0.03.

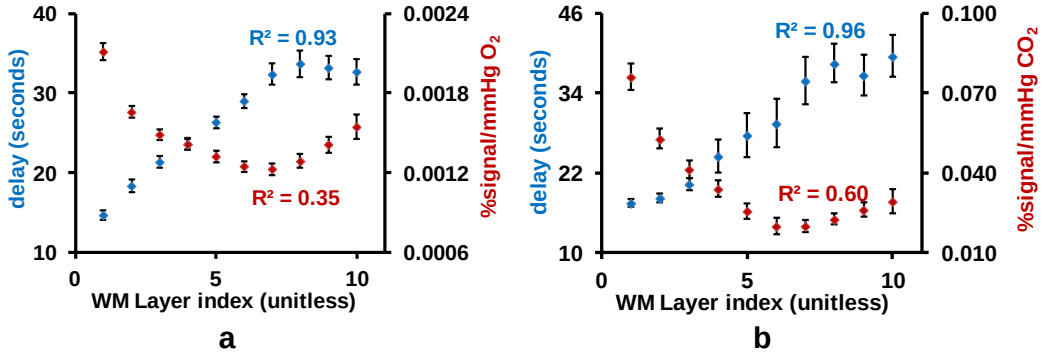

Figure 4-15: Relationship between WM layer index and vascular response delay, which shows a positive correlation, and the relationship between WM layer index and magnitude of vascular response, which is a negative correlation; (a) shows the relationship for the O_2 gas; the correlation between WM layer index and vascular response delay is significant at p = 0.00001, and the correlation between WM layer index and magnitude of vascular response is significant at a trend level of p = 0.07. (b) shows the relationship for the CO_2 gas; the correlation between WM layer index and vascular response delay is significant at p = 0.000001, and the correlation between WM layer index and magnitude of vascular response is significant at p = 0.008. Blue color indicates data from the correlation between WM layer index and vascular response delay and red color indicates data from the correlation between WM layer index and magnitude of vascular response. Error bar = standard error.

4.3.4 Relationship between WM Layer Index and Vascular Response

To understand the relationship between the WM layer indexes with their vascular response delay, we obtained Pearson's correlation coefficient, shown in Figure 4-15; in blue color is the correlation curve. Figure 4-15 a, shows the result of the correlation due to inhalation of the O_2 gas and Figure 4-15 b shows the result of the correlation due to inhalation of the CO_2 gas. The results show that with an increase in WM layer index i.e. as the depth of the WM from the cortical surface increases, the delay in vascular response also increases for both O_2 and CO_2 gas; data represented in blue color in Figure 4-15 a and Figure 4-15 b respectively. The response delay increases up to layer 8 and then it plateaus for layers 9 and 10; no significant difference was found between layers 8, 9 and 10. We also performed the same correlation analysis between the WM layer indexes and the magnitude of vascular response in these layers, shown in Figure

4-15 in red color. An opposite, negative correlation is seen between the magnitude of response (% signal/mmHg gas) and the layer index, i.e. as the layer index increases, the magnitude of response (% signal/mmHg gas) decreases for both O_2 and CO_2 gas; shown in red color in Figure 4-15 a and b respectively. For the O_2 gas, the magnitude of response increases in layers 9 and 10 and was found to be significantly different from layer 8 at a $p < 0.05$. No significant difference in magnitude of response was seen for the CO_2 data between layers 8, 9 and 10.

4.3.5 Reproducibility of Delays

We would also like to see if the measured delays in vascular response in the first BOLD scan are reproducible with those estimated from the second BOLD scan. To test for this, we measured Pearson's correlation coefficient between delays measured in each scan. We obtained the correlation between delays measured in the WM fiber tracts in the first BOLD scan with those measured from the second BOLD scan, separately for inhalation of O_2 and CO_2 gas. A positive correlation was seen to inhalation of the O_2 gas, significant at $p = 0.0001$, as shown in Figure 4-16 a. Delays measured due to inhalation of the CO_2 gas were also positively correlated between scans, significant at $p = 0.005$, shown in Figure 4-16 b.

We performed a correlation of delays measured in the lobes in WM between scans and found a positive correlation for both the O_2 and the CO_2 gas, but were not significant. For the WM layers, we performed this correlation and found that delays measured in the WM layers in the first scan (BOLD # 1) were positively correlated with the delays measured from the second scan (BOLD # 2). The correlations measured due to inhalation of the O_2 gas and that measured due to inhalation of the CO_2 gas were significant at $p < 0.000001$ and $p = 0.0001$ respectively, as shown in Figure 4-17.

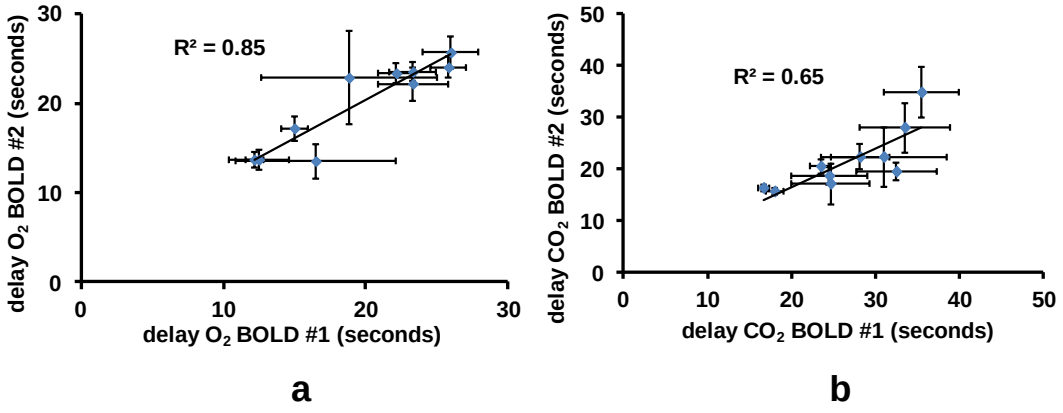

Figure 4-16: Correlation between delays measured for each scan (BOLD #1 and BOLD #2) for O_2 and CO_2 gas for the WM fiber tracts; (a) shows a positive correlation for the O_2 gas, significant at p = 0.0001, and (b) shows positive correlation for the CO_2 gas, significant at p = 0.005. Error bar = Standard error.

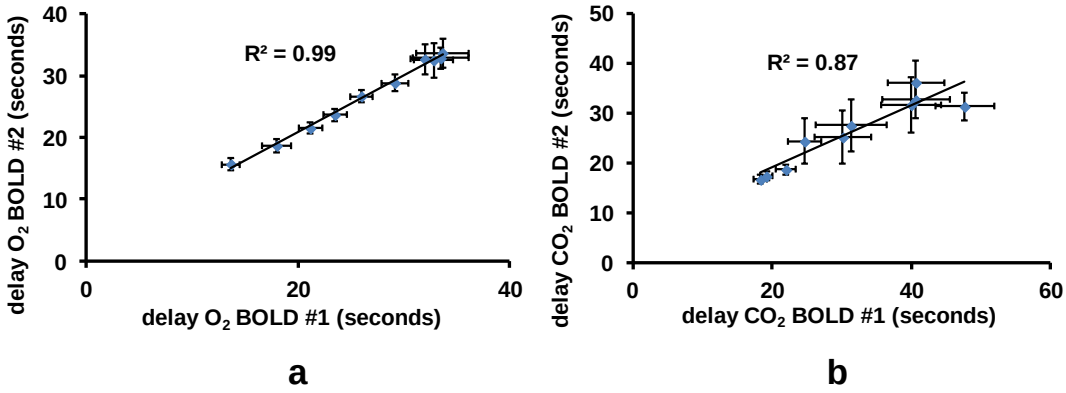

Figure 4-17: Correlation between delays measured for each scan (BOLD #1 and BOLD #2) for O_2 and CO_2 gas for the WM layers; (a) shows the correlation for the O_2 gas, significant at p < 0.000001, and (b) shows the correlation for the CO_2 gas, significant at p = 0.0001. Error bar = Standard error.

To estimate the reproducibility between the delays in vascular response measured in each BOLD scan, we measured the coefficient of variation (COV). The COV is measured by dividing the standard deviation of the delays measured in the first and

second scan by the average delay. The COV shows the extent of variability in relation to the mean.

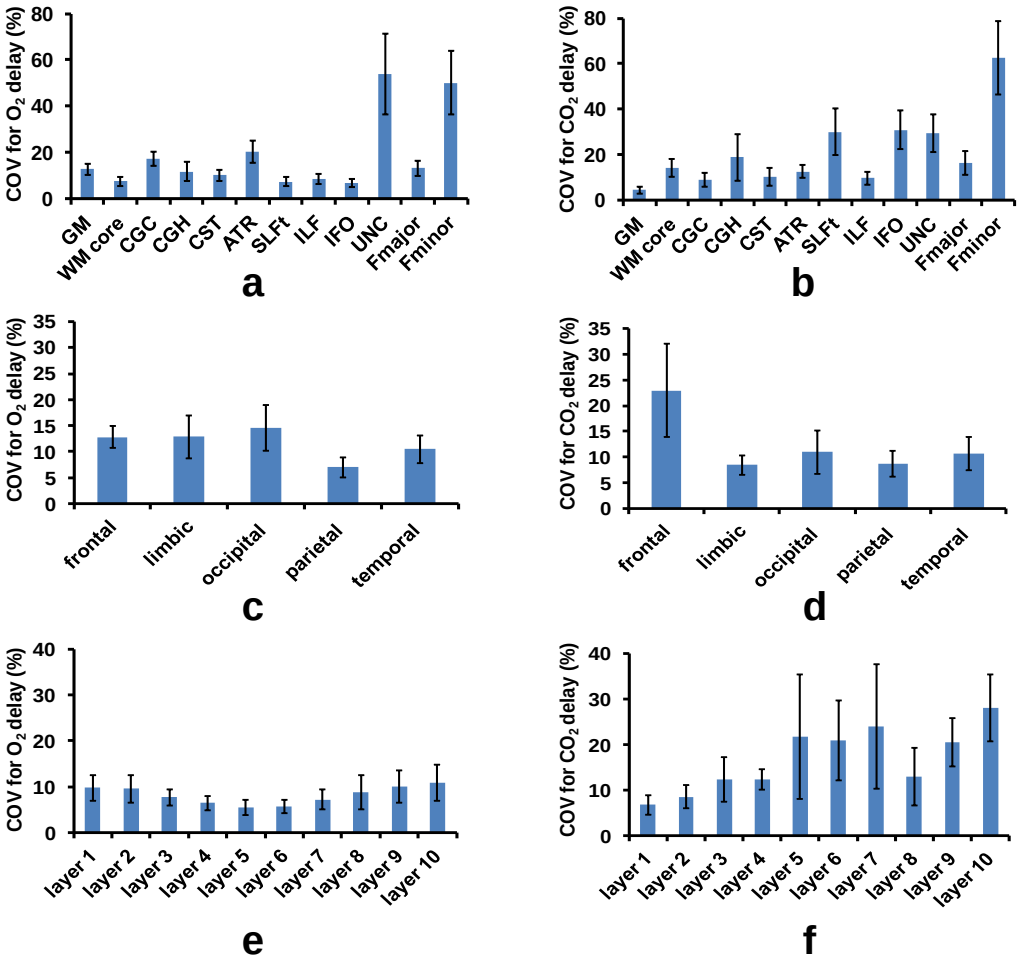

Figure 4-18: Coefficient of variation (COV) of the delays measured from GM, WM core, WM fibers, and the WM classified into cerebral lobes and from the WM layers. In (a) is shown COV of delays measured from GM, WM core and all 10 WM fibers for inhalation of the O_2 gas and (b) shows COV of delays measured due to inhalation of the CO_2 gas; (c) shows COV of delays measured from the WM from all cerebral lobes due to inhalation of the O_2 gas and (d) shows those values measured due to inhalation of the CO_2 gas; (e) shows the COV of delays measured for all WM layers for inhalation of the O_2 gas and (f) shows those values measured due to inhalation of the CO_2 gas. Error bar = Standard error.

The COV of the delays measured from the GM, core of the WM and all WM fibers for the O_2 gas is shown in Figure 4-18 a; and that measured for the CO_2 gas is shown in Figure 4-18 b. The COV for the delay measured from the GM for the O_2 gas is 12.6 ± 2.3 % and that measured from the core of the WM is 7.3 ± 2.1 %. The average COV delays for all 10 WM fibers for the O_2 gas is 19.7 ± 5.5 %; which is large and is mainly due to the COV from the UNC and the Fminor fibers. For the scans performed by inhalation of the CO_2 gas, the COV of delay measured from the GM was 4.4 ± 1.5 %, for the core of the WM it was 14.2 ± 3.8 % and the average COV of delays for all 10 WM fibers was 22.9 ± 7.1 %. The COV for delays measured for the cerebral lobes from the WM are shown in Figure 4-18 c for the O_2 gas and in Figure 4-18 d for the CO_2 gas. The average COV of delays for all lobes due to inhalation of the O_2 gas was 11.5 ± 3.0 % and from inhalation of the CO_2 gas was 12.3 ± 4.2 %. The COV for delays measured from the WM layers is shown in Figure 4-18 e for the O_2 gas and in Figure 4-18 f for the CO_2 gas. The average COV of delays for all WM layers due to inhalation of the O_2 gas was 8.2 ± 2.5 % and from inhalation of the CO_2 gas was 16.8 ± 6.7 %

4.3.6 Relationship between Delays for O_2 and CO_2

To estimate the relationship between the delays measured for the O_2 and the CO_2 gas, we obtained Pearson's correlation between delays measured for each gas. The delays measured for the O_2 and the CO_2 gas for the WM fibers were positively correlated, significant at a $p = 0.005$; shown in Figure 4-19 a. In Figure 4-19 a, a unity line is shown for comparison with the fitted trend line. The slope of the trend line indicates that the delays measured to the WM fibers by inhalation of CO_2 are longer compared to the delays measured due to inhalation of O_2. We found a negative correlation between the delays measured for the WM from the cerebral lobes, and did not find any significance, shown in Figure 4-19 b. For the WM layers we found a positive correlation for the delays

measured for the O_2 and the CO_2 gas, which was significant at a p = 0.000002, shown in Figure 4-19 c. Again the slope of the trend line in Figure 4-19 c indicates that the delays measured to the WM layers are longer due to CO_2 inhalation compared to those measured due to O_2 inhalation.

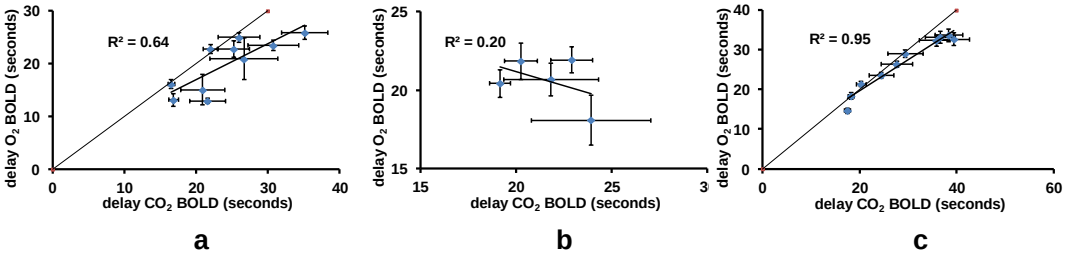

Figure 4-19: Relationship between delays measured for inhalation of O_2 and CO_2 gas for the WM fibers, WM contained within the cerebral lobes and the WM layers; (a) shows a positive correlation for data from the WM fibers, significant at p = 0.005; (b) shows a negative correlation for data from the WM contained within the cerebral lobes and (c) shows a positive correlation for data from the WM layers, significant at p = 0.000002. Error bar = Standard error.

4.3.7 Fractional Anisotropy from the 10 Major Fiber Tracts

For the 10 WM fiber tracts, we have measured the Fractional Anisotropy (FA), which is an index of the structural integrity within the WM, these values are shown in Figure 4-20 and are comparable to those reported previously [115].

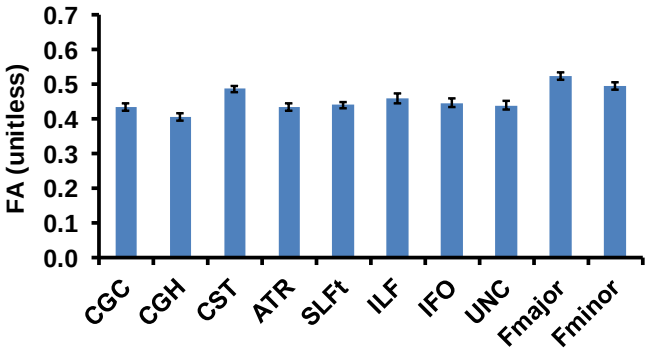

Figure 4-20: Fractional Anisotropy (FA) for individual fiber tracts in the WM

Table 1, Table 2 and Table 3 provide relevant information for the WM fiber tracts, lobes and WM layers respectively.

Table 4-1: FA, magnitude of vascular response and delay in response to O_2 and CO_2 inhalation, probability of WM, and ROI volume for 10 major fiber tracts.

ROI	FA	%BOLD/mmHg O_2	O_2 Delay (s)	%BOLD/mmHg CO_2	CO_2 Delay (s)	Probability	ROI volume (cm^3)
CGC	0.435	0.0018	16.1	0.0788	16.5	0.986	3.01
CGH	0.406	0.0027	12.9	0.0903	21.6	0.971	0.52
CST	0.486	0.0016	22.8	0.0423	22.0	0.989	6.70
ATR	0.434	0.0023	13.1	0.0850	16.8	0.987	7.19
SLFt	0.440	0.0014	24.9	0.0285	26.0	0.991	4.90
ILF	0.460	0.0015	25.8	0.0289	35.2	0.988	4.82
IFO	0.446	0.0015	23.4	0.0295	30.8	0.989	7.94
UNC	0.439	0.0015	15.0	0.0372	20.9	0.985	3.63
Fmajor	0.524	0.0017	22.8	0.0457	25.3	0.983	7.24
Fminor	0.496	0.0010	20.8	0.0039	26.7	0.988	10.53
WM core	0.372	0.0014	32.8	0.0248	37.4	0.999	6.06

Table 4-2: magnitude of vascular response and delay in response to O_2 and CO_2 inhalation, and ROI volume for WM classified into cerebral lobes.

ROI	%BOLD/mmHg O_2	O_2 Delay (s)	%BOLD/mmHg CO_2	CO_2 Delay (s)	ROI volume (cm^3)
frontal	0.0014	20.7	0.0329	21.8	105.63
limbic	0.0015	20.4	0.0476	19.2	24.04
occipital	0.0018	18.1	0.0629	23.9	9.23
parietal	0.0015	21.8	0.0468	20.3	27.28
temporal	0.0017	21.9	0.0429	22.9	29.93

Table 4-3: magnitude of vascular response and delay in response to O_2 and CO_2 inhalation and ROI volume for WM layers

ROI	%BOLD/mmHg O_2	O_2 Delay (s)	%BOLD/mmHg CO_2	CO_2 Delay (s)	ROI volume (cm^3)
layer 1	0.0021	14.7	0.0760	17.5	97.99
layer 2	0.0017	18.3	0.0528	18.3	56.80
layer 3	0.0015	21.3	0.0414	20.3	35.90
layer 4	0.0014	23.6	0.0340	24.5	23.28
layer 5	0.0013	26.3	0.0257	27.7	16.26
layer 6	0.0012	29.0	0.0201	29.4	11.75
layer 7	0.0012	32.3	0.0201	35.8	7.30
layer 8	0.0013	33.7	0.0227	38.4	3.76
layer 9	0.0014	33.2	0.0262	36.7	1.68
layer 10	0.0015	32.7	0.0294	39.5	0.62

4.4Discussion

4.4.1 Delays

The present study conducted a thorough examination of the vascular response in the WM to inhalation of both O_2 and CO_2 gas. This according to us is one of the first few studies to look at the vascular response in the WM to both O_2 and CO_2 gas by classifying white matter in three different ways: fiber tracts, lobes and layers.

One of the main findings in this paper is that the delays measured using the O_2 gas i.e. the time it takes for the O_2 gas to travel from the lungs to the brain and for O_2 to be detected using the BOLD MRI sequence, are long. These delays can primarily be attributed to the time it takes for extravascular (tissue) partial pressure of O_2 to reach steady state. In the GM this delay was 11.5 ± 0.6 seconds and in the core of the WM it was 32.8 ± 1.1 seconds. Delays in the GM and core of the WM to the O_2 gas are comparable to the long delays measured by the CO_2 gas [18]. The delay measured to the core of the WM was significantly longer than that measured to the GM owing to the lower CBF in the microvasculature in the WM, because of which it takes longer for WM partial

pressure of O_2 to reach steady state in the WM. The core of the WM shows vascular response to O_2, 21 seconds after the vascular response to O_2 in the GM. 21 seconds is not a very long time for partial pressure of O_2 to reach steady state within the core of the WM, given that partial pressure of O2 builds up by the process of diffusion, i.e. the O2 gas diffuses through tissue space. This data may suggest that vascular supply may be not be spread too far apart from each other, i.e. blood vessels within the WM tissue space may be present at least few millimeters apart. The average delay measured with the O_2 gas for all fiber tracts was 19.8 ± 1.5 seconds; the average delay in the WM contained within the broad cerebral lobes is 20.6 ± 1.1 seconds, and the average delay in the WM layers is 26.5 ± 1.1 seconds. For the CO_2 gas, the delay in the GM was 15.7 ± 0.5 seconds, which was significantly different compared to that measured for the O_2 gas at $p = 0.0002$. Delay in the GM to inhalation of the CO_2 gas is similar to those reported previously [18]. In the core of the WM, the delay due to the CO_2 gas was measured at 37.4 ± 4.0 seconds and was not significantly different from that measured with the O_2 gas. The delay measured in the core of the WM to inhalation of the CO_2 gas is similar to that reported previously due to CO_2 inhalation, no significant difference was seen between the delay measured in this study and that measured in Chapter 3 [18] ($p = 0.56$). Within the WM fiber tracts, the average delay was 24.2 ± 2.4 seconds and was significantly different at $p = 0.003$ compared to that measured using the O_2 gas. In the WM lobes the average delay to the CO_2 gas was 21.6 ± 1.6 seconds, but not different from that measured using the O_2 gas. Average delay in the WM layers due to the CO_2 gas was 28.8 ± 2.4 seconds, which was not significantly different from that, measured using the O_2 gas. The average delays measured to the core of the WM were the longest compared to all ROIs examined. This core of the WM is comprised of WM layer 8, layer 9 and layer 10, i.e. the core of the WM was obtained after peeling off 7 WM layers. Longest

delays in the core of the WM may suggest that this region may contain the smallest of vasculature compared to vasculature contained in all other ROIs.

Average delays measured due to the CO_2 gas in each ROI: the WM fiber tracts, WM lobes and the WM layers were longer compared to those measured using the O_2 gas. This is also evident in the O_2 and CO_2 delays reported from individual ROIs as shown in Figure 4-4, where delays using the CO_2 gas were longer compared to those measured using the O_2 gas; these delays were significantly different for the GM ROI, the fiber tracts: CGH and ATR and for WM layer 1 and layer 10. These results are confirmed with a significant positive correlation between the delays measured due to O_2 and CO_2 gas to the WM fiber tracts, significant at $p = 0.005$ and the delays measured to the WM layers significant at $p = 0.000002$, as shown in Figure 4-19 a and Figure 4-19 c respectively. Both Figure 4-19 a and Figure 4-19 c support above results that delays measured to the fiber tracts and the layers in the WM due to CO_2 inhalation are longer than those measured due to inhalation of the O_2 gas. This difference in delays measured due to O_2 and CO_2 gas could be because of the difference in the mechanism of vascular response elicited by each of these gases. The CO_2 gas stimulates the smooth muscles on the arterial vessel walls, which causes the arterial vessels to dilate and bring in more oxy-hemoglobin, which is detected in the venous vessels. The O_2 gas acts as a bolus and after achieving steady state within cerebral tissue, it enters the venous vessels where it is detected. Thus the cerebrovascular reactivity caused by the CO_2 gas may be the reason for the longer delays compared to the delays measured due to inhalation of O_2 gas. Among all WM layers, only WM layers 1 and 10 show significant differences between delays measured due to O_2 and CO_2. WM layer 1 contains the largest blood vessels among all WM layers and WM layer 10 contains the smallest of microvasculature compared to all WM layers. This suggests that the most obvious differences between the

delays measured due to O_2 and CO_2 gas are seen in these layers and that CVR is most different in the largest and smallest vessels compared to those intermediate size vessels, located in WM layers 2 through 9.

We also tested the relationship between O_2 and CO_2 delays across all nine subjects for all ROIs. We found a positive correlation between the delays measured due to O_2 and CO_2 for the GM, WM core and all fiber tracts in the WM except in the SLFt fiber in which we found a negative correlation that was not significant. Shown in Figure 4-21 is the correlation between O_2 and CO_2 delays to the UNC fiber tract, which was significant at $p = 0.008$.

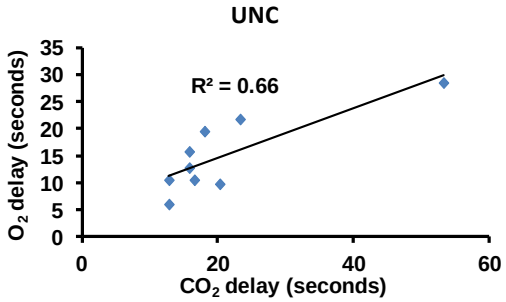

Figure 4-21: Positive correlation between delays measured due to CO_2 and O_2 gas for the UNC fiber tract, significant at $p = 0.008$.

We also tested for the relationship between O_2 and CO_2 delays measured to each of the WM layers across all nine subjects. For each layer, we found a positive correlation between the O_2 and CO_2 delays; the correlation to WM layer 7 was significant at $p = 0.01$. These data suggest that if a subject has a short O_2 delay, then that subject also has a short CO_2 delay as well.

For the WM classified into the broad cerebral lobes, we did not find a correlation ($p = 0.45$) for the delays measured due to inhalation of the O_2 and the CO_2 gas as shown in Figure 4-19 b. It has to be noted that the WM from the cerebral lobes contains all WM

thresholded to contain 95% or more WM; the cerebral lobes contain WM adjacent to the cortical surface as well as deeper WM. So, we speculate that the reason we did not find a correlation between the O_2 and CO_2 delays in the cerebral lobes, could be due to partial volume effects from the WM adjacent to the cortical surface. We also tested for the correlation between O_2 and CO_2 delays in individual lobes across all 9 subjects and found a positive correlation for all lobes except in the temporal lobe, where we found negative correlation.

4.4.2 Differences in Delay between ROIs

To test for differences between delays within WM fiber tracts, we compared a fiber tract's delay to those measured from all other fiber tracts and shown in Figure 4-5 is the difference matrix for delays measured due to O_2 inhalation. Few fiber tracts show significant differences (blue color in Figure 4-5) in delay measured due to inhalation of the O_2 gas. These results suggest that there may be differences in supply of blood vessels to these fiber tracts. The results for the CO_2 inhalation data show differences in delay between the CGC and CST fibers, which may indicate differences in CVR in these fibers. The delays from the CO_2 inhalation data may also be more variable compared to the delays measured for O_2 inhalation which may be the reason why we see differences only between two fiber tracts for the CO_2 data. For the lobe data, we found differences only in the CO_2 data between the temporal and limbic lobes and between temporal and parietal lobes significant at $p < 0.05$, Bonferroni corrected.

For the WM layers, we found that delays measured due to the O_2 gas were different for most layers as shown in Figure 4-6 a. This may be indicative of blood supply differences in the WM layers. This is expected, because as the WM layer index increases, i.e. as the distance of the WM from the cortical surface increases, the size of the blood vessels are expected to decrease. Blood vessels are known to penetrate from

the cortical surface and then perfuse the WM; the vessels are expected to have larger diameter on the cortical surface and vessel diameter is expected to decrease as it penetrates deeper into WM. For delays in WM layers due to inhalation of CO_2 gas, we found that the WM layers closest to the cortical surface (layer # 1,2,3,4) were different from the deepest WM layers (layer # 8, 9 and 10) as shown in Figure 4-6 b. These data may suggest that there are differences in CVR in the arterial vessels present in the WM layers near the cortical surface compared to those present in the WM furthest away from the cortical surface.

4.4.3 Magnitude of Vascular Response

The magnitude of vascular response due to O_2 and CO_2 gas was measured for all ROIs and reported in Figure 4-7. As seen in Figure 4-7, the largest magnitude of signal response was seen in the GM for both O_2 and CO_2 gas and all other WM ROIs showed smaller vascular response. The magnitude of vascular response to O_2 in the GM is approximately four times as large as the magnitude of vascular response in the core of the WM, which may be indicative of the blood volume within each compartment, this finding is similar to those reported previously [21]. The magnitude of response in the GM to CO_2 is approximately 8 to 10 times as large as the magnitude of response in the core of the WM, which may suggest that CVR in the GM is approximately 8 to 10 times as large as the CVR in the WM. For the O_2 gas and the CO_2 gas, the core of the WM shows smaller magnitude of vascular response compared to the fiber tracts in the WM, which may suggest that the core of the WM may have lesser blood supply and smaller CVR compared to the fiber tracts. The average magnitude of vascular response for the WM from the cerebral lobes was higher than the magnitude of response from the core of the WM, which may suggest that the WM from the cerebral lobes may have some partial volume effects from WM regions located closer to the cortical surface. The vascular

response magnitude in the WM layers for the O_2 and the CO_2 gas shows similar findings, i.e. the signal in layer 1 is the highest compared to all other layers and the magnitude keeps decreasing until layer 7 after which the signal increases in WM layers 8, 9 and 10, as seen in Figure 4-7 c and Figure 4-7 f. This decrease in signal in WM layers with increase in depth from the cortical surface is expected as the blood supply and CVR is anticipated to decrease in deeper WM layers. The increase in signal in WM layers 8, 9 and 10, may suggest that blood vessels may be penetrating those layers from the midline of the brain as well as from the lateral cortical surface. This data also indicates that layers 8, 9 and 10 may contain more blood supply, and the combined CVR from these layers is higher than that from adjacent WM layers.

4.4.4 Differences in Magnitude of Vascular Response between ROIs

We also compared the magnitude of vascular response between fibers and found that for the O_2 data, only few fibers show significant differences as shown in Figure 4-9 a, which indicates that the vascular response to O_2 is similar in most fibers, probably due to similar supply of blood vessels to the fiber tracts. For the CO_2 data, we find that more fibers show significant differences between the magnitudes of response as shown in Figure 4-9 c, which may indicate that CVR between fibers are different. An interesting finding from the WM layers is that the magnitude of response to O_2 for WM layer 9 was significantly larger than that for layer 8, as seen in Figure 4-9 b, which may indicate that layer 9 may have larger blood supply compared to layer 8. We do not see a difference between layers 8 and 9 for the CO_2 data.

4.4.5 Relationship between Delay and Magnitude of Vascular Response

We found a negative correlation between the vascular response delay and the magnitude of vascular response in the WM fibers for O_2 inhalation significant at $p = 0.03$. We found a negative correlation for CO_2 inhalation as well, significant at $p = 0.02$,

Bonferroni corrected. This data indicates that in the WM fiber tracts, if a fiber tract has a short delay, that fiber tract shows a large magnitude of vascular response. We also found this negative correlation for all individual fiber tracts across all nine subjects, for both O_2 and CO_2 data. In the WM layers also, we found that the negative correlation between response delay and magnitude of vascular response for both the O_2 and the CO_2 inhalation; data were significant at $p = 0.01$ and at $p = 0.008$ respectively. The cerebral lobes in the WM also show the same negative correlation, but no significance. Thus the relationship between response delay and response magnitude was negative for most ROIs examined in this study. These data suggest that if blood supply to a ROI is high, as indicated by a large magnitude of vascular response then that ROI will have a smaller delay in vascular response. In the case of the CVR response, if the vascular reactivity of the blood vessels from an ROI is large, then that ROI will show a smaller delay in vascular response to CO_2.

4.4.6 Reproducibility of Delays

We found a positive correlation between delays measured from the first BOLD and that measured from the second BOLD scan for the WM fiber tracts (Figure 4-16), for both O_2 and the CO_2 gas, both significant at $p = 0.0001$ and $p = 0.005$ respectively. We found a similar positive correlation for the WM layers (Figure 4-17) for both O_2 and the CO_2 gas, significant at $p < 0.000001$ and $p = 0.0001$ respectively. For the WM lobes, we found a positive correlation, but it was not significant at $p < 0.05$. This indicates that for each ROI, if BOLD scan # 1 has a long delay then that ROI has a long delay for the BOLD scan # 2 as well. We also quantified the variation between BOLD scan # 1 and BOLD scan # 2, by measuring the coefficient of variation between scan # 1 and scan # 2 for each gas; the result is shown in Figure 4-18. We found that the coefficient of variation was highest for the Fminor fiber tract, which was approximately 50% for the O_2 gas and

60% for the CO_2 gas. The Fminor fiber is located in the frontal lobe, very close to the sinuses and high COV in the Fminor fiber tract may suggest that the magnetic field may not be well estimated in this region owing to susceptibility issues caused by air spaces in the sinus cavity. The magnetic field bends in tissue that is near air spaces, which causes distortions in the image that are worse especially in the BOLD image. Average COV for the WM fiber tracts was 19.7 ± 5.5 % for delays estimated using the O_2 gas; COV of delays estimated to WM fiber tracts using the CO_2 gas was 22.9 ± 7.1 %. Thus for the WM fiber tracts, the COV of delays due to the CO_2 gas was higher, but not significantly different from that measured for the O_2 gas. In the WM from the cerebral lobes, we found that average COV of delays for the O_2 gas was 11.5 ± 3.0 % and that for the CO_2 gas was 12.3 ± 4.2 %; not significantly different. In the WM layers, the COV for delays due to the O_2 gas was 8.2 ± 2.5 % and due to the CO_2 gas, was 16.8 ± 6.7 %; the O_2 and CO_2 data were significantly different at $p = 0.006$.

4.4.7 Limitations

The findings from the present study need to be interpreted in view of a few limitations. First, this study has only examined the cerebrovascular reactivity using fixed CO_2 inhalation, but has not tested other types of vasodilatative challenges such as breath hold [80], injection of acetazolamide [81], prospective end-tidal targeting [49], or dynamic end-tidal forcing [48]. Thus, our results should be interpreted within the scope tested. Second, high temporal resolution in data acquisition (e.g. short TR of 1000ms or less) is desired in order to accurately depict time delays in the signal. Third, the resolution of the DTI image is 2.5 × 2.5 × 2.5 mm^3, which may be less and may contribute to partial volume effects from surrounding GM. Acquiring data at a resolution of 2.0 × 2.0 × 2.0 mm^3 or higher is desirable and may lower the contribution of partial volume effects from

GM. This increase in resolution may require multiple averages of DTI data acquisition to obtain similar SNR.

4.4.8 Implications for Future Research

Inclusion of larger number of participants is important to confirm the findings from this study and to establish typical values of vascular response delay and magnitude of vascular response from WM fiber tracts for young healthy volunteers.

Including elderly participants in the study will help examine the effects of age on blood supply and CVR in the fiber tracts and in the layers in WM. An increase in CBF and CVR was seen with age in the core of the WM, as found in Chapter 3; it would be paramount to examine if similar findings are seen in the WM fiber tracts and the layers in WM. Data acquisition with higher resolution and a shorter TR (less than 1000ms) is definitely warranted to confirm the delay measurements from this study. Future studies must include patients that may have insufficiencies in WM for example a study on multiple sclerosis patients is important to confirm if disease processes result in a diminished vascular response to O_2 and CO_2; Multiple sclerosis is associated with axonal demyelination and thus deficits in vascular response are an expected outcome. There is also a possibility that the WM fiber tracts may also suffer from partial volume effects, especially if the tract traverses in close proximity to gray matter structures, for example the Anterior Thalamic Radiation (ATR) tract is adjacent the thalamus and the Cingulum to Hippocampus (CGH) tract is adjacent the hippocampus. A method to erode the fiber tracts would be most appropriate, such that only the core of the fiber tract is used for examination of vascular responses. A post-processing method that can be used in future studies of the WM is Tract Based Spatial Statistics (TBSS) [116], in which the fiber tracts from each participant are transformed into MNI template space and then skeletonized to include only the inner core of the fiber tract. Transforming the fiber tract into MNI space

may smooth the tract, causing partial volume effects, but skeletonizing the tract removes some of the PVE; however the benefits of skeletonization outweighs the ill effects of smoothing.

4.5 Conclusions

The white matter in brain was the focus of the study and it was characterized into fiber tracts, lobes and layers. Brain vascular response to inhalation of both O_2 and CO_2 were measured from these WM regions. One of the main findings from the study is that delays measured from the Et O_2 to the vascular response in all ROIs are long, on similar order as that measured due to CO_2. Another important finding is that the delays due to CO_2 were longer compared to those measured due to O_2. It was suggested that the differences in delay measured due to the O_2 and the CO_2 gas were due to differences in the mechanism of action of these gases on the vasculature in brain. The WM fiber tracts and layers show differences in delays and magnitude of response to both CO_2 and O_2 gas. Differences in ROIs due to the CO_2 gas may indicate differences in CVR, while differences in ROIs due to the O_2 gas may indicate differences in blood supply to those ROIs. Measurement of delays for each of these ROIs was also shown to be reproducible between scans.

Chapter 5

Life-Long Aerobic Exercise Preserved Baseline Cerebral Blood Flow but reduced Vascular Reactivity to CO_2

5.1 Introduction

Beneficial effects of aerobic exercise on human health have been a topic of research for several decades. It is well established that exercise improves cardiovascular function [32, 33, 117]. Recently, improvement in brain health has also been demonstrated as an apparent benefit of aerobic exercise. Older adults undergoing fitness training showed greater cognitive function in multiple domains including executive function, controlled processes, visuospatial processing, and motor speed, compared to non-exercise group [118]. Efforts are now being directed toward understanding the mechanisms of such salutary effects. Previous research has demonstrated several aspects of changes in brain structure and function. Colcombe and colleagues showed that brain tissue density was better preserved in high-fit elderly compared to low-fit ones [119]. Studies have also demonstrated that age-related decline in white matter structural integrity was ameliorated by aerobic exercise [36]. It was also shown that, when performing a spatial processing task, high-fit individuals showed greater brain activity in the prefrontal and parietal cortices [34]. Exercise was also proposed to promote neurogenesis in dentate gyrus of the hippocampal formation [120]. Some of these alterations are thought to be supported or mediated by improvement in cerebrovascular function. Indeed, the effect of short-term (<1 year) aerobic exercise on cerebrovascular health has been reported, primarily in animals [37-39] but also starting to be explored in humans [121].

To probe the prospective benefits of long-term aerobic exercise, we used a cross-sectional design in this study and compared a group of elderly Masters Athletes

(MA) to a sedentary elderly group (SE). MA are individuals who participate in competitive sports at a very high level even at an age that exceeds the typical peak age for the event. The MA recruited in this study were all endurance runners and have undergone life-long aerobic training. Thus, this group of individuals represents a unique group of sample on the highest end of the fitness level spectrum. Previous studies have shown that MA has preserved cardiovascular and peripheral vascular systems compared to sedentary elderly controls, including greater cardiac stroke volume [122], lower aortic stiffness [123, 124], and higher ventricular compliance [122]. However, properties of brain vasculature, in particular microvasculature, in the MA have not been fully characterized.

The cerebrovascular parameters examined in the present study were determined with MRI techniques and included a baseline measure, Cerebral Blood Flow (CBF), and a measure reflecting dynamic properties of the vessels, Cerebral Vascular Reactivity (CVR) to CO2. Previous brain aging studies have established that both parameters decrease with age [9, 125], but CVR was the more age-sensitive vascular marker [9]. We hypothesize that life-long aerobic exercise may promote brain vascular health by "reversing" some of the age-decline effects.

5.2 Methods

5.2.1 Subjects

This study was approved by the Institutional Review board of the University of Texas Southwestern Medical Center. All subjects gave informed written consent before participating in the study. Ten MA, ten SE and nine sedentary young controls (YC) participated in the study. The demographic information of the participants is summarized in Table 5-1. All MA were ranked in either regional or national events and were recruited from running clubs or from records of competitive running events. Masters athletes were consistent age-group place winners at regional and national endurance events and had

participated in regular competitions for 23±8 years with a weekly running mileage of 32±10 miles or equivalent swimming or cycling. SE subjects were recruited with news letters or from senior centers. Subjects recruited into the sedentary groups do not exercise for more than 30 minutes, three times per week [126]. The YC were also sedentary subjects and were recruited to serve as a control group to verify the effect of age on brain vascular health. All subjects were healthy with no medical problems based on medical history data and physical exams. Subjects were excluded if they had any cardiovascular (e.g. hypertension, Type 2 diabetes) or cerebrovascular diseases (e.g. history of stroke, transient ischemic attack), major psychiatric or neurological disorders, dementia or substance abuse, or contraindications to MRI.

Table 5-1: Demographic information of the study participant; MA, Masters Athletes (N=10); SE, Sedentary Elderly (N=10); YC, Young Control (N=9).

	Age (years)	**Gender**	**Education (years)**	**$EtCO_2$ at 5% CO_2 (mmHg)**	**$EtCO_2$ at rest (mmHg)**	**$EtCO_2$ Difference (mmHg)**
MA	74.5±5.8	7M/3F	16.7±1.8	44.8±3.9	35.0±4.4	9.8±1.6
SE	75.4±5.6	8M/2F	16.4±1.9	45.4±2.9	36.1±4.5	9.3±2
YC	27.0±3.6	5M/4F	14.7±1.6	47.2±1.8	39.1±2.2	8.1±1.5

5.2.2 Testing of Peak Oxygen Consumption (Vo_{2max})

Maximal oxygen uptake was assessed in MA and SE groups using a modified Astrand-Saltin protocol on a treadmill described previously [127]. Briefly, prior to Vo_{2max} testing, subjects were asked to undergo two sub-maximal stages of steady state exercise to measure cardiovascular and ventilatory responses. Cardiac output (acetylene re-breathing method) and body oxygen consumption (Vo_2) were measured at rest, during

each steady state, and immediately following peak exercise. Ventilatory gas exchange was assessed with the Douglas bag technique: gas fractions by mass spectrometry (MGA 1100, Marquette, MI); ventilatory volume by a Tissot spirometer. Vo_{2max} were determined by meeting at least 3 of the following criteria: 1) Vo_2 ceased to increase with increasing workloads (plateau), 2) heart rate (HR) reached the age-predicted value (220 – age), 3) respiratory exchange ratio(RER) > 1.1, and 4) blood lactate > 8.0 mmol/l.

5.2.3 MRI Experiment

MRI scans were performed on a 3 Tesla Philips Achieva system (Philips Medical Systems, Best, The Netherlands). An 8 channel transmit/receive head coil was used for all MR scans. CBF data were acquired using a Pseudo-Continuous Arterial Spin Labeling (pCASL) technique, which were previously validated with a radiotracer method [47]. 30 control and label pairs of images were acquired using an EPI acquisition with following parameters: labeling duration 1650ms, post-labeling delay 1525ms, TR/TE/FA = 4000ms/13.81ms/90°, voxel size = 3.0 x 3.0 x 7 mm^3, FOV = 240 x 240 mm^2, 17 slices, and thickness = 7 mm, scan duration = 4 minutes.

CVR response to CO2 was measured using a hypercapnia (inhalation of 5% CO_2 mixed with 21% O_2 and 74%N_2) protocol described previously [17]. Alternating blocks of room air (1 minute) and hypercapnia (1 minute) was inhaled by the subject while Blood-Oxygen-Level-Dependent (BOLD) images were acquired continuously for 7 minutes. Compared to long-duration CO2 paradigm, this 1-min paradigm has been shown to improve subject comfort while maintaining the quality of the data [17]. Another advantage of the short block design is that potential effect of MRI signal drift could be reduced. The imaging parameters were: TR/TE/FA = 3000ms/30ms/90°, voxel size = 1.72 x 1.72 x 6 mm^3, FOV = 220 x 220 mm^2, 25 slices, and thickness = 6 mm. The air/gas mixture was delivered using a Douglas bag and switching between room air and CO_2 was achieved

via a valve on the bag. The air/gas mixture was delivered to the subject via a mouth piece and a nose clip was used to stop nasal breathing. End-tidal CO_2 (Et CO_2) is the partial pressure of CO_2 at the end of an exhaled breath and was measured using a capnography monitor (Capnograd, model 1265, Novametrix Medical Systems, Wallingford, CT) during the experiment; Et CO_2 is an indicator of the vasodilatory input to the brain. Other physiologic parameters including breath rate, heart rate and arterial oxygenation were also measured during the experiment by a physiology monitor (MEDRAD Inc., Pittsburgh, PA). CVR data from two MA were not usable because one subject did not have a stable breathing pattern during the experiment and for the other subject an experimental error occurred during the scan. Data from one YC was not usable as the mouthpiece fell off during the experiment.

A T_1-weighted structural image was acquired for anatomic reference with following parameters: TR/TE/FA = 8.14ms/3.73ms/12°, shot interval 2100ms, TI = 1100ms, voxel size = 1.0 x 1.0 x 1.0 mm^3, FOV = 256 x 256 mm^2, 160 slices, and thickness = 1 mm.

5.2.4 MRI Data Processing

For CBF data, the difference between the label and control images were calculated and the CBF map was obtained using a perfusion kinetic model similar to that described by Chalela et al. [128] and Wang et al. [129]. Specifically, CBF was computed by:

$$CBF = \frac{S_{ASL} \cdot \lambda \cdot e^{w/T1}}{2\alpha \cdot T1 \cdot M_0} \tag{7}$$

where w is the post-labeling delay time (1525ms), α is the labeling efficiency (0.86) [63], λ is the blood-brain partition coefficient (0.9 ml/g) [130]. Note that here we used the average of blood and tissue T_1 for the parameter "T_1" (1279ms) [59, 131],

because the labeled spins will spend some time in the blood and some in the tissue space. M_0 is the equilibrium magnetization of the tissue, which was estimated from the control image but accounting for the T1 relaxation of the static spins.

CVR data were processed using procedures described in the literature [9, 17, 132]. First, the time lag between the Et CO_2 time course and global BOLD response was calculated by shifting the Et CO_2 time course one second at a time until maximum cross correlation was obtained. Note that the BOLD time course always lag behind the EtCO2 because it takes some time for the blood in the lung (where the Et CO_2 was measured) to travel to the heart and be pumped to the brain and for the brain vessels to react to the higher CO_2 level (when the BOLD change occurred). Next, the shifted Et CO_2 trace was used as a regressor in the Statistical Parameter Mapping's General Linear Model to estimate the CVR on a voxel-by-voxel basis. The CVR has units of % BOLD signal change per mmHg of EtCO_2 change (% BOLD/mmHg CO_2).

5.2.5 Statistical Analysis

Before the vascular parameters were compared across groups, the images were spatially registered to the MNI template using an elastic registration algorithm, Hierarchical Attribute Matching Mechanism for Elastic Registration (HAMMER) proposed by Shen and Davatzikos (2002), which detects and corrects for region-specific brain atrophy [133]. This feature is important to ensure that the comparison truly reflects vascular parameters rather than brain volume reduction.

When comparing the vascular data between subject groups, the following strategy was used [134]. Absolute values of the whole-brain were first compared to examine whether a difference is present. If so, Region-of-interest (ROI) or voxel-wise analyses will continue to use the absolute values. On the other hand, if no global difference is present, the ROI and voxel-wise comparisons will use relative values

(normalized against whole-brain value for each subject). When global difference is not present, the use of relative values have been shown to be more sensitive in detecting regional differences owing to its reduction of subject-to-subject physiologic variations [134].

ROI analysis was performed using MNI template space ROIs defined by Automated Anatomical Labeling (AAL) software [135]. ROIs consisted of frontal, temporal, parietal and occipital lobes, subcortical gray matter, insula, cerebellum, and the entire cerebrum. The left and right sides were combined. The T_1-weighted image was segmented into gray matter (GM), white matter (WM) and cerebrospinal fluid (CSF) using a probabilistic algorithm available in SPM. GM and WM segments were used for partial volume effects (PVE) correction. Two PVE corrections were applied to CVR and CBF values obtained from each ROI: first, only data from voxels that contain a minimum of 70% GM were included; second, the voxels that survived this threshold were again corrected for PVE with the formula: $SI_{corr} = SI_{uncorr}/(GM + (0.4 \times WM))$, where SI_{corr} and SI_{uncorr} were corrected and uncorrected data respectively and GM, WM were tissue probability values for GM and WM, respectively, within each voxel [136].

Whole-brain CVR and CBF data were compared across groups using a one-way Analysis-of-Variance (ANOVA) method. Student's t-tests were conducted to compare results between groups for individual ROIs. A two-tailed p-value of 0.05 is considered significant. Voxel-by-voxel comparisons between the groups were conducted using two-sample student's t-test in SPM. Results were considered statistically significant at a voxel-wise p-value of 0.005 and an extent threshold of 250 voxels [137]. Correlation between Vo_{2max} and CVR ROI data were performed using Pearson's correlation; and results were considered significant at a p-value < 0.05 for a two-tailed distribution.

5.3 Results

5.3.1 VO_{2max}

Vo_{2max} for MA and SE were 40.6±2.0 ml/kg/min and 23.4±1.7 ml/kg/min, respectively. As expected, MA showed a significantly better physical fitness compared to SE ($p < 0.001$).

5.3.2 CBF

Whole-brain-averaged CBF values were 37.1±10.4 ml/100g/min and 36.5±7.2 ml/100g/min for MA and SE, respectively, with no statistically significant difference ($p = 0.9$). Similarly, no CBF differences were seen in whole-brain GM (40.2±11.3 ml/100g/min in MA and 39.7±7.8 ml/100g/min in SE, $p = 0.9$) or whole-brain WM (31.6±9.3 ml/100g/min in MA and 30.8±6.9 ml/100g/min in SE, $p = 0.8$) between the two groups. The ROI and voxel-wise comparison of CBF therefore used relative CBF (rCBF). None of the lobular ROIs examined manifested differences in rCBF. Voxel-wise comparison revealed that, when compared to SE, MA showed significantly greater rCBF in posterior cingulate cortex (PCC) and precuneus (Figure 5-1a), regions that are part of the default mode network (DMN) and are known to be sensitive to aging and Alzheimer's Disease. Figure 5-1 b shows averaged rCBF in these voxels. The values in MA were 16.7% greater than those in SE. Figure 5-1 b also revealed that PCC/precuneus rCBF in MA was higher than that in YC (corrected $p = 0.01$). We emphasize, however, that this does not mean blood supply in these regions in MA was greater than YC. Indeed, examinations of absolute CBF suggested that aCBF in PCC/precuneus of MA was slightly (9.7%) lower than that in YC (Figure 5-1 c). Therefore, the interpretation of the data should be that aerobic exercise selectively preserved blood supply in the PCC/precuneus region by showing a milder age effect, considering that the whole-brain-

averaged absolute CBF manifested a 22.1% reduction (from 51.6±8.1 ml/100g/min to 40.2±11.3 ml/100g/min, one-way ANOVA, corrected p = 0.04) when comparing MA to YC (similar to the reduction comparing SE to YC).

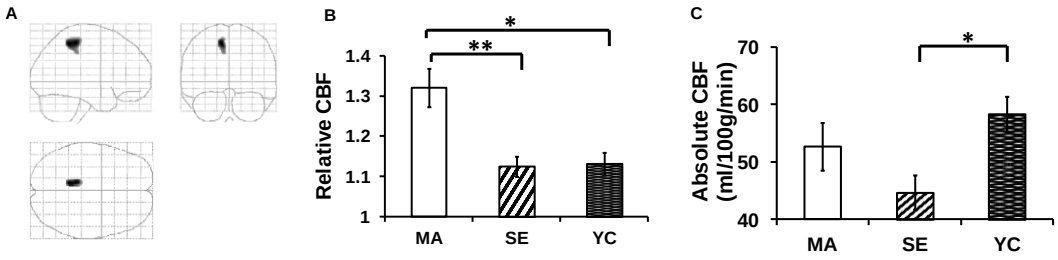

Figure 5-1: Comparison of Cerebral Blood Flow (CBF) across subject groups. (A) Brain regions showing significantly (p<0.005, cluster size 250) greater CBF in Masters Athletes (MA) compared to Sedentary Elderly (SE). These voxels are located in posterior cingulate cortex and precuneus of the Default-Mode-Network (DMN). Results are shown in glass brain view. No clusters showed MA < SE. (B) Relative CBF (normalized against whole-brain value) in the cluster highlighted in (A). (C) Absolute CBF in the cluster highlighted in (A). * corrected p < 0.05, ** corrected p < 0.005. Error bar = standard error.

We have also investigated any potential CBF differences in the opposite direction, but found no regions manifesting a lower rCBF in the MA group when compared to SE.

5.3.3 CVR

Both the MA and SE groups responded to CO_2-inhalation by revealing a significantly higher Et CO_2. However, no differences were seen between the groups in terms of their Et CO_2 values during room-air, during CO_2-inhalation, or the Et CO_2 changes (Table 5-1).

One-way ANOVA showed a main effect of group on whole-brain CVR. Figure 5-2 A shows group-averaged absolute CVR maps for MA and SE. It is apparent from visual inspection of the images that a difference is present throughout the brain. Furthermore, the difference is paradoxical in that the MA group revealed a lower aCVR compared to

the SE. Figure 5-2 B plots CVR values in major brain lobes. A difference with corrected $p<0.05$ was seen in temporal lobe and insula. A difference with uncorrected $p<0.05$ was seen in frontal and parietal lobes, and sub-cortical gray matter. The other regions also showed a trend in the same direction.

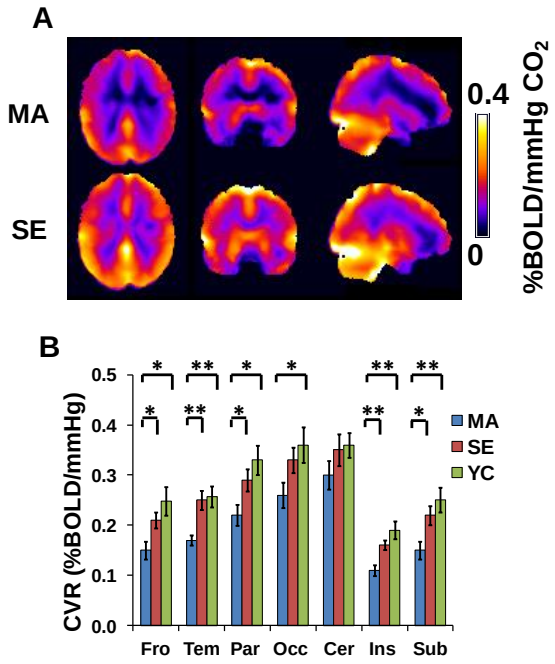

Figure 5-2: Comparison of Cerebral Vascular Reactivity (CVR) across subject groups. (A) Group-averaged CVR maps for Masters Athletes (MA) (N=8) and Sedentary Elderly (SE) (N=10). (B) ROI results for MA, SE, and Young Controls (YC). Fro - Frontal lobe, Tem - Temporal lobe, Par - Parietal lobe, Occ - Occipital lobe, Cer - Cerebellum, Ins – Insula, Sub – Subcortical gray matter. ** corrected $p<0.05$. * uncorrected $p<0.05$. Error bar = standard error.

Voxel-wise comparison confirmed the findings from the ROI analysis. Clusters in which MA had lower CVR were observed throughout the brain (Figure 5-3). Although the significant clusters do not cover all voxels in the brain due to limited sample size and power, the spatial distribution of these clusters suggests that CVR difference between

MA and SE represents a whole-brain feature. We found no clusters in which CVR was greater in the MA group.

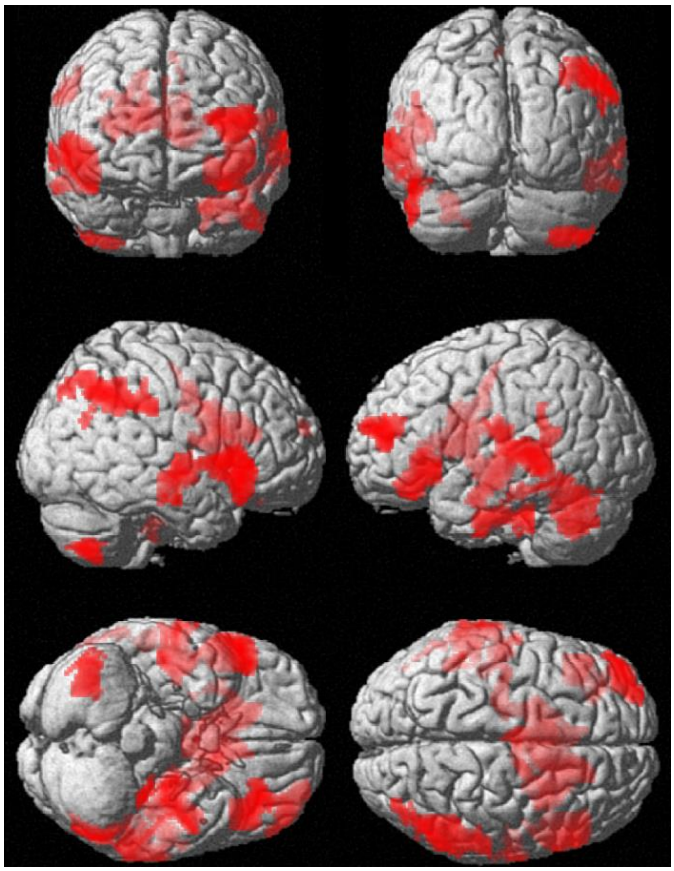

Figure 5-3: Voxel-wise comparison of Cerebral Vascular Reactivity (CVR) between Masters Athletes (MA) and Sedentary Elderly (SE). Red color indicates clusters where MA have lower CVR compared to SE ($p<0.005$, cluster size 250). No clusters showed MA > SE.

We further examined whether, within the MA group, there is a dose-response relationship between physical fitness and CVR by studying the correlation between Vo_{2max} and CVR in each ROI. We observed a negative correlation between CVR and Vo_{2max} (Figure 5-4) in the temporal lobe ROI (cc = -0.81, uncorrected p = 0.027). The other brain regions examined also showed negative correlation coefficients (cc range = -

0.73 to -0.25) but did not reach significance threshold. The negative correlation is congruent with the between-group findings and, collectively, the results suggest that MA in general have lower CVR compared to SE and MA individuals with greater physical fitness have even lower CVR. Across the entire elderly cohort (SE and MA), a negative correlation was also present between whole-brain CVR and Vo_{2max} (cc = -0.73, p = 0.004).

CVR in YC was greater than the other two groups in all brain ROIs examined (Figure 5-2b), consistent with previous reports that CVR shows an age-related decline [9].

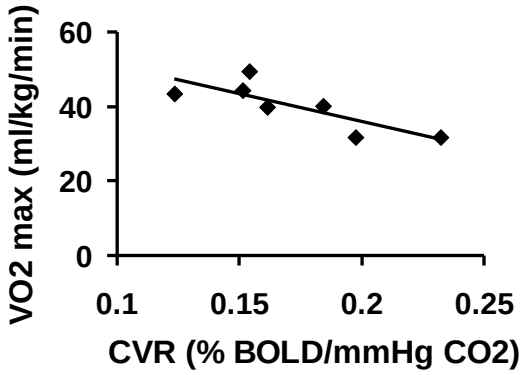

Figure 5-4: Scatter plot between Vo_{2max} and CVR values in the temporal lobe.

5.4 Discussion

The present work suggested that life-long aerobic exercise preserved CBF in posterior cingulate cortex/precuneus, a key region in the default-mode-network and highly sensitive to age and dementia [138]. CBF in this region of the MA subjects still showed an age-related decrease, but its degree was milder compared to that in the SE subjects or to other regions of the MA subjects. This study also suggested that blood

vessels in the MA brain were actually less responsive to vaso-dilatative CO_2 stimuli. This effect was spatially non-specific and was present throughout the brain.

Our finding of an elevated CBF in DMN in MA compared to SE is particularly interesting in view of recent reports that DMN represents pivotal regions responsible for basic brain functions such as maintaining alertness and preparing the brain to react to external stimuli [139], and that its function shows pronounced degradation with aging and with Alzheimer's Disease [140]. The salutary effect of aerobic exercise on DMN CBF is congruent with previous findings that the spatial pattern of age-related CBF decline is similar to that of DMN [125]. Our observation on CBF may be related to recent findings by Voss et al. using another imaging modality, functional connectivity MRI (fcMRI), which showed that connectivities among the DMN regions were significantly correlated with the individual's aerobic fitness [141]. CBF and resting state neural activity in DMN are known to be closely associated. In fact, higher CBF in DMN as compared to the rest of the brain was one of the first evidence that led Raichle and colleagues to propose a default mode of the brain [142], and the findings were reproduced by other groups [143].

CBF increase can be attributed to either healthier vasculature itself or an indirect effect of greater neural activity via neurovascular coupling. Our interpretation of the results is that the elevated CBF in PCC reflects a more active neural activity in this region. Had the vascular changes itself been responsible for our observation, it is hard to conjecture that the vascular changes are limited to this small region, especially given the wide-spread CVR differences observed in the same subjects. In fact, the CVR in PCC of MA was significantly lower (0.18±0.05 %BOLD/mmHg vs. 0.19±0.06 %BOLD/mmHg, $p = 0.012$) than that of SE. These results also suggest that the wide-spread CVR difference cannot be attributed to the resting CBF effect, which is more focal.

Our CVR data showed that MA had a lower value compared to SE and this was in fact opposite from what we had originally hypothesized. One possible reason is that physical exercise may have different effects on different vasculature systems in the body. A wealth of literature has demonstrated that aerobic endurance exercise training is beneficial to the health of cardiovascular system and to some extent the peripheral vascular system [122-124]. In contrast, the benefit on cerebral vasculature is less pronounced. For example, it was shown that the aortic compliance in MA was similar to that in young adults [144], but the carotid compliance was considerably lower than that observed in young subjects [145]. It was also shown that intima-media thickness (IMT) of femoral artery in MA was smaller compared to sedentary elderly, but IMT of carotid artery did not differ between MA and sedentary elderly [146]. Similarly, carotid blood pressure did not show a difference between the two groups [146]. The reason that endurance training markedly improved cardiovascular and peripheral vascular systems but had only modest effect on brain vessels may be associated with the blood flow demands of these organs during the exercise. Cardiac and peripheral systems are known to have drastically higher demands during exercise, whereas the cerebral cortex may receive modestly higher blood supply compared to resting state. Higher flow during exercise may be salutary as it is associated with higher laminar shear in vessel wall, which was shown to be responsible for protective effects such as increased vessel diameter [147] and improved vascular endothelial function [148]. The brain vessels, on the other hand, may receive reduced degree of benefits due to unchanged or only slightly increased blood flow during exercise.

Another mechanism may have also contributed to the lower CO_2-reactivity in MA. CO_2 is a by-product of metabolism and exercise. There is some evidence in the literature that blood CO_2 concentration is elevated during physical exercise at a level below 80% of

Vo_{2max} (beyond 80% of Vo_{2max}, CO_2 concentration will decrease due to hyperventilation) [149]. Blood vessels in MA may thus experience considerably more high-CO_2 exposure time periods during their lifetime, due to the constant exercise they perform. More lifetime exposure to high levels of CO_2 will conceivably cause the vasculature to become "desensitized" to CO_2 stimulation. This could also be a protection mechanism to prevent blood vessels in the brain from over-dilating during exercise when most blood should go to the limbs. It remains to be determined whether only CO_2-reactivity was reduced in MA or reactivity to other stimulants is also affected. For example, it would be interesting to investigate whether their vascular responses to simple visual stimulation or to blood pressure modulation are also reduced, compared to SE.

The findings from the present work should be interpreted in view of a few limitations. One limitation is that the SE group was selected using very stringent criteria, i.e. the absence of any cardiovascular (e.g. hypertension, Type 2 diabetes) or cerebrovascular diseases (e.g. history of stroke, transient ischemic attack). The advantage of using these criteria is that they matched the criteria for the MA group. However, given that they are in their 70's and lead a sedentary lifestyle yet they do not have any cardiovascular conditions, they may represent a "supernormal" group of subjects and may have some genetic predispositions that protect them from age-related vascular conditions. To address this potential confound, we also analyzed data from another elderly group, a healthy control group in our earlier Alzheimer's study (SE-A) [132], and compared their CVR/CBF values to the MA group. It was found that the CVR values in SE-A were still consistently higher than the MA group in all brain regions, suggesting that our findings were valid even using another control group. Similarly, CBF enhancement in the PCC of the MA group was still detected even using the SE-A for comparison.

The other limitation of this study is that we did not report comparisons of cognitive function or brain volume between MA and SE subjects. We did collect cognitive and volumetric data, and the results are being presented in another report [150] in which we found that MA had better performance in a number of cognitive domains including letter fluency, category fluency, and reading skills.

The sample size of ten participants per group is smaller than most other aging and dementia studies, which resulted in lower detection power and precluded us from conducting multiple comparison corrections in certain analyses. This is because of the relatively unique group of subjects, i.e. Masters Athletes, examined in our study. In fact, we had to recruit some of the participants from outside our metropolitan area in order to achieve the present sample size. Indeed, many of the previous studies on MA have used a similar size [122, 123]. Nonetheless, future studies in a larger cohort or multi-site studies should be performed to verify the findings from the present work.

5.5 Conclusions

This study showed that life-long aerobic exercise preserved blood supply in the brain's default-mode-network against age-related degradation. On the other hand, its impact on cerebral vascular system seems to be characterized by a dampening of CO_2 reactivity, but the reason for this observation merits further investigation using non-CO_2 vascular challenges such as brain activation or blood pressure modulation.

Chapter 6

Conclusions

Brain vascular response to physiological challenges such as O_2 and CO_2 were studied using MRI. Physiological mechanisms of BOLD MRI signal change was better understood. This research has revealed that when using typical BOLD imaging parameters to study MR signal response to the hypercapnia challenge, negative CVR is to be expected in brain ventricles. The physiologic underpinning of this observation appears to be a reduction of CSF volume fraction as a consequence of choroid plexus (blood vessel) dilation, causing bright CSF signal being replaced by less intensive blood signal. Measurement of CBF suggested that oxygenation in the ventricles most likely increased rather than decreased during hypercapnia, confirming that blood vessel dilation occurred in the ventricles during CO_2 inhalation. Simulation experiments with assumed parameters helped make future recommendations regarding BOLD MRI parameters, so as to avoid the negative CVR in the ventricles. These findings should be interpreted in view of the limitations from this study. First, this experiment only tested for BOLD response in the ventricles to hypercapnia (CO_2) inhalation and did not examine BOLD signal change mechanisms to other pharmacological agents such as Acetazolamide. Second, this study did not test for possible contribution of CSF inflow or cardiac pulsation effects on the negative BOLD response in the ventricles. But data from the study revealed that the effect of pulsation may be small, otherwise the IR sequence should still show a negative BOLD response in the ventricles. Third, simulations from this study considered only the effect of oxygenation change due to inhalation of O_2, but it did not consider the effect of potential T_1 shortening due to dissolved oxygen in plasma, which could also cause a BOLD signal increase due to O_2 inhalation. Finally it is assumed that brain metabolism is unchanged during a hypercapnia challenge and that hypercapnia

results in a purely vascular response. However there is evidence in literature that metabolism is slightly suppressed during the hypercapnia challenge [82]. However the vascular response to CO2 inhalation is still a large effect in the measured CVR response, considering that a unit (mm Hg) increase in Et CO2 results in approximately 6% increase in CBF, but only around 1.5% decrease in metabolic rate [82].

CVR in white matter was studied and characterized in terms of its magnitude and temporal characteristics. It was found that white matter CVR in response to hypercapnia was different from that of GM in several aspects. Aside from the expected reduction in magnitude, WM response was slower than GM by tens of seconds. This could be attributed to the longer time it takes for WM extravascular CO_2 to accumulate and may be related to the lower perfusion in white matter. It was found that with age, WM CVR becomes greater and faster, which is opposite to the changes seen in the GM. This research helped us better understand the mechanism of BOLD signal change to CO_2 in white matter. These findings should also be considered in light of few limitations. First, given the large delay between brain tissue types, the frequency domain analysis may be the preferred approach over time domain analysis, since it is less sensitive to the delay between time courses. Second, in order to obtain accurate delays, a higher sampling resolution of scanner acquisition is advised, with a TR less than 1000 ms. Third, the gender distribution between the younger and elderly participants was not exactly matched. The elderly group had more male subjects, and it known that males and females could have differences in CBF. Therefore, some of the CBF findings, for example lower GM CBF in old, could be influenced by this gender difference. Future CVR results from pathological conditions in WM, should consider possible changes in both amplitude and delay for results interpretation. It should be noted that if the delay time is not properly

accounted for, the response amplitude may be underestimated, which may lead to mis-interpretation of results.

The white matter in brain was further studied and it was characterized into fiber tracts, lobes and layers. Brain vascular response to inhalation of both O_2 and CO_2 were measured from these WM regions. One of the main findings from this research was that delays measured from the end-tidal (Et) O_2 to the vascular response in all WM regions are long, on similar order as that measured due to the CO_2 gas. It was also found that the delays due to CO_2 were longer compared to those measured due to O_2. The differences in delay measured due to the O_2 and the CO_2 gas were attributed to differences in the mechanism of action of these gases on the vasculature in brain. Differences were found between fiber tracts with respect to delay in response and the magnitude of response, for both the O_2 and CO_2 gas. Differences were also found between the WM layers with respect to delay in response and the magnitude of response, for both the O_2 and CO_2 gas. Measurement of delays in the WM was also shown to be reproducible between scans. This research has few limitations, which need to be considered during the interpretation of these results. First, to compute accurate delays, faster image acquisition is required, with a TR less than 1000ms. Second the results from this study need to be interpreted under the scope tested, i.e. only results to a CO2 inhalation paradigm were tested. Future studies should consider examining vascular responses in WM to other paradigms such as breath hold or pharmacological challenges such as injection of acetazolamide, prospective end-tidal targeting or dynamic end-tidal forcing. The WM fiber tracts may contain partial volume effects from adjacent GM, because of the large voxel size of $2.5 \times 2.5 \times 2.5$ mm^3. A higher DTI acquisition resolution of less than this current resolution may be advised for future studies to avoid partial volume effects from GM.

Research was also conducted on an application of CVR to understand the effect of life-long aerobic exercise on vascular health. This study showed that life-long aerobic exercise preserved blood supply in the brain's default-mode-network against age-related degradation. It was found that the impact of life-long aerobic exercise on cerebral vascular system was characterized by a dampening of CO_2 reactivity. It was suggested that this reduction in CVR because of exercise required further investigation using non-CO_2 vascular challenges such as brain activation or blood pressure modulation. The findings from this research should be interpreted in view of few limitations. First the sedentary elderly participants from this study have a mean age of 75 years and none of them have any cardiovascular diseases or diabetes and neither do they take any medications, so they may represent individuals that are "super normal" with probably a genetic predisposition to protect them from age related vascular degeneration. The MA group was also highly fit and all MA were still undergoing endurance training while volunteering in this research. Future studies may consider recruiting MA that may not actively participate in sports, which may help reduce some exposure to CO_2 during the time the CVR measurements are performed. Second the sample size of 10 participants per group is smaller than most aging and dementia studies, which prevented us from performing corrections for multiple comparisons on certain analysis. Recruitment of a smaller sample size was because of the special subjects, the MA, some of whom had to be recruited outside our metropolitan area to achieve this sample size. Indeed, many of the previous studies on MA have used a similar sample size. Future multi-site studies or studies with a larger sample size are needed to confirm these findings.

6.1 Suggestions for Future Research

Research performed as part of this dissertation has helped better interpret BOLD changes to physiological challenges and paved the steps for future research in the brain

in compartments other than the gray matter. Until now BOLD signal change mechanisms were better understood in GM. These studies have helped us understand the physiologic underpinnings of BOLD signal change mechanisms to O_2 and CO_2 in the brain white matter and CSF. Research on vascular physiology in the ventricles may find future applications in clinic to understand pathophysiology of hydrocephalus and also to understand the choroid plexus and its mechanism of auto-regulation better. Studies to examine BOLD signal change mechanisms in the ventricle to a pharmacological agent such as Acetazolamide are also necessary. Research on the study of CVR in WM fiber tracts may initiate future studies with larger cohort to reproduce these findings. Studies should also aim to eliminate partial volume effects from GM that may be present in the current data; such studies should focus on increasing the resolution of the DTI acquisition. There is great potential that future WM studies will be performed on higher magnetic field strengths to increase the signal to noise ratio (SNR) in WM, especially given that the signal in WM is much weaker (75% less than GM signal), because of less vasculature in WM compared to GM. Future studies to measure other parameters such as CBV from the WM fiber tracts may also be initiated to compare and confirm the results obtained from the vascular response in the WM fiber tracts to O_2 inhalation. Future research should also include patient populations with WM diseases such as multiple sclerosis to find out if disease processes lead to changes in WM vascular response to physiological challenges. Examination of the vascular response in the WM to O_2 and CO_2 can also be applied to predict impending WM lesions or communication problems between brain regions in disorders and diseases such as multiple sclerosis, mild cognitive impairment (MCI), Alzheimer's disease and traumatic brain injury. Future research on Masters Athletes should include examination of BOLD response to simulants

other than CO_2, for example pharmacological agents such as Acetazolamide or neuronal stimulation, both of which have non CO_2 based mechanisms of action on the brain.

References

1. Kety, S.S. and C.F. Schmidt, The Effects of Altered Arterial Tensions of Carbon Dioxide and Oxygen on Cerebral Blood Flow and Cerebral Oxygen Consumption of Normal Young Men. J Clin Invest, 1948. **27**(4): p. 484-92.
2. Kuschinsky, W., Regulation of cerebral blood flow: an overview. 1996, Johns Libbey & Company Ltd, London: Mraovitch, S., Sercombe, R. (Eds.), Neurophysiological Basis of Cerebral Blood Flow Control: An Introduction. p. 245–262.
3. Greenberg, S.M., Small vessels, big problems. N Engl J Med, 2006. **354**(14): p. 1451-3.
4. Mandell, D.M., et al., Mapping cerebrovascular reactivity using blood oxygen level-dependent MRI in Patients with arterial steno-occlusive disease: comparison with arterial spin labeling MRI. Stroke, 2008. **39**(7): p. 2021-8.
5. Fierstra, J., et al., Impaired peri-nidal cerebrovascular reserve in seizure patients with brain arteriovenous malformations. Brain, 2011. **134**(Pt 1): p. 100-9.
6. Mikulis, D.J., et al., Preoperative and postoperative mapping of cerebrovascular reactivity in moyamoya disease by using blood oxygen level-dependent magnetic resonance imaging. J Neurosurg, 2005. **103**(2): p. 347-55.
7. Conklin, J., et al., Impaired cerebrovascular reactivity with steal phenomenon is associated with increased diffusion in white matter of patients with Moyamoya disease. Stroke, 2010. **41**(8): p. 1610-6.
8. Han, J.S., et al., BOLD-MRI cerebrovascular reactivity findings in cocaine-induced cerebral vasculitis. Nat Clin Pract Neurol, 2008. **4**(11): p. 628-32.
9. Lu, H., et al., Alterations in cerebral metabolic rate and blood supply across the adult lifespan. Cereb Cortex, 2011. **21**(6): p. 1426-34.
10. Pillai, J.J. and D.J. Mikulis, Cerebrovascular Reactivity Mapping: An Evolving Standard for Clinical Functional Imaging. AJNR Am J Neuroradiol, 2014.
11. Vagal, A.S., et al., The acetazolamide challenge: techniques and applications in the evaluation of chronic cerebral ischemia. AJNR Am J Neuroradiol, 2009. **30**(5): p. 876-84.
12. Davis, T.L., et al., Calibrated functional MRI: mapping the dynamics of oxidative metabolism. Proc Natl Acad Sci U S A, 1998. **95**(4): p. 1834-9.
13. Hoge, R.D., et al., Linear coupling between cerebral blood flow and oxygen consumption in activated human cortex. Proc Natl Acad Sci U S A, 1999. **96**(16): p. 9403-8.

14. Donahue, M.J., et al., Hemodynamic changes after visual stimulation and breath holding provide evidence for an uncoupling of cerebral blood flow and volume from oxygen metabolism. J Cereb Blood Flow Metab, 2009. **29**(1): p. 176-85.
15. Donahue, M.J., et al., Vascular space occupancy (VASO) cerebral blood volume-weighted MRI identifies hemodynamic impairment in patients with carotid artery disease. J Magn Reson Imaging, 2009. **29**(3): p. 718-24.
16. Hua, J., et al., Physiological origin for the BOLD poststimulus undershoot in human brain: vascular compliance versus oxygen metabolism. J Cereb Blood Flow Metab, 2011. **31**(7): p. 1599-611.
17. Yezhuvath, U.S., et al., On the assessment of cerebrovascular reactivity using hypercapnia BOLD MRI. NMR Biomed, 2009. **22**(7): p. 779-86.
18. Thomas, B.P., et al., Cerebrovascular reactivity in the brain white matter: magnitude, temporal characteristics, and age effects. J Cereb Blood Flow Metab, 2014. **34**(2): p. 242-7.
19. Blockley, N.P., et al., An improved method for acquiring cerebrovascular reactivity maps. Magn Reson Med, 2011. **65**(5): p. 1278-86.
20. Mandell, D.M., et al., Selective reduction of blood flow to white matter during hypercapnia corresponds with leukoaraiosis. Stroke, 2008. **39**(7): p. 1993-8.
21. Lu, H., et al., Novel approach to the measurement of absolute cerebral blood volume using vascular-space-occupancy magnetic resonance imaging. Magn Reson Med, 2005. **54**(6): p. 1403-11.
22. van Osch, M.J., et al., Can arterial spin labeling detect white matter perfusion signal? Magn Reson Med, 2009. **62**(1): p. 165-73.
23. Iannetti, G.D. and R.G. Wise, BOLD functional MRI in disease and pharmacological studies: room for improvement? Magn Reson Imaging, 2007. **25**(6): p. 978-88.
24. Duvernoy, H.M., S. Delon, and J.L. Vannson, Cortical blood vessels of the human brain. Brain Res Bull, 1981. **7**(5): p. 519-79.
25. Aslan, S., et al., White matter cerebral blood flow is inversely correlated with structural and functional connectivity in the human brain. Neuroimage, 2011. **56**(3): p. 1145-53.
26. Bulte, D.P., et al., Cerebral perfusion response to hyperoxia. J Cereb Blood Flow Metab, 2007. **27**(1): p. 69-75.

27. Xu, F., et al., Effect of hypoxia and hyperoxia on cerebral blood flow, blood oxygenation, and oxidative metabolism. J Cereb Blood Flow Metab, 2012. **32**(10): p. 1909-18.
28. Zlokovic, B.V., Neurovascular mechanisms of Alzheimer's neurodegeneration. Trends Neurosci, 2005. **28**(4): p. 202-8.
29. Lublin, F.D. and S.C. Reingold, Defining the clinical course of multiple sclerosis: results of an international survey. National Multiple Sclerosis Society (USA) Advisory Committee on Clinical Trials of New Agents in Multiple Sclerosis. Neurology, 1996. **46**(4): p. 907-11.
30. Etnier, J.L., et al., A meta-regression to examine the relationship between aerobic fitness and cognitive performance. Brain Res Rev, 2006. **52**(1): p. 119-30.
31. Heyn, P., B.C. Abreu, and K.J. Ottenbacher, The effects of exercise training on elderly persons with cognitive impairment and dementia: a meta-analysis. Arch Phys Med Rehabil, 2004. **85**(10): p. 1694-704.
32. Ades, P.A., et al., The effect of weight loss and exercise training on flow-mediated dilatation in coronary heart disease: a randomized trial. Chest, 2011. **140**(6): p. 1420-7.
33. Kavanagh, T., et al., Quality of life and cardiorespiratory function in chronic heart failure: effects of 12 months' aerobic training. Heart, 1996. **76**(1): p. 42-9.
34. Colcombe, S.J., et al., Cardiovascular fitness, cortical plasticity, and aging. Proc Natl Acad Sci U S A, 2004. **101**(9): p. 3316-21.
35. Colcombe, S.J., et al., Aerobic exercise training increases brain volume in aging humans. J Gerontol A Biol Sci Med Sci, 2006. **61**(11): p. 1166-70.
36. Marks, B.L., et al., Aerobic fitness and obesity: relationship to cerebral white matter integrity in the brain of active and sedentary older adults. Br J Sports Med, 2011. **45**(15): p. 1208-15.
37. Black, J.E., et al., Learning causes synaptogenesis, whereas motor activity causes angiogenesis, in cerebellar cortex of adult rats. Proc Natl Acad Sci U S A, 1990. **87**(14): p. 5568-72.
38. Swain, R.A., et al., Prolonged exercise induces angiogenesis and increases cerebral blood volume in primary motor cortex of the rat. Neuroscience, 2003. **117**(4): p. 1037-46.
39. Clark, P.J., et al., Functional analysis of neurovascular adaptations to exercise in the dentate gyrus of young adult mice associated with cognitive gain. Hippocampus, 2009. **19**(10): p. 937-50.

40. Sessa, W.C., et al., Chronic exercise in dogs increases coronary vascular nitric oxide production and endothelial cell nitric oxide synthase gene expression. Circ Res, 1994. **74**(2): p. 349-53.
41. Kuschinsky, W., Regulation of cerebral blood flow: an overview, in Neurophysiological basis of cerebral blood flow control: an introduction, S. Mraovitch and R. Sercombe, Editors. 1996, Johns Libbey & Company Ltd: London. p. 245-62.
42. Donahue, M.J., et al., Relationships between hypercarbic reactivity, cerebral blood flow, and arterial circulation times in patients with moyamoya disease. J Magn Reson Imaging, 2013: p.; In-press. doi: 10.1002/jmri.24070.
43. Bandettini, P.A. and E.C. Wong, A hypercapnia-based normalization method for improved spatial localization of human brain activation with fMRI. NMR Biomed, 1997. **10**(4-5): p. 197-203.
44. Liau, J. and T.T. Liu, Inter-subject variability in hypercapnic normalization of the BOLD fMRI response. Neuroimage, 2009. **45**(2): p. 420-30.
45. Handwerker, D.A., et al., Reducing vascular variability of fMRI data across aging populations using a breathholding task. Hum Brain Mapp, 2007. **28**(9): p. 846-59.
46. Thomason, M.E., L.C. Foland, and G.H. Glover, Calibration of BOLD fMRI using breath holding reduces group variance during a cognitive task. Hum Brain Mapp, 2007. **28**(1): p. 59-68.
47. Liu, P., et al., Comparison of relative cerebral blood flow maps using pseudo-continuous arterial spin labeling and single photon emission computed tomography. NMR Biomed, 2012. **25**(5): p. 779-86.
48. Wise, R.G., et al., Dynamic forcing of end-tidal carbon dioxide and oxygen applied to functional magnetic resonance imaging. J Cereb Blood Flow Metab, 2007. **27**(8): p. 1521-32.
49. Slessarev, M., et al., Prospective targeting and control of end-tidal CO2 and O2 concentrations. J Physiol, 2007. **581**(Pt 3): p. 1207-19.
50. Bright, M.G., et al., The effect of basal vasodilation on hypercapnic and hypocapnic reactivity measured using magnetic resonance imaging. J Cereb Blood Flow Metab, 2011. **31**(2): p. 426-38.
51. Driver, I., et al., The change in cerebrovascular reactivity between 3 T and 7 T measured using graded hypercapnia. Neuroimage, 2010. **51**(1): p. 274-9.
52. Spano, V.R., et al., CO2 blood oxygen level-dependent MR mapping of cerebrovascular reserve in a clinical population: safety, tolerability, and technical feasibility. Radiology, 2013. **266**(2): p. 592-8.

53. Thomas, B.P., et al., Life-long aerobic exercise preserved baseline cerebral blood flow but reduced vascular reactivity to CO2. J Magn Reson Imaging, 2013.
54. Brian, J.E., Jr., Carbon dioxide and the cerebral circulation. Anesthesiology, 1998. **88**(5): p. 1365-86.
55. Lu, H. and P.C. van Zijl, Experimental separation of intra and extravascular BOLD effects using multi-echo VASO and BOLD fMRI at 1.5T and 3.0T. Magn Reson Med, 2005. **53**: p. 808-16.
56. Lin, C., et al. Measurements of T1 relaxation times at 3.0T: implications for clinical MRA. in Proc. 9th Annual Meeting ISMRM. 2001. Glasgow, UK.
57. Lu, H., X. Golay, and P.C. van Zijl, Intervoxel heterogeneity of event-related functional magnetic resonance imaging responses as a function of T(1) weighting. Neuroimage, 2002. **17**(2): p. 943-55.
58. Lu, H., et al., Sustained post-stimulus elevation in cerebral oxygen utilization following vascular recovery. J Cereb Blood Flow Metab, 2004. **24**: p. 764-770.
59. Lu, H., et al., Determining the longitudinal relaxation time (T1) of blood at 3.0 Tesla. Magn Reson Med, 2004. **52**(3): p. 679-82.
60. Zhao, J.M., et al., Oxygenation and hematocrit dependence of transverse relaxation rates of blood at 3T. Magn Reson Med, 2007. **58**(3): p. 592-7.
61. Boxerman, J.L., et al., MR contrast due to intravascular magnetic susceptibility perturbations. Magn Reson Med, 1995. **34**(4): p. 555-66.
62. Shinozuka, T., E.M. Nemoto, and P.M. Winter, Mechanisms of cerebrovascular O2 sensitivity from hyperoxia to moderate hypoxia in the rat. J Cereb Blood Flow Metab, 1989. **9**(2): p. 187-95.
63. Aslan, S., et al., Estimation of labeling efficiency in pseudocontinuous arterial spin labeling. Magn Reson Med, 2010. **63**(3): p. 765-71.
64. Attwell, D. and C. Iadecola, The neural basis of functional brain imaging signals. Trends Neurosci, 2002. **25**(12): p. 621-5.
65. Lu, H., et al., Functional magnetic resonance imaging based on changes in vascular space occupancy. Magn Reson Med, 2003. **50**(2): p. 263-74.
66. Scouten, A. and R.T. Constable, Applications and limitations of whole-brain MAGIC VASO functional imaging. Magn Reson Med, 2007. **58**(2): p. 306-15.

67. Scouten, A. and R.T. Constable, VASO-based calculations of CBV change: accounting for the dynamic CSF volume. Magn Reson Med, 2008. **59**(2): p. 308-15.
68. Donahue, M.J., et al., Theoretical and experimental investigation of the VASO contrast mechanism. Magn Reson Med, 2006. **56**(6): p. 1261-73.
69. Grant, R., et al., Changes in cranial CSF volume during hypercapnia and hypocapnia. J Neurol Neurosurg Psychiatry, 1989. **52**(2): p. 218-22.
70. Nakagawa, Y., et al., Effects of mild hypercapnia on somatosensory evoked potentials in experimental cerebral ischemia. Stroke, 1984. **15**(2): p. 275-8.
71. Waxman, S.G., Ventricles and coverings of the brain, in Clinical Neuroanatomy, S.G. Waxman, Editor. 2009, McGraw-Hill Companies, Inc.: Columbus, OH. p. 149-162.
72. Emerich, D.F., et al., The choroid plexus in the rise, fall and repair of the brain. Bioessays, 2005. **27**(3): p. 262-74.
73. Artru, A.A., Reduction of cerebrospinal fluid pressure by hypocapnia: changes in cerebral blood volume, cerebrospinal fluid volume, and brain tissue water and electrolytes. J Cereb Blood Flow Metab, 1987. **7**(4): p. 471-9.
74. Raichle, M.E. and F. Plum, Hyperventilation and cerebral blood flow. Stroke, 1972. **3**(5): p. 566-75.
75. Wise, R.G., et al., Resting fluctuations in arterial carbon dioxide induce significant low frequency variations in BOLD signal. Neuroimage, 2004. **21**(4): p. 1652-64.
76. Birn, R.M., et al., Separating respiratory-variation-related fluctuations from neuronal-activity-related fluctuations in fMRI. Neuroimage, 2006. **31**(4): p. 1536-48.
77. Kannurpatti, S.S. and B.B. Biswal, Detection and scaling of task-induced fMRI-BOLD response using resting state fluctuations. Neuroimage, 2008. **40**(4): p. 1567-74.
78. Bianciardi, M., et al., Negative BOLD-fMRI signals in large cerebral veins. J Cereb Blood Flow Metab, 2011. **31**(2): p. 401-12.
79. Bright, M.G., et al. Anticorrelated fMRI signal changes of hemodynamic origin in large cerebral vessels. in Proc. 20th Annual Meeting ISMRM. 2012.
80. Kastrup, A., et al., Regional variability of cerebral blood oxygenation response to hypercapnia. Neuroimage, 1999. **10**(6): p. 675-81.

81. Bokkers, R.P., et al., Symptomatic carotid artery stenosis: impairment of cerebral autoregulation measured at the brain tissue level with arterial spin-labeling MR imaging. Radiology, 2010. **256**(1): p. 201-8.
82. Xu, F., et al., The influence of carbon dioxide on brain activity and metabolism in conscious humans. J Cereb Blood Flow Metab, 2011. **31**(1): p. 58-67.
83. Zappe, A.C., et al., The influence of moderate hypercapnia on neural activity in the anesthetized nonhuman primate. Cereb Cortex, 2008. **18**(11): p. 2666-73.
84. Waxman, S.G., J.D. Kocsis, and P.K. Stys, The axon: structure, function and pathophysiology. 1 ed. Vol. 1. 1995, New York, NY: Oxford University Press.
85. Hui, E.S., et al., Stroke assessment with diffusional kurtosis imaging. Stroke, 2012. **43**(11): p. 2968-73.
86. Kantarci, K., et al., Mild cognitive impairment and Alzheimer disease: regional diffusivity of water. Radiology, 2001. **219**(1): p. 101-7.
87. Inglese, M. and M. Bester, Diffusion imaging in multiple sclerosis: research and clinical implications. NMR Biomed, 2010. **23**(7): p. 865-72.
88. Lipton, M.L., et al., Diffusion-tensor imaging implicates prefrontal axonal injury in executive function impairment following very mild traumatic brain injury. Radiology, 2009. **252**(3): p. 816-24.
89. Wakana, S., et al., Fiber tract-based atlas of human white matter anatomy. Radiology, 2004. **230**(1): p. 77-87.
90. Pike, G.B., et al., Multiple sclerosis: magnetization transfer MR imaging of white matter before lesion appearance on T2-weighted images. Radiology, 2000. **215**(3): p. 824-30.
91. van Gelderen, P., J.A. de Zwart, and J.H. Duyn, Pittfalls of MRI measurement of white matter perfusion based on arterial spin labeling. Magn Reson Med, 2008. **59**(4): p. 788-95.
92. Kastrup, A., et al., Assessment of cerebrovascular reactivity with functional magnetic resonance imaging: comparison of CO(2) and breath holding. Magn Reson Imaging, 2001. **19**(1): p. 13-20.
93. Rostrup, E., et al., Regional differences in the CBF and BOLD responses to hypercapnia: a combined PET and fMRI study. Neuroimage, 2000. **11**(2): p. 87-97.
94. Murphy, K., A.D. Harris, and R.G. Wise, Robustly measuring vascular reactivity differences with breath-hold: normalising stimulus-evoked and resting state BOLD fMRI data. Neuroimage, 2011. **54**(1): p. 369-79.

95. Kannurpatti, S.S., et al., Non-neural BOLD variability in block and event-related paradigms. Magn Reson Imaging, 2011. **29**(1): p. 140-6.
96. Zaca, D., J. Hua, and J.J. Pillai, Cerebrovascular reactivity mapping for brain tumor presurgical planning. World J Clin Oncol, 2011. **2**(7): p. 289-98.
97. Tancredi, F.B. and R.D. Hoge, Comparison of cerebral vascular reactivity measures obtained using breath-holding and CO2 inhalation. J Cereb Blood Flow Metab, 2013. **33**(7): p. 1066-74.
98. Bright, M.G. and K. Murphy, Reliable quantification of BOLD fMRI cerebrovascular reactivity despite poor breath-hold performance. Neuroimage, 2013.
99. Sicard, K.M. and T.Q. Duong, Effects of hypoxia, hyperoxia, and hypercapnia on baseline and stimulus-evoked BOLD, CBF, and CMRO2 in spontaneously breathing animals. Neuroimage, 2005. **25**(3): p. 850-8.
100. Uludag, K., et al., Coupling of cerebral blood flow and oxygen consumption during physiological activation and deactivation measured with fMRI. Neuroimage, 2004. **23**(1): p. 148-55.
101. Zappe, A.C., K. Uludag, and N.K. Logothetis, Direct measurement of oxygen extraction with fMRI using 6% CO2 inhalation. Magn Reson Imaging, 2008. **26**(7): p. 961-7.
102. Chen, J.J. and G.B. Pike, MRI measurement of the BOLD-specific flow-volume relationship during hypercapnia and hypocapnia in humans. Neuroimage, 2010. **53**(2): p. 383-91.
103. Chen, J.J. and G.B. Pike, Global cerebral oxidative metabolism during hypercapnia and hypocapnia in humans: implications for BOLD fMRI. J Cereb Blood Flow Metab, 2010. **30**(6): p. 1094-9.
104. Folstein, M.F., S.E. Folstein, and P.R. McHugh, "Mini-mental state". A practical method for grading the cognitive state of patients for the clinician. J Psychiatr Res, 1975. **12**(3): p. 189-98.
105. Wong, E.C., Vessel-encoded arterial spin-labeling using pseudocontinuous tagging. Magn Reson Med, 2007. **58**(6): p. 1086-91.
106. Dai, W., et al., Continuous flow-driven inversion for arterial spin labeling using pulsed radio frequency and gradient fields. Magn Reson Med, 2008. **60**(6): p. 1488-97.
107. Alsop, D.C. and J.A. Detre, Reduced transit-time sensitivity in noninvasive magnetic resonance imaging of human cerebral blood flow. J Cereb Blood Flow Metab, 1996. **16**(6): p. 1236-49.

108. D'Esposito, M., L.Y. Deouell, and A. Gazzaley, Alterations in the BOLD fMRI signal with ageing and disease: a challenge for neuroimaging. Nat Rev Neurosci, 2003. **4**(11): p. 863-72.
109. Liu, P., et al., Comparison of relative cerebral blood flow maps using pseudo-continuous arterial spin labeling and single photon emission computed tomography. NMR Biomed, 2011. **25**: p. 779-786.
110. Ge, Y., et al., Dirty-appearing white matter in multiple sclerosis: volumetric MR imaging and magnetization transfer ratio histogram analysis. AJNR Am J Neuroradiol, 2003. **24**(10): p. 1935-40.
111. Catani, M., et al., Virtual in vivo interactive dissection of white matter fasciculi in the human brain. Neuroimage, 2002. **17**(1): p. 77-94.
112. Waxman S.G., K.J.D., Stys P.K., The Axon: Structure, Function and Pathophysiology. 1st ed. Oxford University Press: New York, NY, 1995.
113. Woods, R.P., et al., Automated image registration: I. General methods and intrasubject, intramodality validation. J Comput Assist Tomogr, 1998. **22**(1): p. 139-52.
114. Jiang, H., et al., DtiStudio: resource program for diffusion tensor computation and fiber bundle tracking. Comput Methods Programs Biomed, 2006. **81**(2): p. 106-16.
115. Wakana, S., et al., Reproducibility of quantitative tractography methods applied to cerebral white matter. Neuroimage, 2007. **36**(3): p. 630-44.
116. Smith, S.M., et al., Tract-based spatial statistics: voxelwise analysis of multi-subject diffusion data. Neuroimage, 2006. **31**(4): p. 1487-505.
117. Steinhaus, L.A., et al., Cardio-respiratory fitness of young and older active and sedentary men. Br J Sports Med, 1988. **22**(4): p. 163-6.
118. Colcombe, S. and A.F. Kramer, Fitness effects on the cognitive function of older adults: a meta-analytic study. Psychol Sci, 2003. **14**(2): p. 125-30.
119. Colcombe, S.J., et al., Aerobic fitness reduces brain tissue loss in aging humans. J Gerontol A Biol Sci Med Sci, 2003. **58**(2): p. 176-80.
120. Pereira, A.C., et al., An in vivo correlate of exercise-induced neurogenesis in the adult dentate gyrus. Proc Natl Acad Sci U S A, 2007. **104**(13): p. 5638-43.
121. MacIntosh, B.J., et al., "Abstract."Cerebral blood flow changes associated with a single aerobic exercise session. ISMRM Scientific Workshop 11-14 October, 2012. **Oral session 4:17:39**.
122. Arbab-Zadeh, A., et al., Effect of aging and physical activity on left ventricular compliance. Circulation, 2004. **110**(13): p. 1799-805.

123. Shibata, S. and B.D. Levine, Effect of exercise training on biologic vascular age in healthy seniors. Am J Physiol Heart Circ Physiol, 2012. **302**(6): p. H1340-6.
124. Vaitkevicius, P.V., et al., Effects of age and aerobic capacity on arterial stiffness in healthy adults. Circulation, 1993. **88**(4 Pt 1): p. 1456-62.
125. Chen, J.J., H.D. Rosas, and D.H. Salat, Age-associated reductions in cerebral blood flow are independent from regional atrophy. Neuroimage, 2011. **55**(2): p. 468-78.
126. Haskell, W.L., et al., Physical activity and public health: updated recommendation for adults from the American College of Sports Medicine and the American Heart Association. Circulation, 2007. **116**(9): p. 1081-93.
127. Levine, B.D. and J. Stray-Gundersen, "Living high-training low": effect of moderate-altitude acclimatization with low-altitude training on performance. J Appl Physiol, 1997. **83**(1): p. 102-12.
128. Chalela, J.A., et al., Magnetic resonance perfusion imaging in acute ischemic stroke using continuous arterial spin labeling. Stroke, 2000. **31**(3): p. 680-7.
129. Wang, J., et al., Arterial transit time imaging with flow encoding arterial spin tagging (FEAST). Magn Reson Med, 2003. **50**(3): p. 599-607.
130. Herscovitch, P. and M.E. Raichle, What is the correct value for the brain--blood partition coefficient for water? J Cereb Blood Flow Metab, 1985. **5**(1): p. 65-9.
131. Lu, H., et al., Routine clinical brain MRI sequences for use at 3.0 Tesla. J Magn Reson Imaging, 2005. **22**(1): p. 13-22.
132. Yezhuvath, U.S., et al., Forebrain-dominant deficit in cerebrovascular reactivity in Alzheimer's disease. Neurobiol Aging, 2012. **33**(1): p. 75-82.
133. Shen, D. and C. Davatzikos, HAMMER: hierarchical attribute matching mechanism for elastic registration. IEEE Trans Med Imaging, 2002. **21**(11): p. 1421-39.
134. Aslan, S. and H. Lu, On the sensitivity of ASL MRI in detecting regional differences in cerebral blood flow. Magn Reson Imaging, 2010. **28**(7): p. 928-35.
135. Tzourio-Mazoyer, N., et al., Automated anatomical labeling of activations in SPM using a macroscopic anatomical parcellation of the MNI MRI single-subject brain. Neuroimage, 2002. **15**(1): p. 273-89.
136. Johnson, N.A., et al., Pattern of cerebral hypoperfusion in Alzheimer disease and mild cognitive impairment measured with arterial spin-labeling MR imaging: initial experience. Radiology, 2005. **234**(3): p. 851-9.

137. Gale, S.D., et al., Traumatic brain injury and grey matter concentration: a preliminary voxel based morphometry study. J Neurol Neurosurg Psychiatry, 2005. **76**(7): p. 984-8.
138. Lustig, C., et al., Functional deactivations: change with age and dementia of the Alzheimer type. Proc Natl Acad Sci U S A, 2003. **100**(24): p. 14504-9.
139. Harrison, B.J., et al., Consistency and functional specialization in the default mode brain network. Proc Natl Acad Sci U S A, 2008. **105**(28): p. 9781-6.
140. Greicius, M.D., et al., Default-mode network activity distinguishes Alzheimer's disease from healthy aging: evidence from functional MRI. Proc Natl Acad Sci U S A, 2004. **101**(13): p. 4637-42.
141. Voss, M.W., et al., Functional connectivity: a source of variance in the association between cardiorespiratory fitness and cognition? Neuropsychologia, 2010. **48**(5): p. 1394-406.
142. Raichle, M.E., et al., A default mode of brain function. Proc Natl Acad Sci U S A, 2001. **98**(2): p. 676-82.
143. Zou, Q., et al., Static and dynamic characteristics of cerebral blood flow during the resting state. Neuroimage, 2009. **48**(3): p. 515-24.
144. Tanaka, H., C.A. DeSouza, and D.R. Seals, Absence of age-related increase in central arterial stiffness in physically active women. Arterioscler Thromb Vasc Biol, 1998. **18**(1): p. 127-32.
145. Tanaka, H., et al., Aging, habitual exercise, and dynamic arterial compliance. Circulation, 2000. **102**(11): p. 1270-5.
146. DeVan, A.E. and D.R. Seals, Vascular health in the ageing athlete. Exp Physiol, 2012. **97**(3): p. 305-10.
147. Dinenno, F.A., et al., Regular endurance exercise induces expansive arterial remodelling in the trained limbs of healthy men. J Physiol, 2001. **534**(Pt 1): p. 287-95.
148. Seals, D.R., et al., Habitual exercise and arterial aging. J Appl Physiol, 2008. **105**(4): p. 1323-32.
149. Seifert, T. and N.H. Secher, Sympathetic influence on cerebral blood flow and metabolism during exercise in humans. Prog Neurobiol, 2011. **95**(3): p. 406-26.
150. Tseng, B.Y., et al., Masters athletes exhibit larger regional brain volume and better cognitive performance than sedentary older adults. J Magn Reson Imaging, 2013. **38**(5): p. 1169-76.

Biographical Information

Binu Panjikattil Thomas, raised in Mumbai, India, received his Bachelors of Engineering from the Mahatma Gandhi Missions college of Engineering and Technology, Mumbai University in June 1999. He worked for a year in Larsen & Tuobro Biotechnologies Pvt. Ltd. as a Service Engineer. In August 2000 he came to U.S.A to pursue his M.S. in Biomedical Engineering in the joint Biomedical Engineering program between UT Arlington, UT Southwestern and UT Dallas. During his M.S., Binu worked on Magnetic Resonance Spectroscopy in the lab of Dr. James Fleckenstein; he was awarded the degree in December 2002. During his M.S., he got interested in the fMRI technique to study brain function and wanted to pursue fMRI research. In March 2003 he began a full time position as Computer Programmer III in the Department of Psychiatry under the supervision of Dr. Carol Tamminga. This job entailed Binu to perform all aspects of fMRI research like data acquisition, data analysis, psychological task development, which he enjoyed. During his full time work, he realized his interests and decided to pursue the doctorate degree. In January 2010 he began his graduate work as a PhD student in the joint Biomedical Engineering program between UT Arlington, UT Southwestern and UT Dallas. He worked in the laboratory of Dr. Hanzhang Lu, at the Advanced Imaging Research Center (AIRC) at UT Southwestern, where he performed work on mapping and characterizing the properties of brain vascular reactivity to physiological challenges using MRI. He was awarded the PhD degree in August 2014. His thesis was titled “MRI assessment of brain vascular reactivity to physiological challenges”. He plans to pursue a postdoctoral research position in future.